
65
356

THE UNIVERSITY OF OKLAHOMA

GRADUATE COLLEGE

INFLUENCE OF SURFACE WAVES UPON MASS TRANSFER INTO LIQUID FILMS FLOWING ON INCLINED PLATES

A DISSERTATION

SUBMITTED TO THE GRADUATE FACULTY

in partial fulfillment of the requirements for the

degree of

DOCTOR OF PHILOSOPHY

BY

HSIANG SUNG LU

Norman, Oklahoma

1965

INFLUENCE OF SURFACE WAVES UPON MASS TRANSFER INTO LIQUID FILMS FLOWING ON INCLINED PLATES

APPROVED BY

O. Hougen

Arthur Bernhart

J. M. Dorrance

Charles Colver

DISSERTATION COMMITTEE

ACKNOWLEDGEMENT

It is a pleasure for the author to express his sincere appreciation to all who have contributed to this work, particularly to his advisor, Dr. Orrin K. Crosser, for his direction and encouragement during the entire course of this research.

Appreciation is expressed to Dr. Robert H. Perry for his guidance and encouragement during the first year of this research.

The author would also like to express gratitude to Mr. H. Warner Merritt, Jr. and Mr. Jerry Turner for their evaluation of the data.

Appreciation is expressed to the National Science Foundation for the financial support in making this work possible.

Finally, most sincere thanks are due to my wife, Lily, for her encouragement and help during the entire graduate program.

TABLE OF CONTENTS

APPENDICES Page

LIST OF TABLES

LIST OF ILLUSTRATIONS

INFLUENCE OF SURFACE WAVES UPON MASS TRANSFER INTO LIQUID FILMS FLOWING ON INCLINED PLATES

CHAPTER I

SUMMARY

In order to know more about the diffusion process in a falling liquid film, the absorption of carbon dioxide and the hydrodynamic properties of a falling water film at different inclination angles for various water flow rates were examined both theoretically and experimentally. In this research work, the concentration profiles in the falling water film were determined by means of Mach-Zehnder interferometer. The local eddy diffusivity in the falling water film was obtained by combination of the concentration profile with the material balance in the falling water film.

The experimental values of the film thickness were compared with theoretical values predicted in this thesis and with those suggested by Dukler, Portalski, and Kapitsa. These latter theories were originally derived for the vertical falling liquid films, and were modified to describe the falling water film at smaller angles. The theories parallel each other and do not agree with the slope of the experimental values. The data cross the theories in the neighborhood of

Reynolds number 800 at 5° and at 435 for 15°. Over the range studied from Reynolds numbers of ~~272~~ 435 to 1917 the experimental film thickness was within about 20% of the theoretical suggestions.

The ratio of the wave velocity to the average velocity and the frequency were also measured, and it was found that the frequency increased as the inclination angle was increased or as the Reynolds number of the water film was increased.

Experimental values of the increase of the interfacial area due to the waves were compared with the theory derived and found to be larger than the theoretical values. This increase in surface area could not account for the changes in mass transfer observed. The data show that a transition appeared in the behavior of the falling water film which was a function of inclination angle. This transition did not seem to be directly related to the laminar-turbulent transition and could be detected by changes in the film thickness, the frequency of the waves on the falling water film, and even the numerical value of the eddy diffusivities.

The concentration profiles indicated that for a 30 inch contact length, the diffusion process took place only in the upper part of the water film at Reynolds numbers larger than 1000, and that the carbon dioxide could penetrate to the bottom of the film at low Reynolds numbers (435).

A maximum value for the local eddy diffusivity occurred in the middle region of the film. Theoretical expressions for the behavior of total diffusivity were

obtained for logarithmic and parabolic velocity profiles. Both expressions show that the total diffusivity depends strongly upon Reynolds number, and weakly upon angle of inclination and have a maximum for the total diffusivity in the central region of the film.

CHAPTER II

INTRODUCTION

The diffusion of a pure gas into a falling liquid film has been examined theoretically and experimentally by many authors (10,11,12,17,27). A significant increase in mass transfer rate has been reported when ripples appear on the liquid surface (10,11,31). Emmert and Pigford (10) observed the absorption and desorption of oxygen and carbon dioxide in a falling water film. In some cases the ripples on the falling water film were eliminated by the addition of 5 to 25% wetting agent. In their experiment, the mass transfer rates were measured in a 3.75 foot long wetted wall column with an inside diameter of 0.99 inch. Their data showed that when ripples appeared on the falling water film, the mass transfer rates were severalfold greater than those encountered when ripples were removed by addition of the wetting agent. In order to find out how much of the reduction of mass transfer might be due to the concentration of wetting agent at the surface of the falling water film, a 1.524 inch long column was used instead of the long wetted wall column. Whether the wetting agent was added to the water or not, the ripples did not exist in the short wetted wall column. Their

data indicated an 11% decrease in absorption rate due to the presence of the wetting agent, when the shorter column was used. This effect is so much smaller than the change in mass transfer accompanying the removal of the ripples that one concludes the ripples are responsible for the higher transfer rate.

The persistent accumulation of these surface active agents at some position on the surface always complicates the interpretation of data from such short columns. However, although the precise role played by the surface active agent in these studies has not been defined, these results, combined with those of Grimley (12) show that the primary role of the surface active agent in reducing the mass transfer is to reduce the wave action, even though some surface area inhibition may result.

Stirba and Hurt (36) studied the absorption of pure carbon dioxide by a vertical falling water film at Reynolds numbers from 380 to 1270. Their results indicated that the mass transfer rates were manyfold greater than values predicted when molecular diffusion was the only transfer process.

These experimental results of previous workers on vertical columns, therefore, show that mass transfer of a gas into laminar flowing liquid films markedly increases when waves appear. The most likely causes for this effect would be the increase in interfacial area resulting from the wave disturbance of the surface, or an increase in dynamic action

within the film which begins where the waves appear.

The change in surface area caused by the waves was studied by Stirba and Hurt (36), who found that the maximum increase in surface area caused by the ripples as judged by visual observation and photographs was probably less than 50%. By an extension of Kapitsa's theory (18), Portalski derived an equation to calculate the fractional surface increase caused by surface waves on a laminar film. As mentioned in his paper, his equation should apply only below Reynolds numbers of 1200, the transitional Reynolds number of a falling water film from laminar flow to turbulent flow. According to the equation of Portalski, the interfacial area would increase 22% at a Reynolds number of 1060, 36% at Reynolds number of 1414, and 52% at Reynolds number of 1766. A capacitometer was used by Portalski to measure the interfacial area of an 82% glycerine water solution falling as a film with the Reynolds number equal to 11.2 and 12.0. The results agreed with his theoretical predictions. The theoretical fractional increase in surface area due to wave motion was 3.3%, and the experimental fractional increase in surface area due to wave motion ranged from 2.3 to 3.5%. Jepsen (17) modified a capacitometer designed by Dukler (8) to measure the interfacial area of a falling water film with inclination angles, equal to $9°44'$, $18°27'$ and $25°42'$. Above the liquid film was quiet air. Jepsen's results indicated that the maximum increase in interfacial area was less than 3%. The range of the liquid Reynolds number in Jepsen's experiments

was from 732 to 1834. At this time, there ~~is~~ are no accurate data concerning the fractional surface increase caused by the wave motion and ripples at these higher Reynolds numbers.

From the above observations, the increase in interfacial area would not explain the severalfold increase in mass transfer rate by the wave motion and ripples. This conclusion is accepted by most workers (31,36).

The second possibility for the increase in mass transfer is a bulk mixing effect caused by the wave motion and ripples. This possibility has been examined by the following authors:

Stirba and Hurt (36) introduced a stream of dye on the surface of a water film and found it spread out in the form of a cone downstream from the point of introduction. They indicated that at no time was a laminar dye thread observed in the rippling film, although the Reynolds number was reduced to as low as 200. This observation indicated a turbulence in the liquid.

The wave phenomena in the falling liquid film was explained theoretically in Kapitsa's paper (18). He started with a Navier-Stokes equation and assumed the velocity distribution in the falling liquid film was parabolic. Then he obtained a periodic solution for the film thickness and velocity. According to his periodic solution, there should be a region of reversed flow in the falling liquid film. Intuitively this region of reversed flow in the falling liquid film might cause an increase in the rate of mass transfer

although the exact consequences of this motion are not fully understood. Recently, his theory was modified by Portalski (30,31,38) who also performed experiments on the properties of the waves in the falling liquid films.

This second possibility has been accepted by most investigators (6,22,24,31,36). For example Danckwerts (6) assumed that various parts of the liquid surface were renewed with fresh material from time to time by some sort of mixing process. Based on his idea, he derived expressions for the rate of absorption in different cases such as instantaneous reaction between dissolved gas and reagent in solution; second order reaction between dissolved gas and reagent in solution; no chemical reaction in solution; and so on. These expressions contained the rate of renewal of liquid surface which must be determined experimentally. Recently, Danckwerts and his coworkers (7) performed experiments on the absorption of CO_2 into Na_2SO_4; NA_2CO_3; NaOH solutions and pure water. They used both a wetted wall column and a column packed with 1/2 inch Raschig rings. They found that after the fractional rate of surface renewal was determined by experimental data, the renewal models could predict these rates of absorption of CO_2 into various liquid solutions within 10 percent.

The above investigation showed that when ripples appeared on the falling water film, the mass transfer rate became very complicated. Besides, the various surface renewal models (6), several studies (18,20,22,24) have started from the hydrodynamic theory of thin falling films to find the

mechanism of the mass transfer in a wetted wall column.

Lewis and Whitman (35) postulated a stagnant film on the surface of the liquid layer and that the remainder of the layer was mixed. Therefore, the concentration gradient occurred only in the stagnant film.

Higbie's penetration theory was based on the assumption that the falling film was in laminar motion and no waves appeared on the surface. He also assumed a constant saturated concentration at the surface of the liquid, with the negligible diffusion in the direction of the flow. Therefore, the entire liquid film corresponded to the stagnant layer of the film theory.

Pigford (35) assumed that the velocity distribution in the falling liquid film was parabolic. He also assumed that the interfacial concentration was constant, that only molecular diffusion within the liquid, and that no waves were present on the surface. Pigford solved the resulting equations to obtain an expression for the average concentration in the falling liquid film. Stirba and Hurt found that this expression would represent their data for the case of wavy flow if an apparent diffusivity was used instead of the molecular diffusivity. They suggested that the apparent diffusivity was the arithmetic sum of the molecular diffusivity (D) and eddy diffusivity (ϵ).

Levich (24) postulated that near the gas interface of a falling liquid film there existed a zone of liquid of thickness δ and in this zone the turbulence was severely

damped. From dimensional analysis he showed that

$$\delta = \frac{\sigma}{\rho U^*}$$

where σ is the surface tension between the gas phase and the liquid phase; ρ is the density of the liquid and U^* is the friction velocity or shear velocity defined as the square root of the wall shear divided by the fluid density. In his theory, he assumed that the eddy diffusion coefficient should decrease near the liquid surface and would be equal to the molecular diffusion coefficient within this thickness δ.

Jepsen (17) observed the concentration profiles for carbon dioxide diffusing into water flowing on an inclined plate by means of a Mach-Zehnder interferometer. He indicated in his thesis that with an inclination angle of 10°, the CO_2 penetrated immediately to the bottom of the film when the waves appeared. He also found that the eddy diffusivity in a falling liquid film was a function of location in the film, and the liquid flow rate. At a Reynolds number of 732 or less, the diffusivity was higher than the molecular diffusivity but was constant through the liquid film.

All of these suggestions to explain the dynamic action utilize a single parameter combined with various assumptions about the flow character. In most cases an effective film thickness or an effective diffusivity must be evaluated from overall mass transfer data.

This discussion shows that the fundamental conception of the mass transfer process for the film with waves depends

greatly upon the flow characteristics of the falling liquid film. Therefore, the actual flow behavior of the falling liquid film will be necessary basic knowledge for the understanding of the mass transfer rates into such a film.

The properties of the falling liquid film which were examined by various investigators are summarized below:

1. Film thickness of a falling liquid film:

In the references (4,8,12,16,18,30,32,41,45) are the results of film thickness which were measured by the different investigators by various methods. Some of them are summarized in the following paragraphs.

In 1948 Kapitsa (18) solved the Navier-Stokes equation for a thin liquid falling film when waves were present on the surface and showed that the film thickness was 7% less than the value calculated for the film without waves.

In 1952 Dukler (8) designed a capacitometer to measure the film thickness of a vertical falling water film. His results showed that the measured film thickness was thicker than the value calculated from laminar flow equation at Reynolds numbers larger than 1080.

In 1960 Portalski (30) investigated the film characteristics of thirteen different liquids. The viscosity range of these thirteen liquids ranged from 0.602 cp. up to 64.4 cp. and the surface tension ranged from 21.7 dyne/cm. up to 66.2 dyne/cm. For the vertical falling water film, he found that when the Reynolds number was greater than 1130, the measured film thickness was larger than the value

calculated for smooth laminar flow, and when the Reynolds number was less than 990, the measured film thickness was smaller than the value calculated for smooth laminar flow. He also found that at the same volumetric flow rate the average value of the rippled film thickness was smaller than the corresponding value with no ripples. In order to suppress the ripples on the liquid surface, a suitable amount of surface active agent was added to the liquid.

2. The velocity distribution:

The parabolic velocity distribution is accepted by most investigators for the falling liquid film. Wilkes and Nedderman (43) measured the velocity distribution by means of stereoscopic photography of small air bubbles moving with the thin falling film. They found that the velocity distribution was very nearly parabolic at a Reynolds number of 4.

Both Kapitsa (18) and Benjamin (1) used the parabolic velocity distribution for the thin wavy falling film in their theoretical development of the characteristics of the waves. Dukler (8) used von Karman's universal velocity distribution to calculate the average film thickness of the falling liquid film. When an universal velocity distribution was used at $Re > 1080$ a better agreement with his experimental film thickness was obtained.

Grimley (12,36) observed suspended illuminated particles within the falling liquid film by a series of high-speed photographs to determine that the peak velocity

occurred not at the air interface but at some distance within the falling liquid film at a Reynolds number of 500.

3. Transitional Reynolds number:

The transitional Reynolds number for the vertical falling liquid film from laminar flow to turbulent flow was examined by several investigators. Dukler's (8) results showed that the transitional Reynolds number was 1080; Emmert's (10) found 1200; Portalski's (30,41) found 1160; Levich (24) indicated in his book that the transitional Reynolds number was 1500.

4. Critical Reynolds number:

The critical Reynolds number for the wave inception of the vertical falling water film was obtained by the following investigators:

Kirkbride (43)	Re=2
Friedman & Miller (11)	Re=6
Grimley (12)	Re=6
Binnie (3)	Re=4.4
Jackson (16)	Fr=1 (ie. Re=3)
Kapitsa (18)	Re=5.8

Benjamin (1) argued that theoretically there was no critical Reynolds number for wave inception. He suggested that the falling liquid film was always unstable. The amplitude of the waves became very small when the Reynolds number was fairly small and the wave length would become very large. Recent theoretical calculations of Whitaker (43a) support this idea.

Taibly and Portalski (39,40) made a complete study for the critical Reynolds number of wave inception, and gave the following conclusions: There was a critical Reynolds number for wave inception, and above the critical Reynolds number for wave inception, waves appeared over the entire column except for some distance at the top. The distance free of wave motion was a function of the Reynolds number of the liquid. Their experiments gave a critical Reynolds number of 7.0 for 82% glycerine water solution, and no wave appeared at Reynolds numbers of 4.6 and 6.4.

5. Wave properties:

Jepsen (17) used a capacitometer with a visicorder to record the wave properties of a falling liquid film at different inclination angles. He indicated in his thesis that both the frequency and amplitude of the waves were irregular and statistically random. Therefore, he used the Probit method to analyze the wave amplitude data and wave frequency data. He found that all his wave amplitude data could be represented by a logarithmic normal distribution and all the wave frequency data were correlated by a normal distribution. His results showed that the frequency varied from 6.0 to 16.0 $sec.^{-1}$ at inclination angles of 9°44', 18°27' and 25°42' with the water Reynolds number varying from 732 to 1834. The maximum wave amplitude was from 0.085 to 0.095 cm. at an inclination angle β of 9°44' with Reynolds number changing from 732 to 1834; from 0.06 to 0.11 cm. and β of 18°27' with Reynolds number of 732 to 1834, and from

0.05 to 0.10 cm. at β of 25°42' with Reynolds number of 732 to 1834.

6. Concentration profiles:

The fundamental description of diffusion into the liquid film would be contained in the concentration profile. The only measurements are those of Jepsen (17), who used a Mach-Zehnder interferometer to measure the concentration profile of a carbon dioxide-water system at an inclination angle of 9°44', with liquid Reynolds numbers from 732 to 1834.

These measurements determined the total diffusivity as a function of position within the film. He found diffusivities considerably higher than the molecular diffusivity and accordingly interpreted his results as eddy diffusivities. His results clearly establish a maximum diffusivity in the central region of the film. Unfortunately, previous work does not include concentration profiles accompanying mass transfer into a vertical film. The interferometer technique becomes unsuitable at higher angles because the films are too thin and the penetration of a diffusing species too shallow. If the relationship between eddy diffusivity and the inclination angles at various Reynolds numbers could be established, it should be possible to predict the relation between the eddy diffusivity and the Reynolds number for vertical films. Therefore, the primary purpose of this thesis was to determine concentration profiles at several inclination angles with various water Reynolds numbers to determine their effect upon the diffusivity. The

second purpose of this thesis was to develop the theoretical and extend the experimental study of the characteristics of the wave motion of the film.

CHAPTER III

THEORETICAL DEVELOPMENT

I. Formulation of the differential equation:

The basic theoretical description of the wave motion of a falling laminar film was that of Kapitsa (18) for the fluid film falling vertically (cf. Levich (24)). The analysis is presented here in some detail because a number of modifications were required to account for the effect of lower angles.

The coordinate system is shown in figure 1: β is the angle of inclination from the horizontal, h is the film thickness, h_o is the average film thickness, x is the distance along the plate, y is the distance perpendicular to the plate.

If there were a slow steady motion of the fluid in a gravitational field, then

$$\nu \frac{\partial^2 V_x}{\partial y^2} + g \sin \beta = 0$$

where g is the gravitational acceleration, ν the kinematic viscosity and V_x the x component of the velocity. The boundary conditions would be:

$$\text{when} \quad y = 0, \quad V_x = 0$$
$$y = h, \quad \frac{\partial V_x}{\partial y} = 0$$

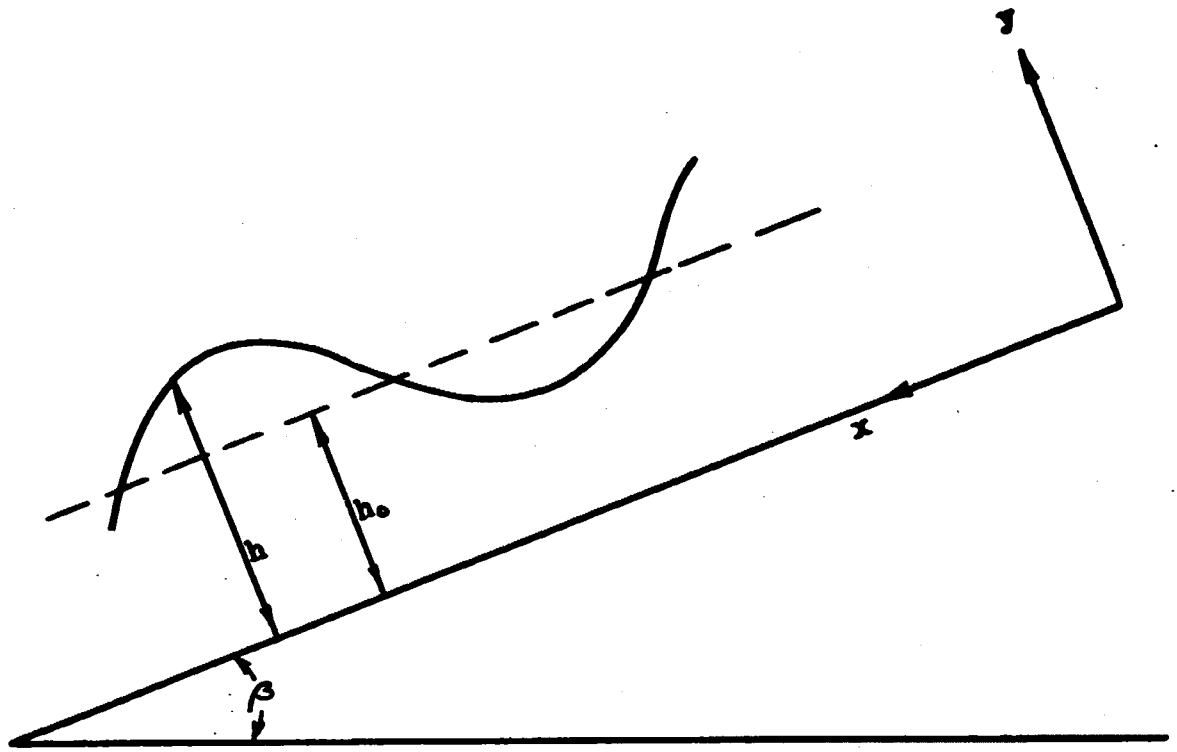

Figure 1. DIAGRAM OF FALLING FILM FLOW ON INCLINED PLANE.

The solution of this differential equation is

$$V_x = \frac{g \sin \beta}{\nu} y \left(h - \frac{y}{2} \right)$$

Let the average velocity be $\overline{V}$, then

$$\overline{V} = \frac{1}{h} \int_0^h V_x \, dy = \frac{g \sin \beta \, h^2}{3\nu} \qquad (1)$$

and

$$V_x = 3\overline{V} \left(\frac{y}{h} - \frac{y^2}{2h^2} \right) \qquad (2\text{-a})$$

For wave motion, the average velocity, $\overline{V}$, would be a function of x and time t. Therefore the above equation becomes

$$V_x = 3\overline{V}(x,t) \left(\frac{y}{h} - \frac{y^2}{2h^2} \right) \qquad (2\text{-b})$$

From the Navier-Stokes equation,

$$\frac{\partial V_x}{\partial t} + V_x \frac{\partial V_x}{\partial x} + V_y \frac{\partial V_x}{\partial y} = \frac{-1}{\rho} \frac{\partial P}{\partial x} + \nu \frac{\partial^2 V_x}{\partial y^2} + g \sin \beta \qquad (3)$$

where

$$P = (h - y)\rho g \cos \beta - \sigma \frac{\partial^2 h}{\partial x^2} \qquad (4)$$

$$V_y = - \int \frac{\partial V_x}{\partial x} \, dy \qquad (5)$$

where ρ is the density of fluid and σ is the surface tension. Substitution of equations 4 and 5 into equation 3 gives

$$\frac{\partial V_x}{\partial t} + V_x \frac{\partial V_x}{\partial x} - \int \frac{\partial V_x}{\partial x} dy \frac{\partial V_x}{\partial y} = -g \cos \beta \frac{\partial h}{\partial x} + \frac{\sigma}{\rho} \frac{\partial^3 h}{\partial x^3} + \nu \frac{\partial^2 V_x}{\partial y^2} + g \sin \beta \qquad (6)$$

Differentiating equation 2-b with respect to x:

$$\frac{\partial V_x}{\partial x} = 3 \frac{\partial \overline{V}}{\partial x} \left(\frac{y}{h} - \frac{y^2}{2h^2} \right)$$

Then,

$$\int \frac{\partial V_x}{\partial x} dy = \frac{\partial \overline{V}}{\partial x} \left(\frac{3}{2} \frac{y^2}{h} - \frac{y^3}{2h^2} \right)$$

Substituting the above equations into equation 6 gives

$$3 \left(\frac{y}{h} - \frac{y^2}{2h} \right) \frac{\partial \overline{V}}{\partial t} - \left(\frac{3}{2} \frac{y^2}{h} - \frac{y^3}{2h^2} \right) \frac{\partial \overline{V}}{\partial x} 3\overline{V} \left(\frac{1}{h} - \frac{y}{h^2} \right)$$

$$+ 9 \left(\frac{y}{h} - \frac{y^2}{2h^2} \right)^2 \overline{V} \frac{\partial \overline{V}}{\partial x}$$

$$= -g \cos \beta \frac{\partial h}{\partial x} + \frac{\sigma}{\rho} \frac{\partial^3 h}{\partial x^3} + \nu \frac{\partial^2 V_x}{\partial y^2} + g \sin \beta \qquad (7)$$

If one averages this equation over y, by integrating with respect to y and dividing by h:

$$\frac{\partial \overline{V}}{\partial t} + 0.9\overline{V} \frac{\partial \overline{V}}{\partial \xi_x} = -g \cos \beta \frac{\partial h}{\partial x} + \frac{\sigma}{\rho} \frac{\partial^3 h}{\partial x^3} + \nu \frac{\partial^2 V_x}{\partial y^2} + g \sin \beta \qquad (8)$$

Let

$$h = h_o(1 + \varphi) \qquad (9)$$

If the capillary waves are not damped, then the film thickness and average liquid velocity are functions of (x - ct), where c is the phase velocity of the wave. Then:

$$\frac{\partial h}{\partial t} = -c \frac{\partial h}{\partial x} \qquad (10)$$

and

$$\frac{\partial \overline{V}}{\partial t} = -c \frac{\partial \overline{V}}{\partial x} \qquad (11)$$

Differentiating equation 9 with respect to x

$$\frac{\partial h}{\partial x} = h_o \frac{\partial \varphi}{\partial x} \tag{12}$$

Equations 10 and 12 give

$$\frac{\partial h}{\partial t} = -ch_o \frac{\partial \varphi}{\partial x} \tag{13}$$

An integral mass balance is:

$$\frac{\partial}{\partial x} \int_o^h V_x \, dy + \frac{\partial h}{\partial t} = 0$$

or

$$\frac{\partial h}{\partial t} = - \frac{\partial (\overline{V}h)}{\partial x} \tag{14}$$

Substituting equations 9, 11 and 13 into equation 8:

$$-c \frac{\partial \overline{V}}{\partial x} + 0.9\overline{V} \frac{\partial \overline{V}}{\partial x} = -g \cos \beta \, h_o \frac{\partial \varphi}{\partial x} + \frac{\sigma}{\rho} h_o \frac{\partial^3 \varphi}{\partial x^3} - \nu \frac{3\overline{V}}{h^2} + g \sin \beta \tag{15}$$

Equations 10 and 14 give

$$\frac{\partial h}{\partial t} = - \frac{\partial (\overline{V}h)}{\partial x} = -c \frac{\partial h}{\partial x}$$

That is, $$\frac{\partial}{\partial x} [(c - \overline{V}) h_o (1 + \varphi)] = 0$$

$$(c - \overline{V}) h_o (1 + \varphi) = \text{constant} = h_o (c - V_o) \tag{16}$$

where V_o is the velocity at the average stream cross section h_o.

Let $$U = c - \overline{V}$$

From equation 16, $$Uh = U_o h_o = \text{constant}$$

If $$Q = \text{volumetric flow rate}$$

Then

$$Q = \frac{1}{t_o}\int_o^{t_o} \bar{V}h\,dt = \overline{\bar{V}h} = \overline{(c - U)h} = \overline{ch} - \overline{Uh} = ch_o - U_o h_o = V_o h_o \tag{17}$$

From equation 16, solve for $\bar{V}$,

$$\bar{V} = c - \frac{c - V_o}{1 + \varphi} = V_o + (c - V_o)\varphi - (c - V_o)\varphi^2 + \ldots \tag{18}$$

and differentiate with respect to x:

$$\frac{\partial \bar{V}}{\partial x} = \frac{c - V_o}{(1 + \varphi)^2}\frac{\partial \varphi}{\partial x} = (c - V_o)(1 - 2\varphi)\frac{\partial \varphi}{\partial x} + \ldots \tag{19}$$

Substituting equations 18 and 19 into equation 15 gives

$$(1 + \varphi)^3 \frac{\sigma h_o}{\rho}\frac{d^3\varphi}{dx^3} + \left[(c - V_o)(c - 0.9V_o)\left(1 + \frac{0.1c\varphi}{c - 0.9V_o}\right) - gh_o \cos\beta\,(1 + \varphi)^3\right]\frac{d\varphi}{dx} + g \sin\beta\,(1 + \varphi)^3 - \frac{3\nu V_o\left(1 + \frac{c}{V_o}\varphi\right)}{h_o^2} = 0 \tag{20-a}$$

If $\varphi^2 << 1$ equation 20-a becomes

$$(1 + 3\varphi)\left\{\frac{\sigma h_o}{\rho}\frac{d^3\varphi}{dx^3} + \left[(c - V_o)(c - 0.9V_o) - g\cos\beta\, h_o - (2.9c - 2.7V_o)(c - V_o)\varphi\right]\frac{d\varphi}{dx}\right\} + 3\left(g \sin\beta - \frac{\frac{c}{V_o}\nu V_o}{h_o^2}\right)\varphi + \left(g \sin\beta - \frac{3\nu V_o}{h_o^2}\right) = 0 \tag{20-b}$$

II. Solution of the differential equation: First an approximation to equation 20-b will be solved.

A. First modify the equation 20-b, so that it becomes a linear differential equation:

$$\frac{\sigma h_o}{\rho}\frac{d^3\varphi}{dx^3} + [(c - 0.9V_o)(c - V_o) - g\cos\beta\, h_o]\frac{d\varphi}{dx}$$

$$+ 3\left(g\sin\beta - \frac{\frac{c}{V_o}\nu V_o}{h_o^2}\right)\varphi + \left(g\sin\beta - \frac{3\nu V_o}{h_o^2}\right) = 0 \qquad (20\text{-}c)$$

By elementary procedures the solution of equation 20-c is

$$\varphi = Ae^{m_1 x} + \alpha e^{px}\sin(\kappa_1 x + B) \qquad (21\text{-}a)$$

where A, B, α, p, κ_1 and m_1 are all constants. In order to have a sinusoidal solution, both m_1 and p must be zero. Therefore,

$$\varphi = A + \alpha\sin(\kappa_1 x + B)$$

The boundary condition:

$$\int_0^\lambda \varphi\, dx = 0$$

requires that A be zero. The equation 21-a becomes

$$\varphi = \alpha\sin(Kx + B) \qquad (21\text{-}b)$$

If $\varphi = 0$, when $x = 0$, then $B = 0$, and,

$$\varphi = \alpha\sin Kx \qquad (21\text{-}c)$$

where

$$K = \left\{ \frac{\rho}{\sigma h_o} [(c - V_o)(c - 0.9V_o) - gh_o \cos \beta] \right\}^{\frac{1}{2}} \quad (22)$$

B. For a more accurate solution with a periodic character, let $c/V_o = 3$. Equation 20-b becomes

$$\frac{\sigma h_o}{\rho} \frac{d^3\varphi}{dx^3} + [(c - V_o)(c - 0.9V_o) - g \cos \beta \, h_o - (2.9c - 2.7V_o)(c - V_o)\varphi] \frac{d\varphi}{dx} + \left(g \sin \beta - \frac{3\nu V_o}{h_o^2} \right) = 0$$

or

$$\varphi''' + (K^2 - j\varphi)\varphi' + \text{constant} = 0 \quad (20\text{-d})$$

where

$$j = \frac{(2.9c - 2.7V_o)(c - V_o)}{\sigma h_o/\rho} \quad (23)$$

Equation 20-d is solved by the method of successive approximation. First, let

$$\varphi = \alpha \sin Kx$$

Equation ~~20~~ 24-d becomes,

$$\varphi''' + (K^2 - j\alpha \sin Kx)\varphi' + \text{constant} = 0 \quad (20\text{-e})$$

Try $\varphi = \alpha \sin Kx + B \cos 2Kx$

Find $B = \frac{\alpha^2 j}{12 K^2}$

Then, let

$$\varphi = \alpha \sin Kx + \frac{\alpha^2 j}{12 K^2} \cos 2Kx$$

Equation 20-d becomes,

$$\varphi''' + (K^2 - j\alpha \sin Kx + \frac{\alpha^3 j}{12\ K^2} \cos 2Kx)\varphi'$$

$$+ \text{constant} = 0$$

Try

$$\varphi = \alpha \sin Kx + \frac{\alpha^2 j}{12\ K^2} \cos 2Kx + \delta \sin 2Kx + \Gamma \sin 3Kx$$

and find $$\Gamma = - \frac{\alpha^3 j^2}{12 \times 16\ K^4}$$

Whence:

$$\varphi = \alpha \sin Kx + \frac{\alpha^2 j}{12\ K^2} \cos 2Kx - \frac{\alpha^3 j^2}{12 \times 16\ K^4} \sin 3Kx$$

$$+ \ . \ . \ . \qquad (24)$$

The numerical value of amplitude α is defined by the condition that in order to maintain an undamped regime, the energy dissipated by the wave motion must be balanced exactly by the work done by gravity. Thus:

$$- \frac{dE}{dt} = \mu \int_0^h \left(\frac{\partial V_x}{\partial y} \right)^2 dy = 3\mu \frac{\overline{V}^2}{h}$$

and over a wave length,

$$\frac{dE}{dt} = -3\mu \frac{1}{\lambda} \int_0^\lambda \frac{\overline{V}^2}{h} dx \qquad (25)$$

The average work done by gravity is

$$W = \rho g \sin \beta\ Q \qquad (26)$$

From equations 25 and 26, the following equations are obtained.

$$\rho g \sin\beta\, Q = 3\mu \frac{1}{\lambda}\int_0^{\lambda} \frac{\left(1 + \frac{c}{V_o}\varphi\right)^2 V_o^2}{h_o(1+\varphi)^3}\,dx = 3\mu \frac{V_o^2}{h_o}\Phi = 3\mu \frac{Q^2}{h_o^3}\Phi$$

where

$$\Phi = \frac{1}{\lambda}\int_0^{\lambda} \frac{\left(1 + \frac{c}{V_o}\varphi\right)^2}{(1+\varphi)^3}\,dx \qquad (27)$$

and

$$h_o^3 = \frac{3\nu Q}{g \sin\beta}\Phi \qquad (28)$$

As mentioned by Kapitsa, the minimum Φ corresponds to the smallest film thickness with which the balance between energy dissipated and work done by gravity can be maintained. This is the most stable flow. The minimum value of Φ is obtained as follows:

$$\frac{\left(1 + \frac{c}{V_o}\varphi\right)^2}{(1+\varphi)^3} = \frac{1}{(1+\varphi)^3} + \frac{2\frac{c}{V_o}\varphi}{(1+\varphi)^3} + \frac{\frac{c^2}{V_o^2}\varphi^2}{(1+\varphi)^3}$$

$$= (1 - 3\varphi + 6\varphi^2 - 10\varphi^3 + \ldots)$$

$$+ 2\frac{c}{V_o}(\varphi - 3\varphi^2 + 6\varphi^3 - \ldots)$$

$$+ \frac{c^2}{V_o^2}(\varphi^2 - 3\varphi^3 + 6\varphi^4 - \ldots) \qquad (29)$$

as long as $\varphi < 1$, the equation 29 is convergent. Since α and c/V_o are independent of x, equation 27 becomes,

$$\Phi = \frac{1}{\lambda}\int_0^{\lambda}(1 - 3\varphi + 6\varphi^2 - 10\varphi^3 + \ldots)dx + \frac{2c}{V_o}\frac{1}{\lambda}\int_0^{\lambda}(\varphi - 3\varphi^2 + 6\varphi^3 - \ldots)dx$$

$$+ \frac{c^2}{V_o^2}\frac{1}{\lambda}\int_0^{\lambda}(\varphi^2 - 3\varphi^3 + 6\varphi^4 - \ldots)dx \qquad (30)$$

From equation 24

$$\varphi = \alpha \sin Kx + \frac{\alpha^2 j}{12 K^2} \cos 2Kx \ . \ . \ .$$

and

$$K\lambda = 2\pi$$

After integration, equation 30 becomes,

$$\begin{aligned} \Phi = 1 + 3\alpha^2 + (3R^2 + 7.5R + 5.625)\alpha^4 + \ . \ . \ . \\ - \frac{c}{V_o} [3\alpha^2 + (3R^2 + 9R + 7.5)\alpha^4 + \ . \ . \ . \ ] \\ + \frac{c^2}{V_o^2} [0.5\alpha^2 + (0.5R^2 + 2.25R + 2.25)\alpha^4 + \ . \ . \ . \ ] \end{aligned} \tag{31}$$

where

$$R = \frac{j}{12 K^2} \tag{32}$$

Differentiating equation 31 with respect to α^2

$$\begin{aligned} \frac{\partial \Phi}{\partial(\alpha^2)} = 3 + (6R^2 + 15R + 11.25)\alpha^2 + \ . \ . \ . \\ - [3 + (6R^2 + 18R + 15)\alpha^2 + \ . \ . \ .] \frac{c}{V_o} \\ + [0.5 + (R^2 + 4.5R + 4.5)\alpha^2 + \ . \ . \ .] \frac{c^2}{V_o^2} \end{aligned} \tag{33}$$

In order to find the minimum value of Φ, for a given value of c/V_o equation 33 must equal zero. More complete forms of equations 31 and 33 were put in Appendix I. The minimum value of Φ is found by the following steps. A value of α_1

was assumed and the value $(c/V_o)_1$, calculated from equation 33. These were substituted into equation 31 to obtain Φ_1. These steps were repeated, assuming different value of α, to calculate values c/V_o and Φ. A plot of Φ against α located the minimum value of Φ and the corresponding value of α and c/V_o. The values of Φ, α, and c/V_o were computed as functions of β and Re, and listed in Table 1.

TABLE 1

$\beta = 5°$	Re	435	1144	1917
	α	0.603	0.615	0.620
	c/V_o	1.595	1.570	1.580
	Φ	0.675	0.668	0.662
$\beta = 15°$	Re	435	1144	1917
	α	0.605	0.615	0.620
	c/V_o	1.590	1.595	1.590
	Φ	0.676	0.673	0.671
$\beta = 25°$	Re	435	1144	1917
	α	0.610	0.620	0.620
	c/V_o	1.600	1.585	1.585
	Φ	0.676	0.674	0.674

Following the procedure of Levich and Portalski the effect of the waves on the interfacial area can be computed. Let

ΔS = percentage increase of interfacial area due to waves.

Since $$y = h = h_o(1 + \varphi)$$

then, $$y' = h_o\varphi'$$

and, $$\Delta S = \frac{\int_0^{\lambda} \sqrt{1 + y'^2}\, dx - \lambda}{\lambda} \times 100\%$$

From equation 24:

$$y = h_o(1 + \varphi) = h_o\left(1 + \alpha \sin Kx + \frac{a^2 j}{12 K^2} \cos 2Kx - \ldots\right)$$

$$y' = h_o\left(\alpha K \cos Kx - \frac{a^2 j}{6K} \sin 2Kx - \ldots\right) = G \cos Kx - H \sin 2Kx \tag{34}$$

where $$G = h_o \alpha K \tag{35-a}$$

$$H = h_o \frac{a^2 j}{6K} \tag{35-b}$$

If $$a < 1$$

then $$(1 + a)^{1/2} = 1 + \frac{a}{2} - \frac{a^2}{8} + \frac{a^3}{16} \ldots$$

It was proved (see Appendix H) that $y'^2 < 1$. Hence

$$\Delta S = \frac{\int_o^\lambda \left(1 + \frac{y'^2}{2} - \frac{y'^4}{8} + \frac{y'^6}{16} - \ldots\right) dx - \lambda}{\lambda} \times 100\%$$

$$= \frac{1}{\lambda} \int_o^\lambda \left(\frac{y'^2}{2} - \frac{y'^4}{8} + \frac{y'^6}{16} - \ldots\right) dx \times 100\% \tag{36}$$

Substitute equation 34 into equation 36, and integration gives

$$\Delta S = \frac{1}{4}(G^2 + H^2) - \frac{3}{64}(G^2 + H^2)^2 + \frac{5}{256}(G^2 + H^2)^3 - \ldots \tag{37}$$

Values of ΔS calculated from equation 37 are presented in the discussion of the results of the experimentally measured wave properties.

The film thickness of a turbulent falling liquid film can be calculated following Dukler and Portalski. Dukler

used the universal velocity distribution of pipe flow for the turbulent falling liquid film to calculate the film thickness. The procedure was as follows:

Let $$U^+ = \frac{V_x}{U^*} \tag{38}$$

$$y^+ = \frac{U^*\rho y}{\mu} \tag{39}$$

From von Karman's analysis, the velocity distribution was:

$$U^+ = y^+ \qquad 0 < y^+ < 5 \tag{40}$$

$$U^+ = -3.05 + 5.0 \ln y^+ \qquad 5 < y^+ < 30 \tag{41}$$

$$U^+ = 5.5 + 2.5 \ln y^+ \qquad y^+ \gtrless 30 \tag{42}$$

The mass flow rate per unit width, Γ, would be

$$\Gamma = \mu \int_0^{\eta} U^+ \, dy^+ \tag{43}$$

Substituting equations 40, 41 and 42 into equation 43 gives

$$\frac{\Gamma}{\mu} = \int_0^5 y^+ \, dy^+ + \int_5^{30} (-3.05 + 5.0 \ln y^+) dy^+ + \int_{30}^{\eta} (5.5 + 2.5 \ln y^+) dy^+$$

$$= + 3.0\eta + 2.5\eta \ln \eta - 64 \tag{44}$$

Equation 39 gives $$\eta = \frac{U^*\rho h_o}{\mu} \tag{45}$$

where $$U^* = \sqrt{\frac{\tau_o g}{\rho}} \tag{46}$$

and the wall shear $$\tau_o = h_o \rho \sin \beta \tag{47}$$

Substituting equations 46 and 47 into equation 45 gives

$$\eta = \frac{U^* \rho h_o}{\mu} = \frac{\rho \sqrt{g \sin \beta}\, h_o^{3/2}}{\mu} \qquad (48)$$

From equation 48 $$h_o^3 = \frac{\eta^2 \nu^2}{g \sin \beta} \qquad (49)$$

For a given flow rate, the value of η could be found from equation 44, and h_o calculated from equation 49. Comparison of equation 49 and equation 28 gives

$$\Phi = \frac{\eta^2 \mu}{3\rho Q} = \frac{\eta^2}{3\frac{\Gamma}{\mu}} \qquad (50)$$

~~Both equations 49 and 50 are~~ plotted in figure 2.

Portalski (30-a) used his experimental value to modify equations 40, 41 and 42. The Φ can be calculated from Portalski's modified equation for the velocity distribution in a falling water film, and the results are plotted in figure 2.

Equation 28 gives $$h_o^3 \sin \beta = \frac{3\nu Q}{g} \Phi \qquad (28\text{-a})$$

and equation 49 gives $$h_o^3 \sin \beta = \frac{\eta^2 \nu^2}{g} \qquad (49)$$

At a constant Reynolds number, from Dukler's method, only one value of η could be obtained from equation 44. This means that η would be independent of the inclination angle β, and $h_o^3 \sin \beta$ = constant, when Re = constant. In the course of the present work, Φ was found to be a function of Reynolds number and inclination angle, and, therefore, Dukler's method had to be modified. More detailed discussion on the relation

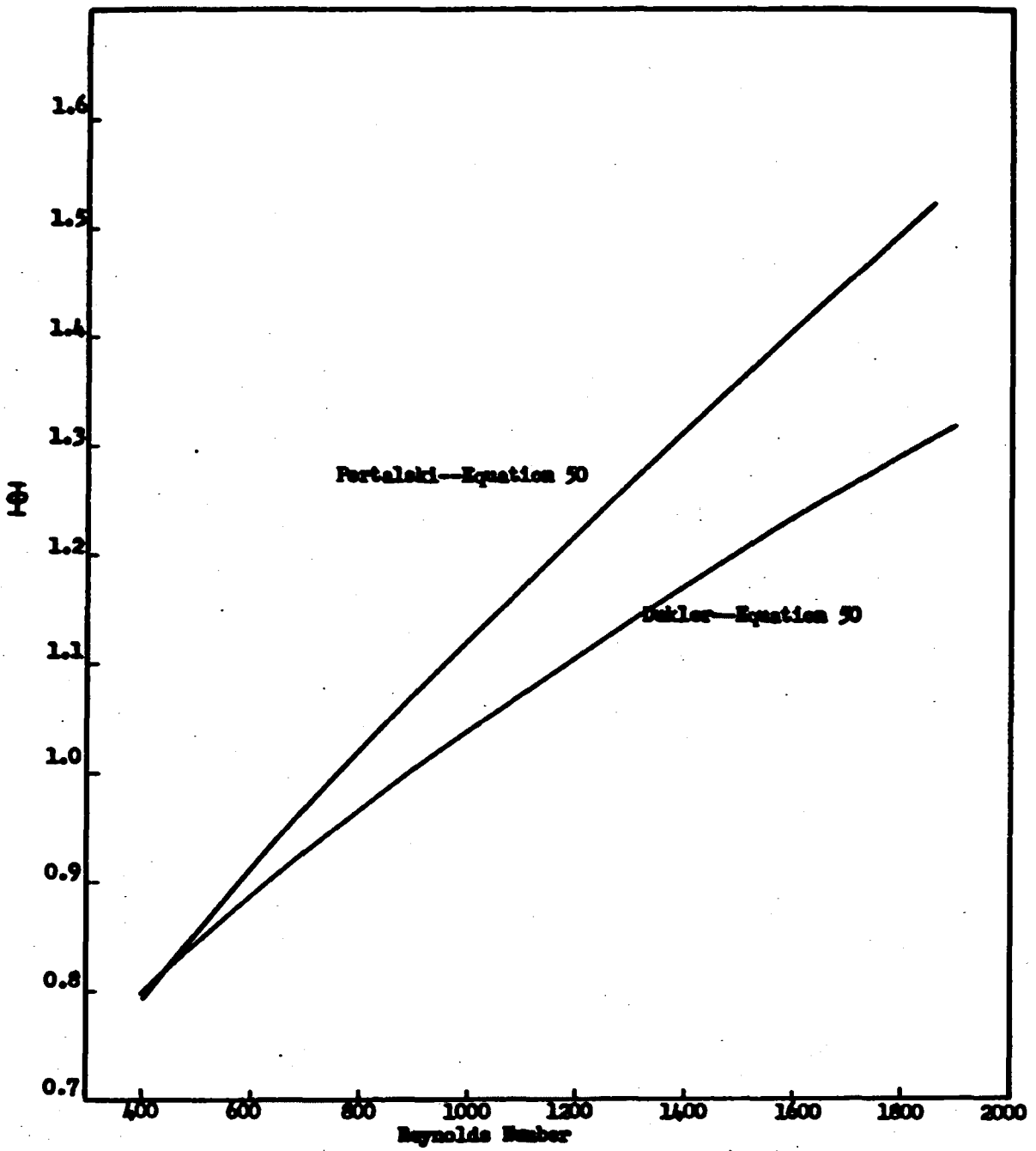

Figure 2. CORRECTION FACTOR FOR THE FILM THICKNESS OF WAVY FLOW.

between ϕ and the flow rate and inclination angle is given in Chapter V.

CHAPTER IV

EXPERIMENTAL WORK

The experimental measurements of wave properties and the diffusion of carbon dioxide into a falling water film were made in a cell constructed of aluminum plates 0.438 inches thick, 2.95 inches wide, 35.33 inches long. An optically flat glass plate 0.0625 inches thick, 2.95 inches wide, 34.83 inches long was cemented to the bottom. The two sides of the cell were optically flat glass windows with a dimension of 1 inch wide, 0.4 inches thick, 36 inches long. The gas and liquid first entered into two separated calming chambers located at the end of the diffusion cell, before entering the diffusion cell. The inlet ports for gas and liquid were sufficiently large (1/4 inches x 2.95 inches) to provide for smooth flow of the fluids. The diffusion process started after the calming chambers. Figure 3C is a drawing of the cell.

Temperature and flow control were provided for both gas and liquid streams. The cell could be tilted from zero to 35° from the horizontal. Details of design may be found in the thesis of Jepsen (17). A flow chart of the experimental apparatus is shown in figure 3A.B

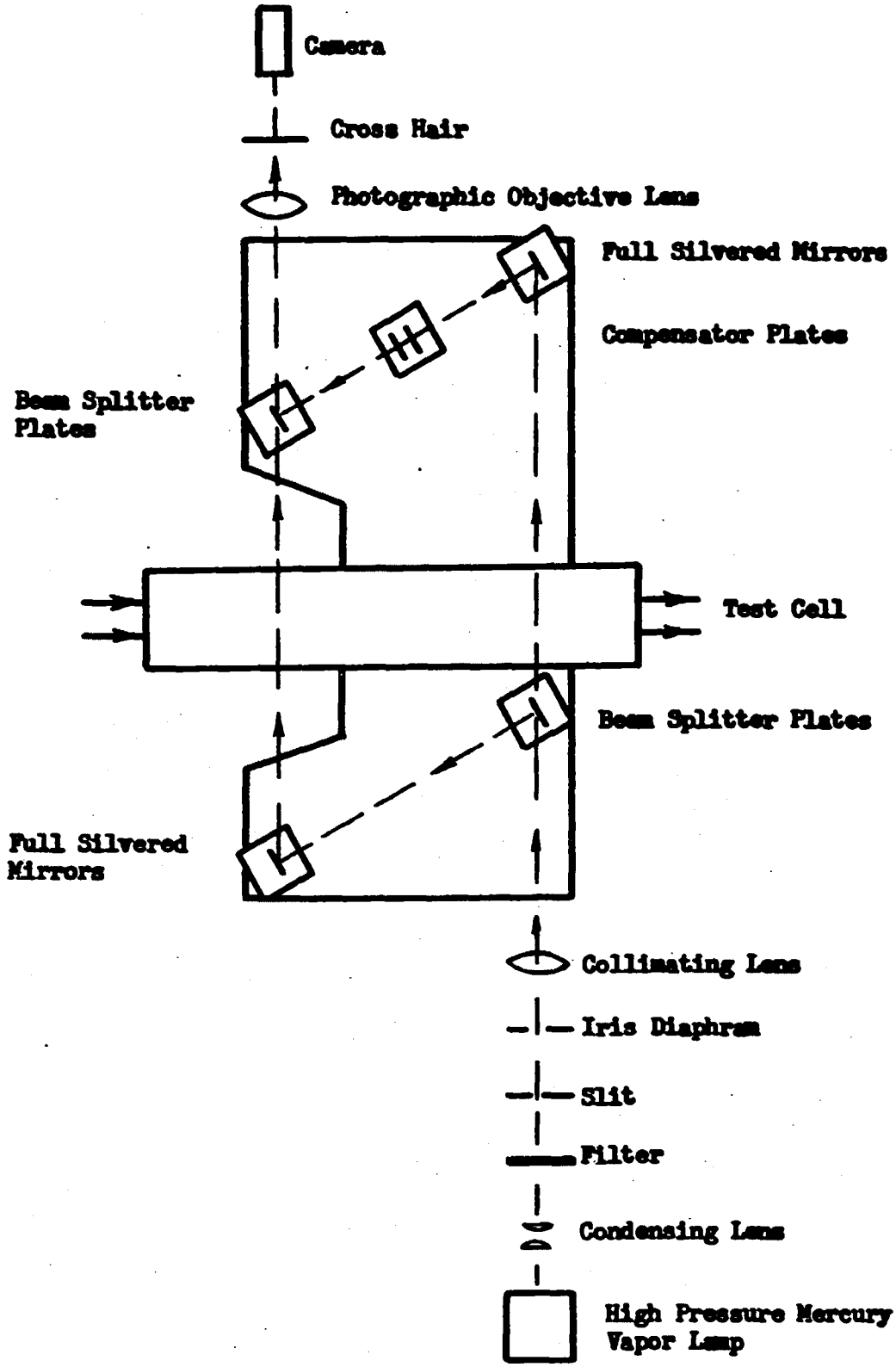

Figure 3A. DIAGRAM OF INTERFEROMETER ASSEMBLY

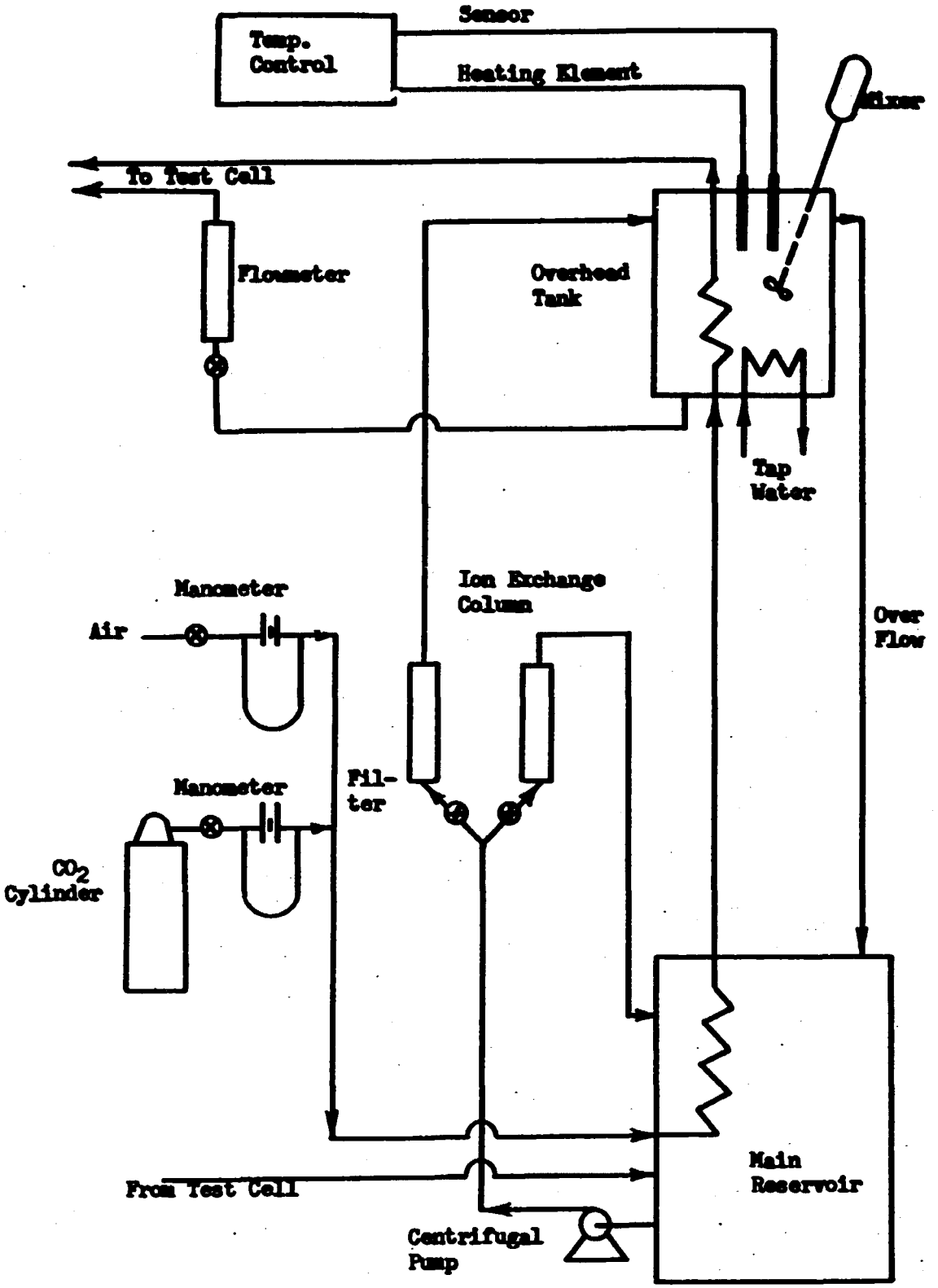

Figure 3B. FLOW CHART OF EXPERIMENTAL APPARATUS.

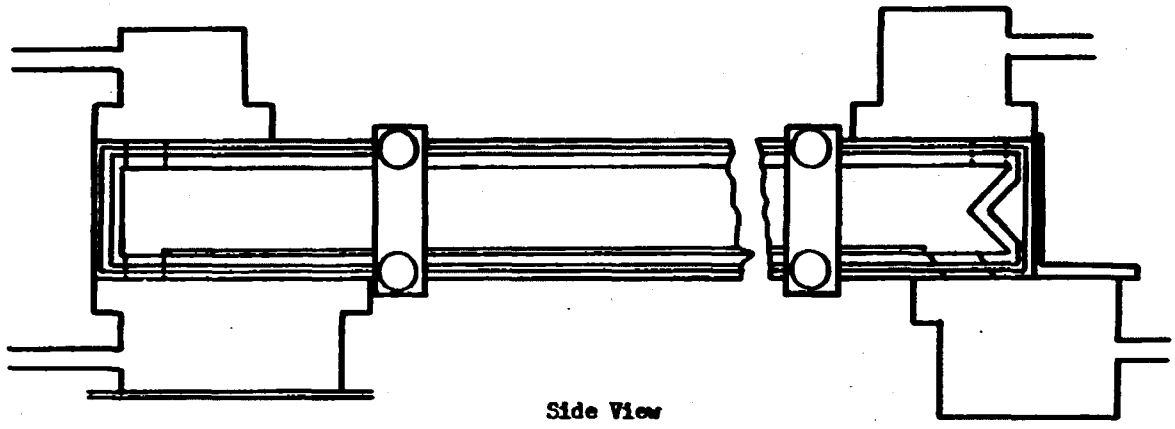

Side View

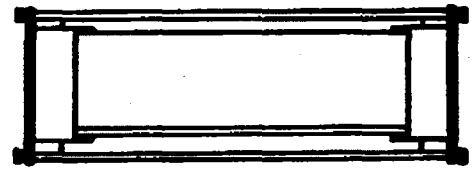

End View

Figure 3C. DIAGRAM OF TEST CELL.

There were three phases to the experimental studies. The first phase was concerned with the determination of the wave properties of the falling water film using a capacitometer. This particular device was first designed by Dukler (8) and later modified by Jepsen (17). The output of the capacitometer was recorded by a Minneapolis-Honeywell Model 906c Visicorder with a mechanically damped galvanometer with a maximum frequency response 270 cps ± 10%. The capacitance to be measured was between the liquid surface and the metal probe. The size of the probes used were 2 mm. by 5.5 mm. and 6 mm. by 8 mm. Each probe was fixed to a micrometer attached to the top of the cell. The bottom of the cell was an optically flat glass plate, so that the micrometer reading of the bottom was obtained within ± 0.0002 inch and the measurement of the film thickness of a quiet pool was within ± 0.0005 inch. Tap water was used in these studies because of the very low conductivity of the distilled water used in the diffusion studies. Because of the high conductivity of the tap water, the capacitance measured was between the surface of the water and the probe, and was proportional to the dielectric constant of the gas above the water surface and the area of the probe, and inversely proportional to the air gap. The dielectric constant and the area of the probe both were constant in this case, so a calibration curve could be obtained by plotting the air gap measured by the micrometer against the capacitance or visicorder reading.

Figures 4, 5, and 6 show that the calibration was

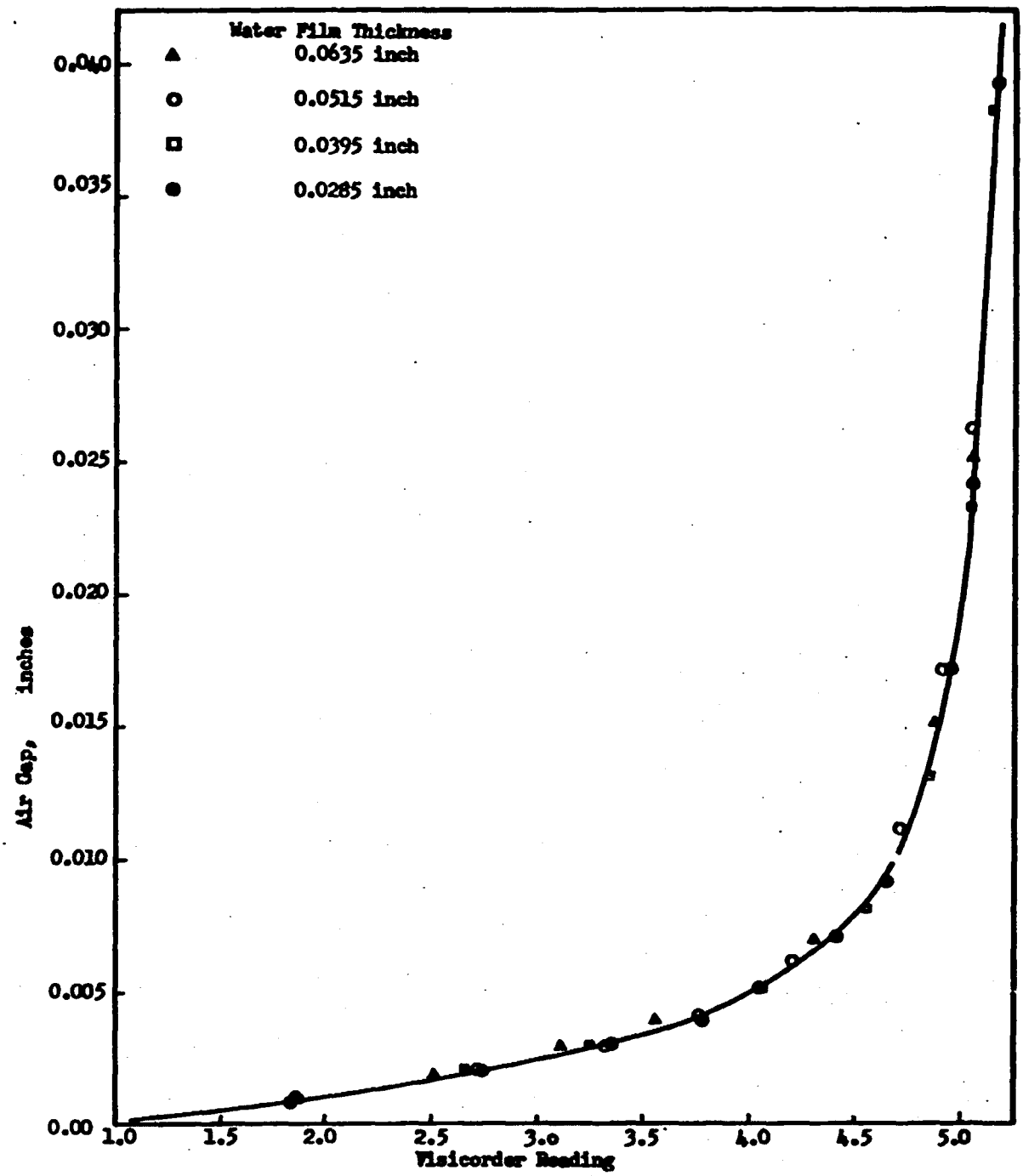

Figure 4. CALIBRATION CURVE

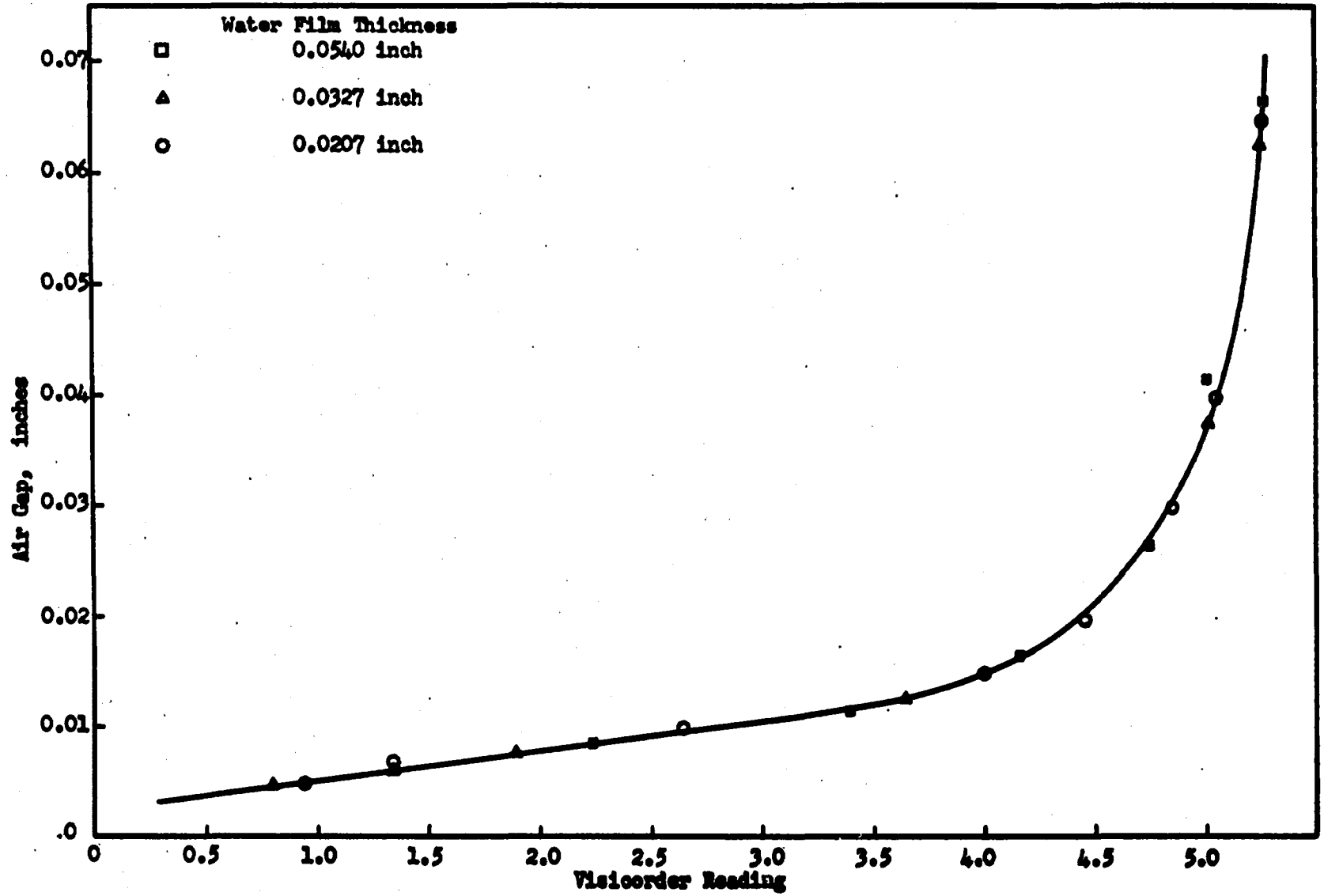

Figure 5. CALIBRATION CURVE

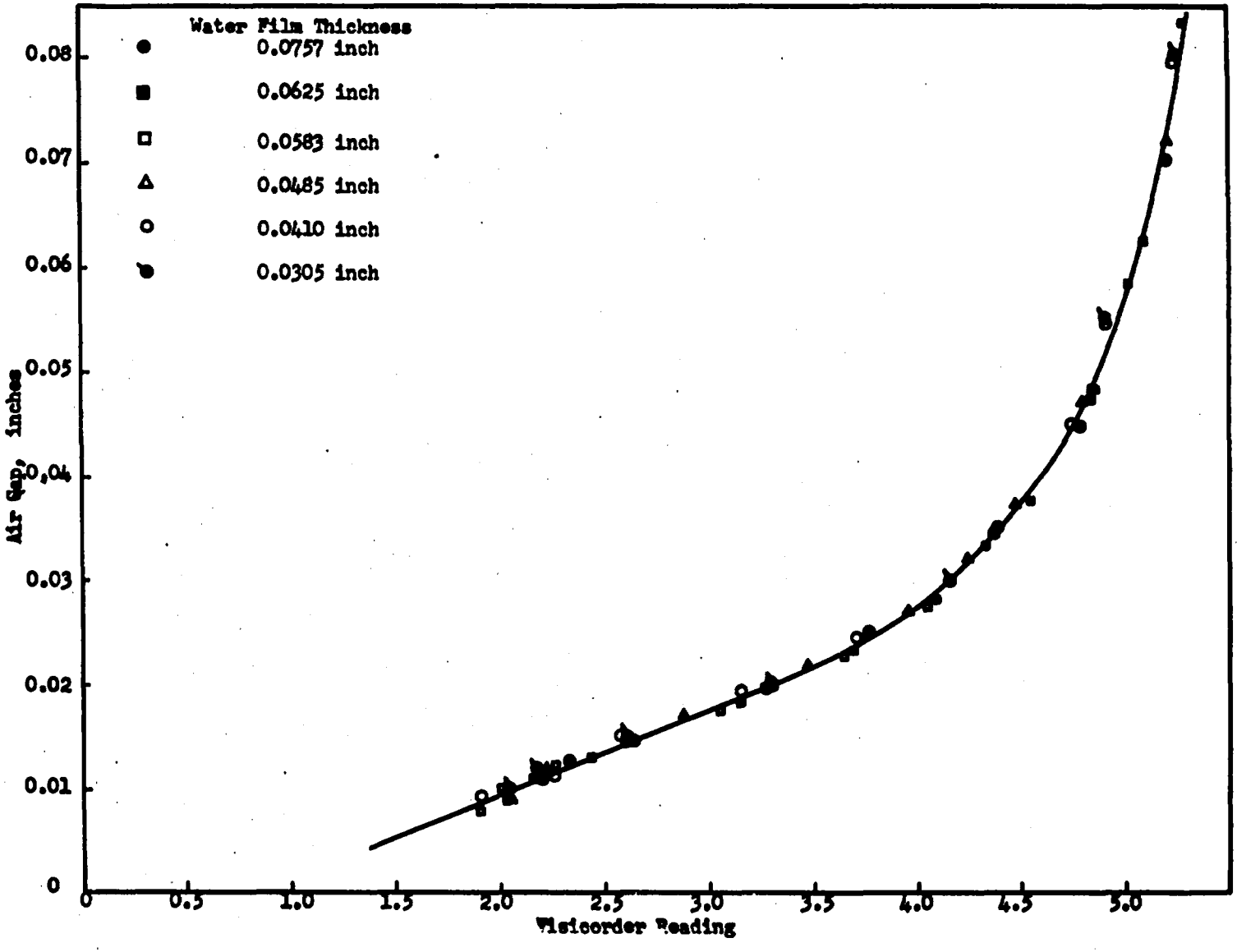

Figure 6. CALIBRATION CURVE

independent of the water film thickness, as the water film thickness changed from 0.02 inch to 0.08 inch and the air gap changed from 0.005 to 0.08 inch. For all the water film thicknesses, the measured air gaps deviated from each other less than ± 0.0005 inch for the same value of visicorder reading.

The capacitometer was always adjusted to give maximum response. The visicorder gave a reading from 1.0 to 5.0 on its scale when the air gap changed from 0.005 to 0.05 inch, and there was a linear relationship between the air gap and visicorder reading over a substantial range, and the wave data taken within this range. The wave properties of a falling water film were obtained by attaching a probe to the top of the cell at 25 inches from the water inlet. At that point the water film thickness was independent of the distance down the cell (see Appendix E). The larger probe was used to measure film thickness and the smaller probe was used to measure frequency. In both cases, the probe was fixed tightly to the top of the cell and was then adjusted to have an average air gap from 0.015 to 0.035 inch. The size of the air gap used depended upon the inclination angle and the Reynolds number of the flow rate. In order to get the best results, the air gap was adjusted as small as possible. The wave properties of a falling water film were investigated at Reynolds numbers ranging from 435 to 1917 with inclination angles equal to 5°, 15° and 25°. The water temperature was 24°C.

The wave velocity was measured by means of two copper probes, 1 mm. by 2 mm. The two probes were set 20.95 inches apart and either probe could be individually connected to the capacitometer by a switch.

When a sudden change in visicorder reading indicated that a wave had touched the first probe, the circuit was switched to the second probe downstream. The wave velocity was measured by the distance between the probe contacts indicated by wave trace, and the chart speed. For each water flow rate, the above measurement was repeated at least five times, and the deviation of these measurements was less than ± 4%.

The following procedures were used to measure the wave properties of a falling water film. The cell was first set horizontally using a cathetometer. One of the probes was attached 25 inches from the water inlet and the capacitometer and the visicorder adjusted to give maximum sensitivity.

The probe was set with an air gap of 0.01 to 0.03 inch from a quiet water surface and the variable capacitor of the capacitometer was adjusted until a maximum sensitivity on the microammeter was obtained. The galvanometer zero of the visicorder was set to give a reading from 1.0 to 5.0 when the air gap varied from 0.005 to 0.05 inch. A large air gap of 0.2 inch was used as a reference point and the corresponding visicorder reading recorded. The calibration data were obtained as values of visicorder reading, corresponding to air gap distances from about 0.1 inch down to 0.01 using the

6 mm. by 8 mm. probe and air gaps from 0.05 to 0.001 inch, were measured with the 2 mm. by 5 mm. probe.

The calibration was repeated at least once each day and whenever the cell was tilted to a new inclination angle. The angle of the cell was determined by measurements with a cathetometer. Before each wave trace, the probe was returned to an air gap of 0.2 inch and the visicorder reading recorded. The probe was then placed as close to the water surface as possible, and the wave trace recorded.

The second part of the experimental work was to determine the concentration profile in the falling water film. The primary apparatus was the Mach-Zehnder interferometer, whose design and utilization is completely described in Jepsen's thesis (17). General information about the measurement of the diffusion concentration profiles by means of an interferometer has been presented in Lin's thesis (26) and in Harvey's thesis (14). Harvey showed that the change in the refractive index of a carbon dioxide-water solution was directly proportional to the concentration of the carbon dioxide. The shift of the fringes of the interference pattern was, therefore, proportional to the refractive index of the solution, and the concentration of carbon dioxide in the solution could be obtained from the fringe shift of the interference pattern. Fringe shift is defined as the distance a fringe moves divided by the length of the fringe spacing. The concentration profile was given by the shape of an interference fringe, and relative values computed directly

from:

$$\frac{C(y)}{C_s} = \frac{N(y)}{N_s}$$

where y is the distance into the film, C(y) is the concentration profile, C_s is the saturation concentration, N_s is the total number of fringe spacings (fringe shifts) a fringe moved as a solution was completely saturated, and N(y) was the number of fringe spacings a fringe was shifted at y. Since the saturation concentration depends upon the temperature of the solution, N_s also is a function of temperature. For this study at 24°C, N_s was 2.847.

Jepsen concluded that there was a pressure effect on the cell windows due to fluctuations in the gas phase pressure. Changes in liquid loading would give similar results but for either cause it was necessary to brace the cell windows from the outside. This was accomplished by attaching 1/4 inch thick, 3/4 inch wide, 2 inch long plexiglass plates outside each cell window by means of 1/4 inch by 5 inch steel bolts that extended laterally across the top and bottom of the cell. The windows were clamped in this manner both immediately upstream and downstream from the field of view.

The light source used in this experiment was a 1000 watt, D.C. high pressure mercury vapor lamp. Only half of the light reduced by the green filter can be collected by the camera, and the final light intensity was very weak. The patterns were photographed using Kodak spectroscopic plates

type 1-D, developed 5 minutes in Kodak developer D-19. Since the surface velocity of the falling water film was 70 cm. per sec. at an inclination angle of 15° and Reynolds number of 1917, it was necessary to use very short exposure times to stop the surface phenomena. The light intensity had to be as high as possible for short exposures and Jepsen's apparatus was modified to permit this. A larger objective lens was obtained and the distance between the lens and the negative plate reduced. The shutter speed possible for these measurements was increased to 1/125 sec., using a camera with a 4.8 cm. focal length lens. The distance between the lens and the plate was one foot. A temperature control system was placed in the overhead tank. The temperature control system is also described in Jepsen's thesis (17). The room temperature was controlled to 24° ± 2°C. In order to make sure there was no temperature effect on the system, the air-water system was first passed through the cell. If there were a temperature difference between the gas phase and the liquid phase or between the liquid and the diffusion cell, the fringes produced by the interferometer would not be straight.

At each cell position, for each water flow rate, four photographs were taken; one for the air-water system and three for the CO_2-water system. Two additional photographs were taken showing a cross hair and the probe which was set a known distance from the bottom. The purpose of the last two photographs was to find the exact location of the bottom

of the film.

Before starting to take the concentration profile data, the air-water system was passed through the diffusion cell to check for straight fringes, indicating no temperature effects on the system. The carbon dioxide was admitted to the cell and when the fringes no longer changed shape or position three photographs were taken. Finally air was readmitted and when the fringes became vertical, another reference photograph was taken.

In the third part of the experimental work the average CO_2 concentration in the falling water film, at each cell position, was determined by titration. The sample at each cell position was collected by flooding the downstream portion of the cell up to the desired position. After maintaining this water level for 3 to 6 minutes, a 250 ml. sample was collected in a flask and sealed by a rubber plug. One-fifth of the sample was taken from the flask by syringe for titration. The CO_2 in the sample was precipitated by excess NaOH and $BaCl_2$ solution and then back titrated with HCl solution using phenolphthalein as indicator. The details of the titration are in Appendix D. These measurements were repeated at least five times, and the results deviated less than $\pm$ 5%. This deviation was acceptable for the procedures used in collecting the sample and performing the titration.

All diffusion studies were made with pure carbon dioxide absorbing into distilled, deionized water.

CHAPTER V

HYDROMECHANICAL RESULTS AND DISCUSSION

The wave data consisted of visicorder traces for various flows at several angles of inclination. These traces were combined with their calibration curves to obtain the average film thickness, average crest and trough height, frequency and wave velocity, A typical wave trace is shown in figure 7.

All the film thickness and frequency data were repeated at least five separate times during the entire experimental study extending over 8 months. In all cases the variation of the measured properties was less than 10%.

Film Thickness

The film thickness of the falling water film was measured at angles of 5°, 15° and 25° for Reynolds numbers from 435 to 1917. Since the micrometer reading of the bottom and of the probe were known, the average film thickness was the difference between the micrometer reading for the bottom plate of the cell and sum of the average air gap and probe position. The average air gap was determined from the calibration curve by using average visicorder reading of the surface of the falling water film. Two different methods

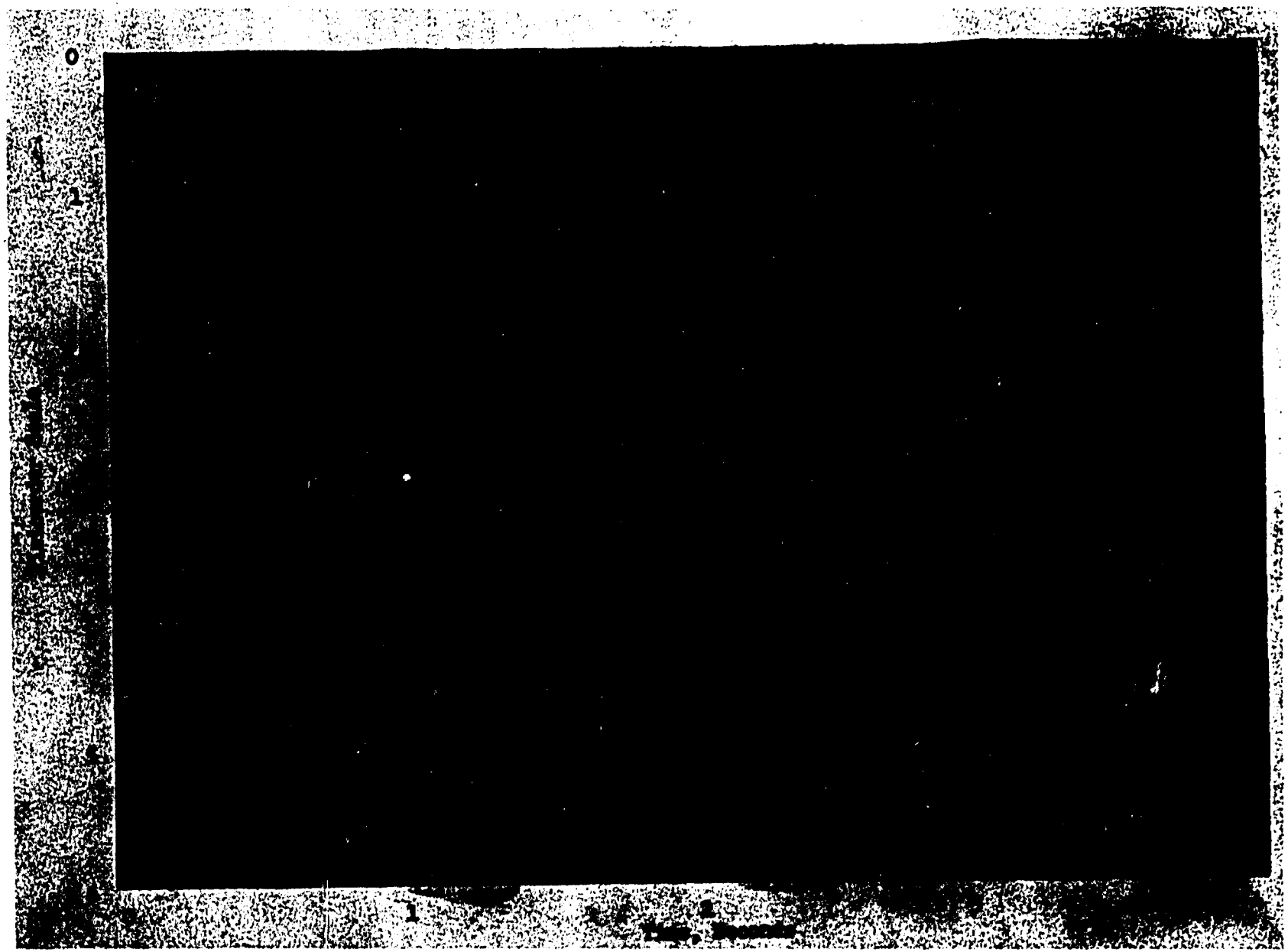

Figure 7. WAVE TRACE.

were used to find the average visicorder reading of the water surface. First, since the wave traces were taken within the linear range of the calibration curve, the average visicorder reading of the wave trace could be found by integration of the area under the curve, divided by the length of the wave trace. Second, the air gaps at each crest and trough were obtained by means of the calibration curve. Then, assuming the wave was triangular in shape, the average air gap was found from the arithmetic mean of the air gap at each crest and trough. The average film thicknesses found by these two methods differed by about 5%. The results of the average film thickness are plotted in figures 8 to 12. Each set of symbols refers to a particular series of determinations for several angles and given date.

The film thickness calculated from Jeffrey's laminar flow equation is different from the film thickness calculated by Dukler's method. If the average film thickness is plotted against the Reynolds number, it is easy to see that the slopes of these lines are also different. Referring to figure 10, the laminar (curve 2) and Kapitsa (curve 3) have constant slope, and the empirical curve of Dukler (curve 1) and equation 28 (curve 4) have variable slope. The curve of Dukler (curve 1) has the biggest slope. At constant Reynolds number, the film thickness of Kapitsa (curve 3) is 7% less than laminar (curve 2); and equation 28 is about 15% less than laminar (curve 2).

By comparing the experimental value of the film

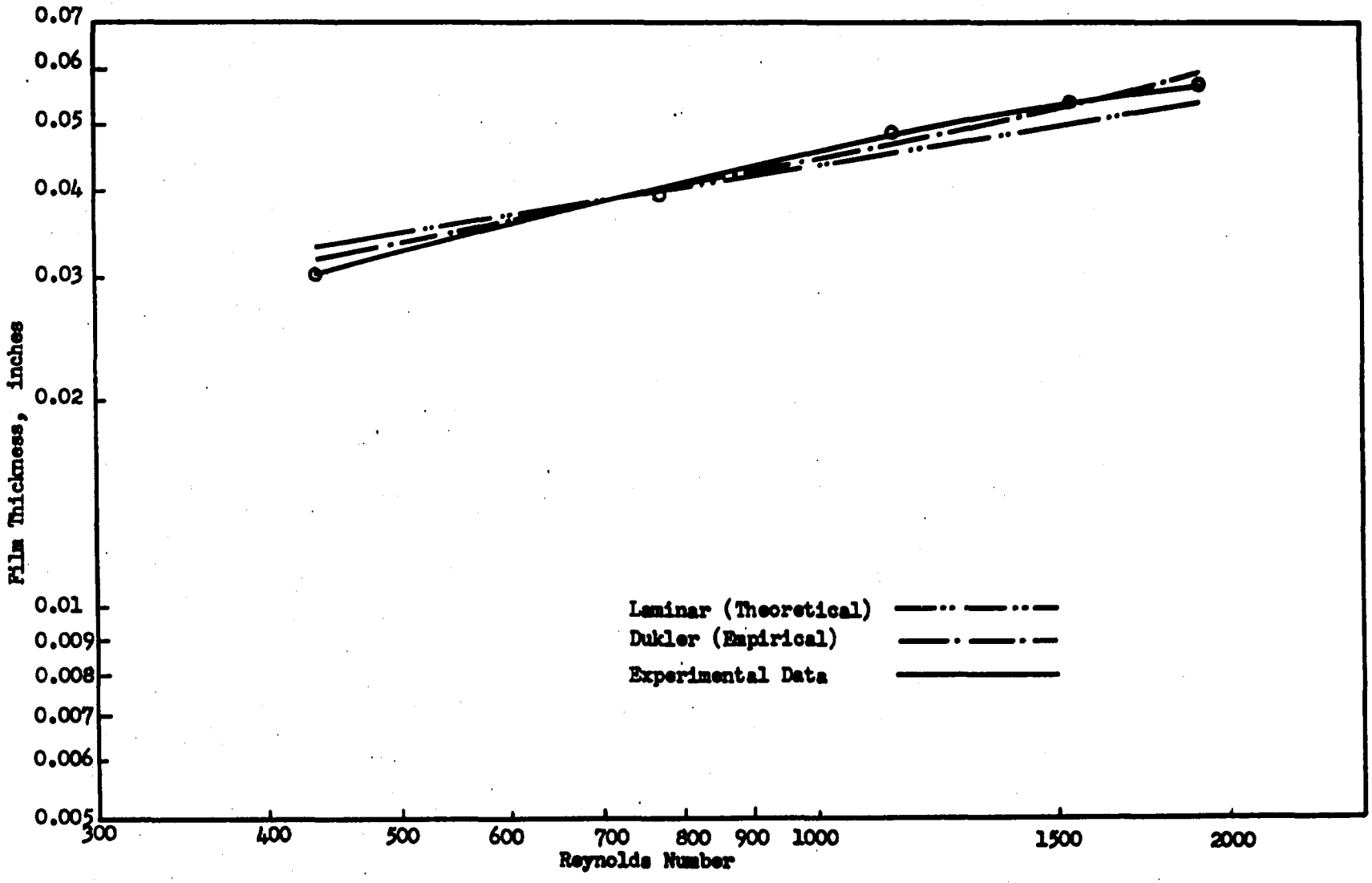

Figure 8. FILM THICKNESS AS A FUNCTION OF REYNOLDS NUMBER FOR AN ANGLE OF INCLINATION OF $2^{\circ}23'$.

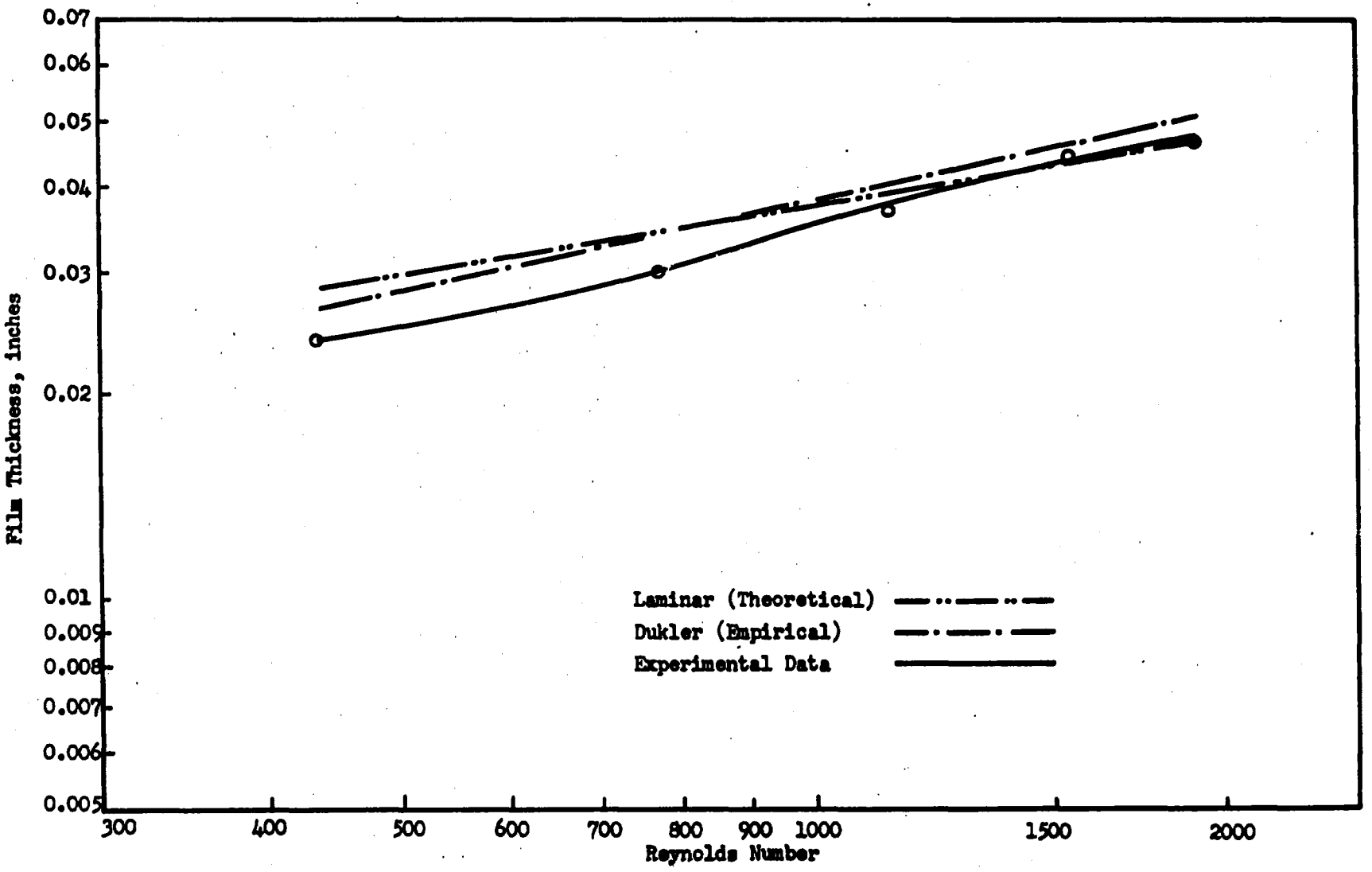

Figure 9. FILM THICKNESS AS A FUNCTION OF REYNOLDS NUMBER FOR AN ANGLE OF INCLINATION OF 4°5'.

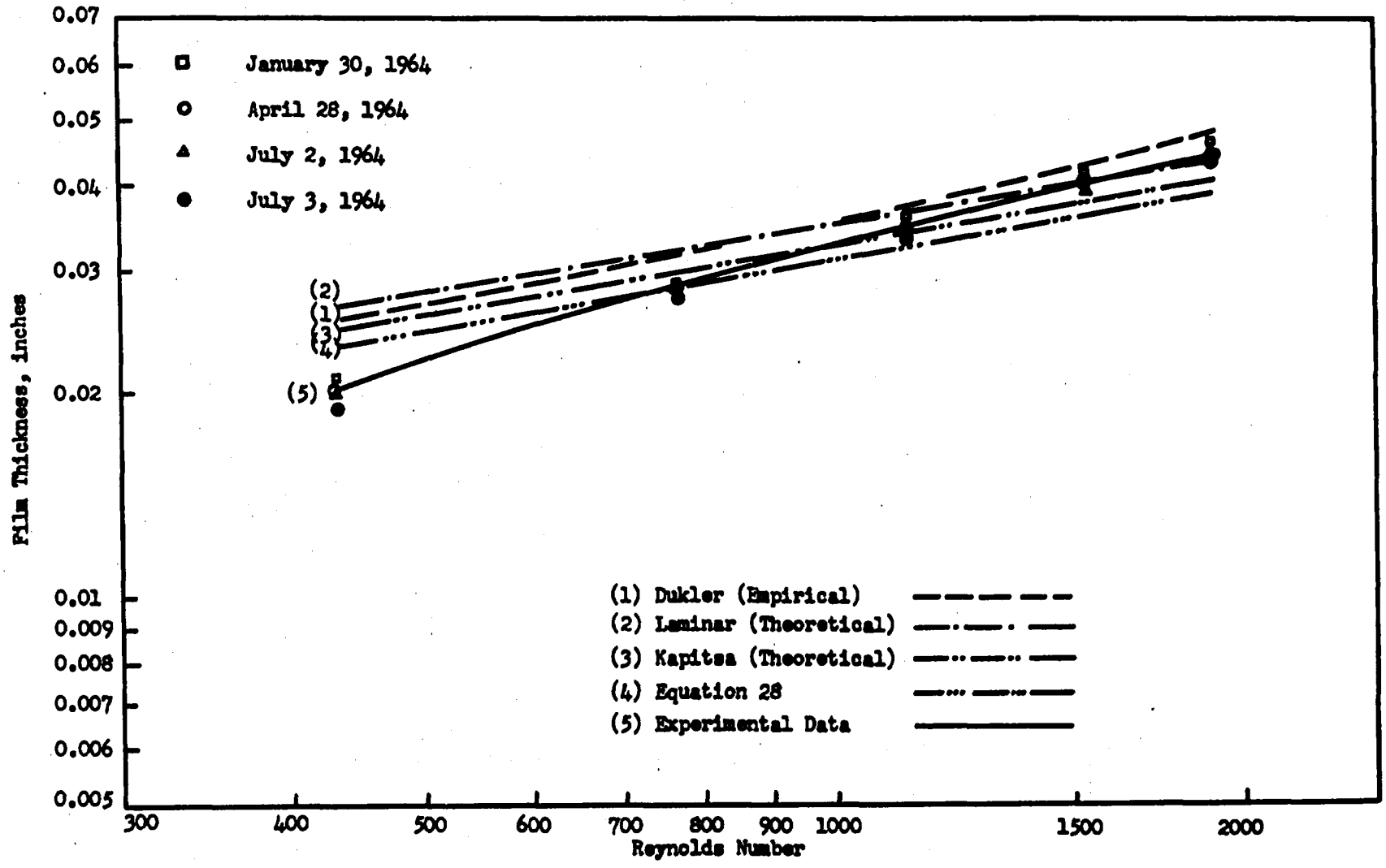

Figure 10. FILM THICKNESS AS A FUNCTION OF REYNOLDS NUMBER FOR AN ANGLE OF INCLINATION OF 5°.

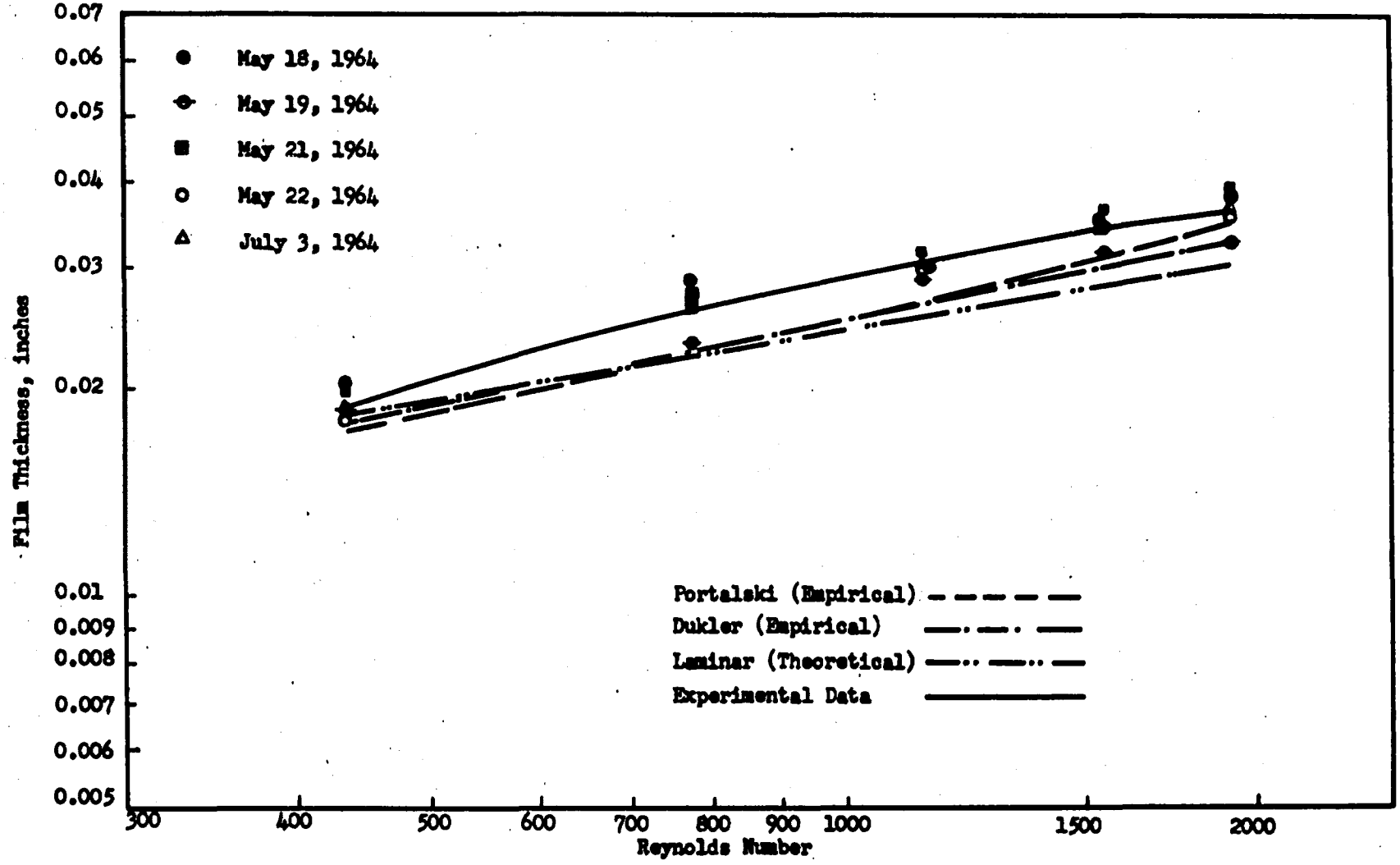

Figure 11. FILM THICKNESS AS A FUNCTION OF REYNOLDS NUMBER FOR AN ANGLE OF INCLINATION OF 15°.

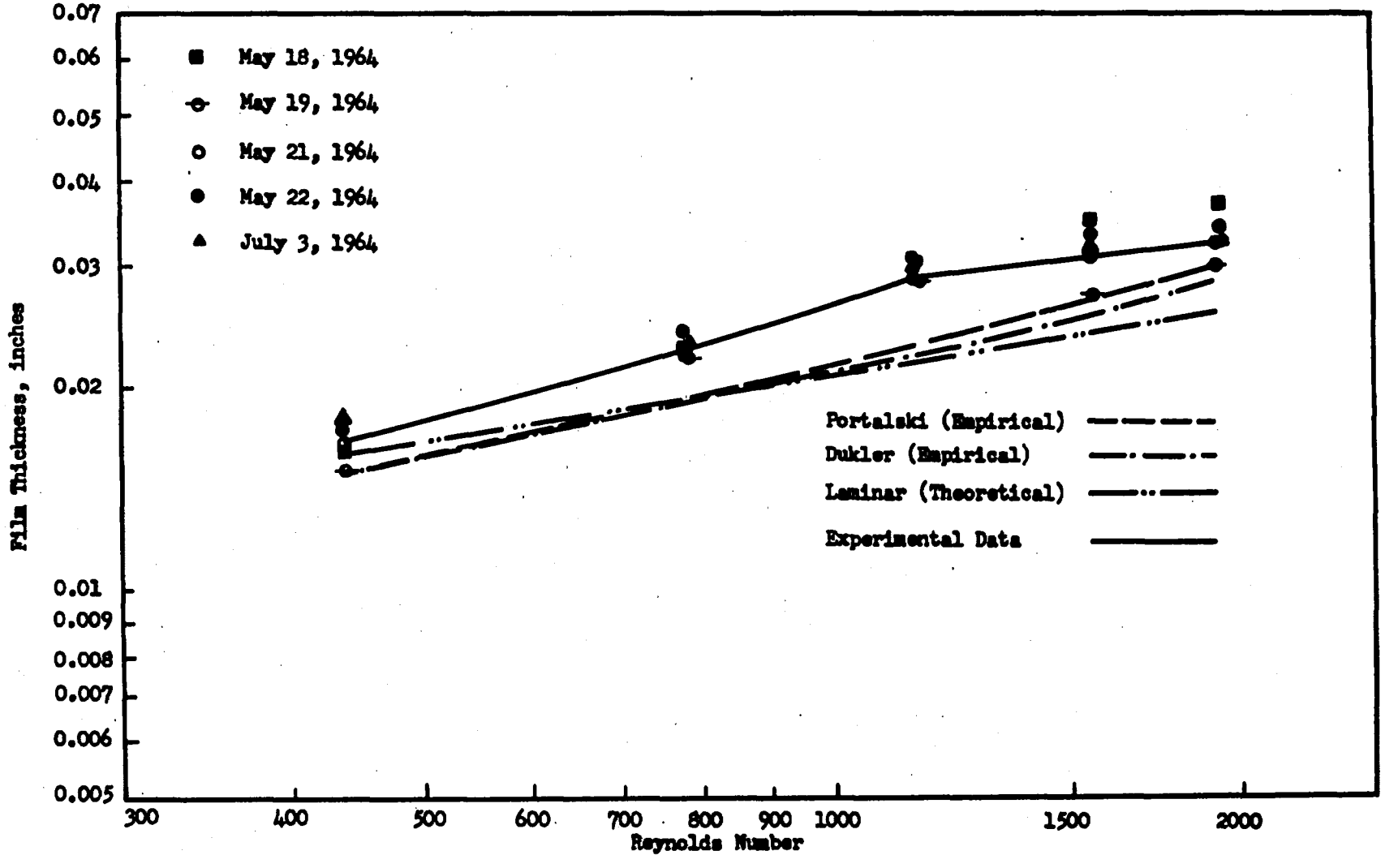

Figure 12. FILM THICKNESS AS A FUNCTION OF REYNOLDS NUMBER FOR AN ANGLE OF INCLINATION OF 25°.

thickness with these theoretical values one finds that over the range of Reynolds numbers of 435 to 1917, at an inclination angle of 5° with low Reynolds number the measured film thickness is close to Kapitsa's theory and equation 28; the film thickness is closer to Dukler's theory at higher Reynolds number. At β of 15° or 25°, the measured film thickness, is larger than all theoretical values at higher Reynolds number, but it is close to equation 28 at low Reynolds numbers. The average film thickness measured by the capacitometer was about 5 to 10% larger than that suggested by the interferometer photograph at β of 5°. When the inclination angle β was 15°, the value of average film thickness measured by the capacitometer was much larger than average film thickness measured from a photograph (see Chapter VI). This kind of deviation was also shown by Jepsen's results. From figures 11 and 12 a transition point is indicated between Reynolds numbers of 1144 and 1544, and shows very clearly at an angle of 25°. After the transition point, the thickness increases slowly as Reynolds number is increased. The transition point did not appear at an angle of 5°. In Jepsen's thesis (pages 207 to 211) at an angle of 25° there was also a transition point at a Reynolds number of 1544. The character of this transition seems to be completely different from that observed by Portalski (41) and Dukler (8) for vertical films. They show that at a Reynolds number of 1100 the film thickness changes from increasing as the cube root of Reynolds number (viscous laminar theory) to increasing as the first power

of the Reynolds number (uniform velocity turbulence). In any case, since no transition was observed at 5°, the transition to turbulence must depend upon inclination angle. This contrast was not the result of undeveloped flow, because Jepsen showed that measurements of wave properties were the same over essentially the entire length of the cell. The average film thickness data of this thesis shows that when the angle increases the transition Reynolds number decreases. Jepsen's measurements of mean film thickness indicated that the experimental value was always larger than the theoretical value predicted by laminar theory. Figures 24, 25 and 26 of Jepsen's thesis for angles of 25°, 18° and 10°, indicate that the slope of those curves (both theoretical and experimental value of the mean film thickness) were the same, and the experimental value of the mean film thickness is about 20 to 30 percent larger than the theoretical value.

The significant features of the results were that the experimental average film thickness disagrees with the laminar theory in magnitude and Reynolds number dependence and that a transition appears which is apparently different from the laminar-turbulent transition observed by other workers at 90°.

Ratio of the Wave Velocity to the Average Velocity

The experimental value of the ratio of the wave velocity to the average velocity, c/V_o, at an inclination angle of 5° was 1.65 to 1.89; and at 15° was 2.02 to 2.28. The theoretical values calculated in Chapter II ranged from

1.57 to 1.60. The experimental value of c/V_o was a little higher than the theoretical value. This agreement was very important because the value of c/V_o seriously affects the values of frequency and amplitude predicted. The experimental data of the c/V_o of other authors are listed in the following table:

Binnie (4)	Re=59 145,	$\beta=1°\sim2.75°$,	c/V_o=1.73 1.89
Benjamin (2)	Re=14.9,	$\beta=13°$,	Wave velocity is about twice surface velocity.
Portalski (30a)	Re=0-400 =400-1100 =1100-2400	$\beta=90°$,	c/V_o=2.9 =2.9-1.9 =1.9-1.5

The wave velocity was calculated by the following equation:

$$c = \frac{L}{\ell/\text{chart speed}} = \frac{106.4}{\ell}\ \frac{\text{cm}}{\text{sec}} \qquad (51)$$

where c was the wave velocity; L was the distance between the two probes--20.95 inches; ℓ was the distance the wave traveled on the visicorder trace; the chart speed was 2 inches per second. The results are shown in figure 13.

The average velocity V_o was calculated from the volumetric flow rate Q and the experimental mean film thickness h_o. The values of c, V_o, c/V_o are listed in Appendix A.

There are few c/V_o data available for the thin flowing

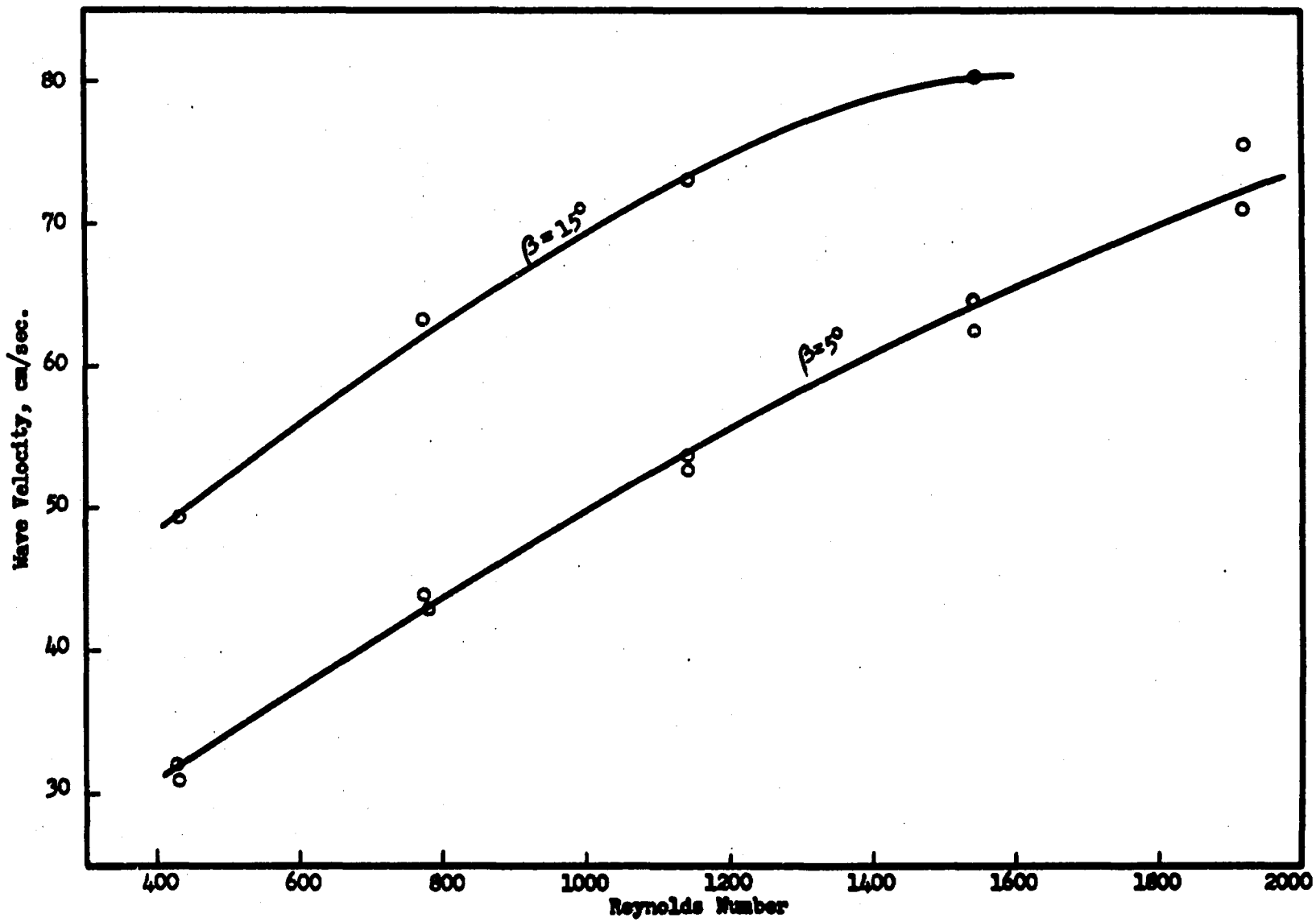

Figure 13. WAVE VELOCITY AS A FUNCTION OF REYNOLDS NUMBER.

films, and all the methods used by the previous investigators to measure the wave velocity were not too accurate. Both Portalski and Binnie used a stop watch to determine the time a visually observed wave traveled a measured distance. Binnie used a 1/4 inch long hair floating down the channel about 22 inches. The method used in this study cannot measure high wave velocities; because a manual switch was used to change the input to the capacitometer from the upstream to the downstream probe. This is the reason why the value of c/V_o at 25° could not be measured accurately enough to report. The proper method for measuring the wave velocity would require two capacitometers. The phase velocities obtained, however, are consistent with those of other studies, are dependent on angle of inclination, and disagree with the theoretical predictions.

Wave Properties

The frequency of the falling water film was obtained by counting the changes in direction of the trace over each one second interval, and the arithmetic average was used to find the average frequency. The statistical method was not used to find the average, because the range of frequencies for the intervals was only a factor of two in the worst case, and at low flow rates was a constant. The results are shown in figure 14. The wave number was calculated from the frequency by the following equation, and the results were listed in Appendix A:

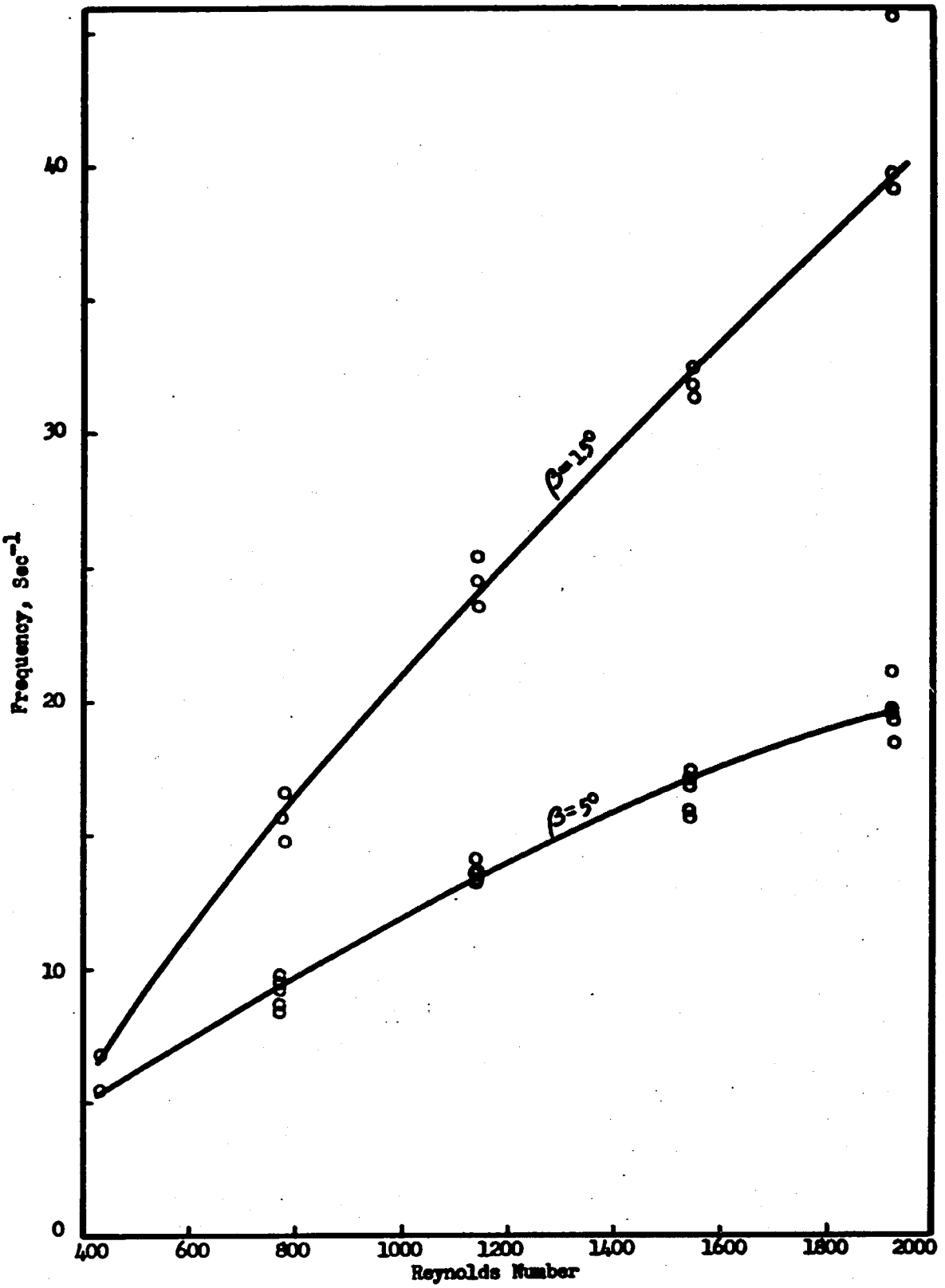

Figure 14. WAVE FREQUENCY AS A FUNCTION OF REYNOLDS NUMBER FOR $\beta=5°$ AND $\beta=15°$.

$$K = \frac{\omega}{c} 2\pi$$

where K is the wave number, ω is the wave frequency and c is the wave velocity.

Figure 14 shows that the frequency of the waves increased as the Reynolds number and the angle increased. The frequency was well defined at low Reynolds number. For example, at a Reynolds number of 435 the frequency of each one second period was the same and there was negligible random effect. As shown in Table 2, the experimental value of the frequency was smaller than the theoretical value. When the Reynolds number increased, random components began to appear.

TABLE 2

Theoretical and Experimental Values of Frequency

$\beta = 5°$					
Re	435	774	1144	1544	1917
Exp. ω, sec^{-1}	5.32	9.05	13.39	16.98	19.6
Theo. ω, sec^{-1}	17.3	31.17	41.87	54.5	67.57
$\beta = 15°$					
Re	435	774	1144	1544	1917
Exp. ω, sec^{-1}	6.77	15.73	24.50	31.85	39.70
Theo. ω, sec^{-1}	48.5	67.5	98.8	11.8	

The transition behavior indicated by the change in film thickness dependence upon Reynolds number, for various angles of inclination, was not reflected by a change in frequency dependence on Reynolds number.

These experimental results do not agree with those

of Jepsen. Jepsen's measurements of frequency indicated that the frequency increased as the Reynolds number increased, but did not increase as the inclination angle increased. However his range of angles was relatively small ranging only from 10°-25°.

Comparison of the predictions for frequency and amplitude of the Kapitsa theory (18,24) showed it to be very unsatisfactory. The more complete analysis suggested by Chapter III is compared in Tables 2 and 3. Although the

TABLE 3

Theoretical and Experimental Values of Amplitude

$\beta = 5°$					
Re	435	774	1144	1544	1917
Exp. $\alpha = 1 - \frac{y_T}{h_o}$	0.305	0.24	0.182	0.167	0.121
Theo. α	0.603		0.615		0.620
$\beta = 15°$					
Re	435	774	1144	1544	1917
Exp. $\alpha = 1 - \frac{y_T}{h_o}$	0.16	0.18	0.102	0.148	0.135
Theo. α	0.605		0.615		0.620

trend of frequency with Reynolds number agrees quite well, the experimental values are about a factor of three below theoretical at 5° and about a factor of four below at 15°. This is difficult to explain. Normally in analysis of this type one anticipates that the experimental frequencies will be higher than the theoretical if they do not agree. The assumptions of the theory are well founded for these disturbances especially at the lower Reynolds numbers and

smaller angle. It is conceivable, that subharmonic phenomena are involved so that future study should examine the wave theory from that point of view. Benjamin (2) suggests that predicting the observed frequencies may be very difficult.

The theoretical value of amplitude was 0.6, which means that the crest height should be 3 to 4 times the height of the trough. From Table 2, the maximum experimental value of $\alpha = 0.305$ was at $\beta = 5^\circ$ with the lowest Reynolds number of 435. Moreover, the trend of amplitude with Reynolds number was considerably larger than the theoretical prediction and in the wrong direction. Since the frequencies do not agree with the theory it is not surprising that the amplitude behavior shows no correspondence with theory.

This general disagreement between theoretical predictions for frequency and experimental values also occurs in measurements at 90°. Both Portalski (30a) and Wilkes (43) report serious disagreement for wave frequencies obtained over a range of Reynolds numbers from 10 to 150. However, Benjamin (1) found excellent agreement at a Reynolds number of 17.

Interfacial Area

Equation 37 was derived in Chapter III to calculate the increase in interfacial area due to the wave motion. The values of ΔS at different inclination angles are shown in figure 15. These values are smaller than the value of ΔS calculated from Portalski's equation. This is not only due

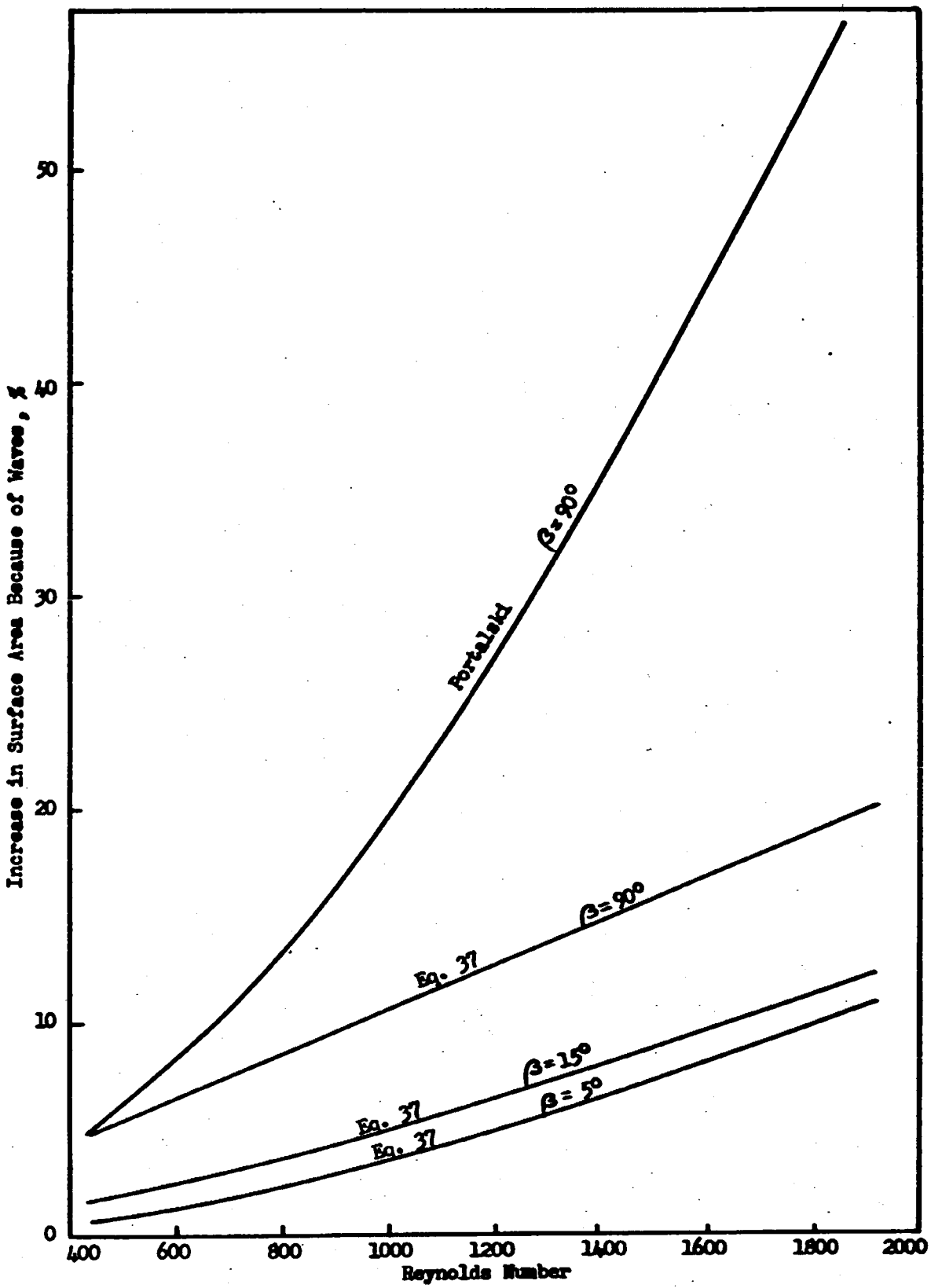

Figure 15. INCREASE IN SURFACE AREA CAUSED BY THE PRESENCE OF WAVES.

to the different values of c/V_o and amplitude used but also because additional terms were included in the analysis, which affect the ΔS substantially. Since the basic equation was derived for laminar flow, it should not be expected to calculate the increasing interfacial area at large Reynolds numbers. At low Reynolds numbers where longer waves predominate, the measurement would be more accurate than for shorter waves. Serious error can occur if the width of the probe were bigger than wave length and this might be the reason why Jepsen (17) found ΔS to be larger at low Reynolds numbers than at higher Reynolds numbers. The capacitometer was satisfactory for measuring frequency, film thickness and wave velocity, but may not be accurate for measuring the value of ΔS and amplitude. Portalski indicated in reference 30 that the experimental value of ΔS agreed with his theoretical value. Because he only measured waves at Reynolds numbers of 11.2 and 12, for an 82% glycerin-water solution, his conclusion about the increasing interfacial area was established only for low Reynolds numbers. On page 95 of Jepsen's thesis, he reported the increase in the interfacial area of the falling water film at three different inclination angles, $9°44'$, $18°27'$ and $25°42'$. His results indicated that for the same flow rate the maximum increase in the surface area was at the lowest inclination angle $9°44'$. This result disagrees with equation 37. The deviation could come from the apparatus and the accuracy of the experimental value of the ΔS as measured by the capacitometer.

Nevertheless, for the lowest Reynolds number of 732 and lowest inclination angle of 9°44', Jepsen's experimental results gave an increase in the surface area, ΔS of 1.45%, and the theoretical value of the ΔS was 2.31% at inclination angle of 5° and Reynolds number of 774. If the sensitivity of the capacitometer could be improved it is possible that the experimental value of ΔS at low Reynolds number and low inclination angle would be in better agreement.

In this thesis, the increase in the interfacial area of one wave trace at inclination angle of 5° with a Reynolds number of 774 was measured by fitting a thread on to the wave curve. A 3.46% increase in the interfacial area was obtained in this case. Sample calculations are presented in Appendix H.

None of the experimental values agree with the theoretical predictions at Reynolds numbers beyond Portalski's studies at Re = 11.2 and 12 for the glycerine solution. The disagreement was not surprising since neither amplitudes nor frequencies agreed with theory. In general, however, all values were too small to account for the increase in mass transfer observed when waves appeared.

CHAPTER VI

RESULTS AND DISCUSSION OF CONCENTRATION MEASUREMENTS

The concentration measurements consisted of photographs of interferometer fringe patterns at several positions for angles of 5° and 15° and six liquid Reynolds numbers ranging from 272 to 1917. Several photographs were taken for each test, including air fringe patterns and probe positions for reference. The position and shape of the interferometer fringes are a measure of the concentration of carbon dioxide concentration.

The photographs presented in figure 16 for 5° inclination angle, 22 inches from the entrance show that the fringes are bent at the bottom at low flow rates. The bottom of the liquid film is located at the bottom end of a bright band. The surface of the film is located at the top of a bright band at low Reynolds numbers. At higher Reynolds numbers the wave action may cause the pattern at the interface to be indistinct and the surface lies slightly above the top of a bright band. At higher flow rates, the fringes are only bent on the top half of the film, and the fringes in the bottom half of the film are straight. When the flow rate was reduced to a Reynolds number of 272, the fringes were not

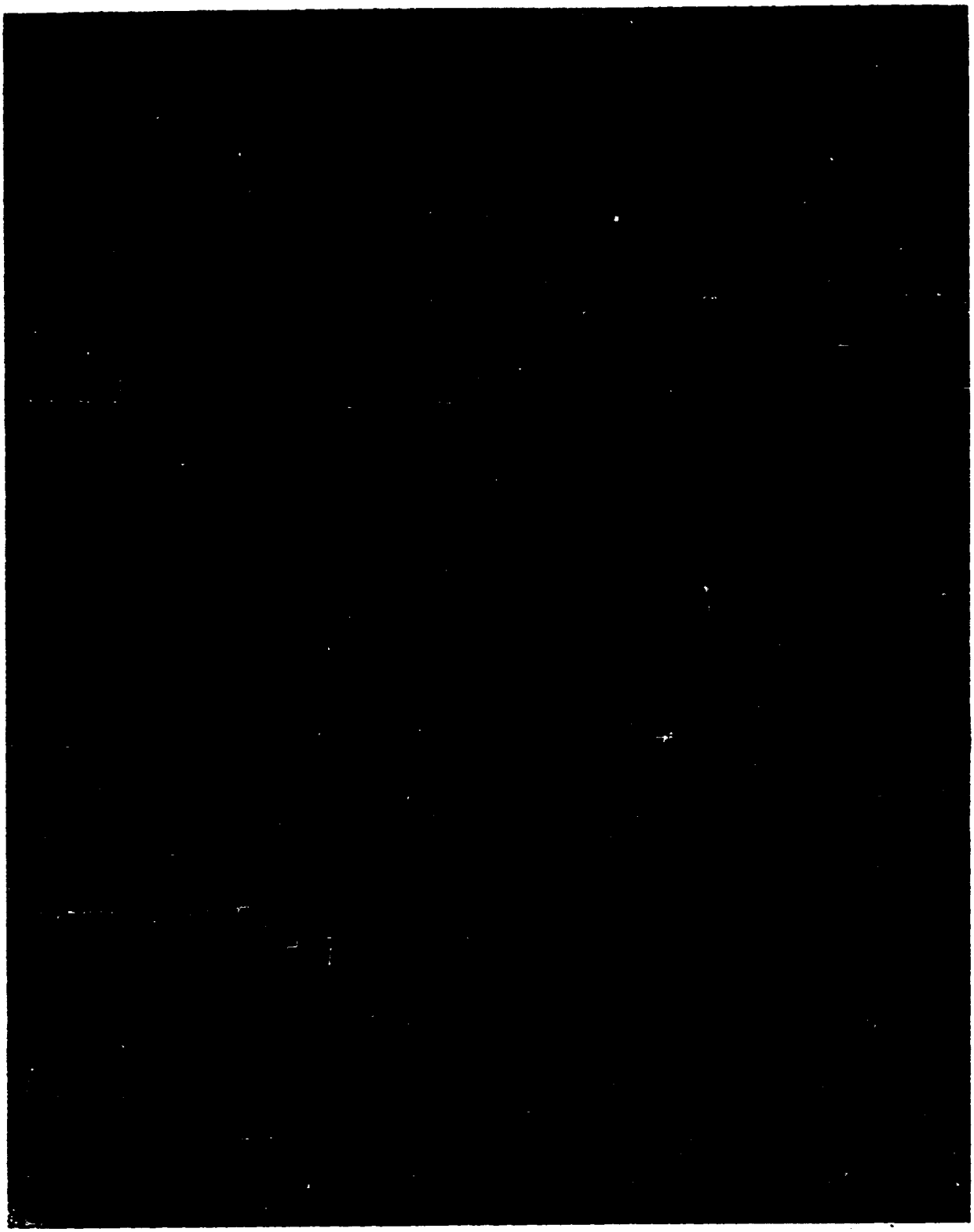

Figure 16. PHOTOGRAPH OF CO_2-WATER INTERFERENCE PATTERN AT AN ANGLE OF 5°, 22 INCHES FROM ENTRANCE.

only bent, but also shifted along the bottom. As the flow rate increased, the bent part of the fringes became smaller and the straight portions increased.

For each cell position, liquid Reynolds numbers 272, 435, 774, 1144, 1544, 1917 were studied. At Reynolds numbers of 272 and 435, the fringes were bent to the bottom; when a Reynolds number of 774 was reached, the fringe was bent only from the surface to the middle of the film 22 inches from the entrance, but at 30 inches from the entrance it was bent almost to the bottom. At a Reynolds number of 1144, the fringe in the bottom half of the film was not bent at all.

The saturated fringe shift was about 2.8 as shown in figure 17 which includes a 0.5 cm. scale to show the magnification. From figure 16 at a Reynolds number 1144, as an example, the total fringe shift on the surface of the liquid film was close to 2.5, this means that if the straight section of the fringes in the bottom part of the water film had zero concentration of carbon dioxide, the concentration at the surface of the water film was still close to the saturated concentration.

Therefore, at the low inclination angle of 5°, the carbon dioxide did not penetrate to the bottom at higher flow rates within the short distance of 30 inches from the water inlet. This was the result of a combination of larger film thickness and high surface velocity. For example, at a Reynolds number of 1917, the film thickness and the surface velocity were about twice the film thickness and the surface velocity

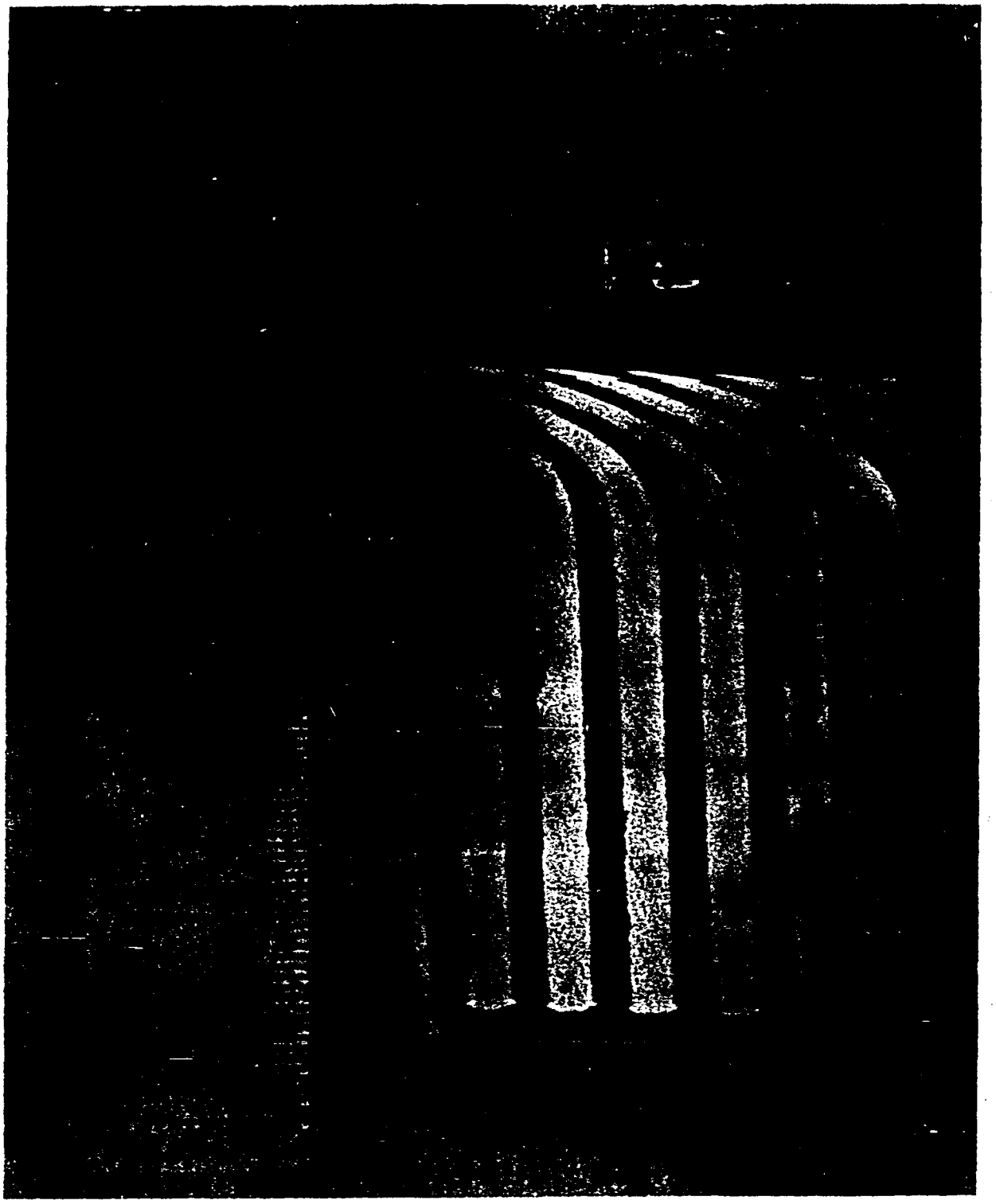

Figure 17. CO_2-WATER INTERFERENCE PATTERN (WITH 0.5 cm. SCALE) SHOWING SATURATED FRINGE SHIFT AT SURFACE UNDER NO FLOW CONDITIONS.

at a Reynolds number of 435, and before the carbon dioxide could penetrate to the bottom, the solution would have already reached the end of the diffusion cell. At lower flow rates (Reynolds number of 435) the residence time was twice that at a Reynolds number of 1917.

Even at 15°, the bottom part of the fringes was not shifted at higher flow rates, corresponding to Reynolds numbers of 1544 and 1917. Although a comparison of the photograph of the air-water system and the CO_2-water system at the same cell position and conditions may indicate a fringe shift, this did not indicate a substantial change in concentration but was caused partly by changes in pressure within the cell and partly by effects present in the room air in the path of the light beam of the interferometer.

The location and shape of a particular interferometer fringe gave both the concentration value and the concentration profile. The technique, however, was complicated because the fringe system was shifted considerably by other effects. The result was that the shape of the concentration profile was well established, but the level of concentration was not, particularly at higher angles and flow rates. Jepsen (17), for example, was convinced that substantial penetration to the wall occurred at high flow rates as soon as the waves formed, even though the CO_2 fringe was still largely straight. The usual experimental information about the concentration level was the titration concentration which gave the average value. The use of this value as a check on the fringe shift

was also complicated because the exact velocity profile was not known, especially for the higher Reynolds numbers and angles.

The concentration profiles obtained, basically agree with Jepsen's results, especially in the shape of the concentration profiles.

The fringe shift in all the photographs was measured by a cathetometer, to ± 0.001 cm. Sometimes the definition of the water surface was not complete but the bottom of the cell could always be located by the reference cross hair and probe. As mentioned before, two photographs were taken at each cell position in order to establish the location of the bottom plate. In these two photographs, the micrometer was set with a known distance above the bottom, and the cross hair was included in the photographs. The cross hair then located the bottom surface for the rest of the photographs.

The fringe shift was calculated from measurements of the distance between the center of the fringe and the cross hair for the CO_2-water system (X_{CO_2}) and air-water system (X_{air}) at the same height from the bottom. The fringe spacing (X_s) was measured as the distance between two fringes and the number of fringe shifts due to CO_2 was calculated:

$$N = \frac{X_{CO_2} - X_{air}}{X_s} \tag{52}$$

The numerical value of N at various locations in the falling water film was listed in Appendix B and some of these are shown in figure 18. For the saturated CO_2 solution, the

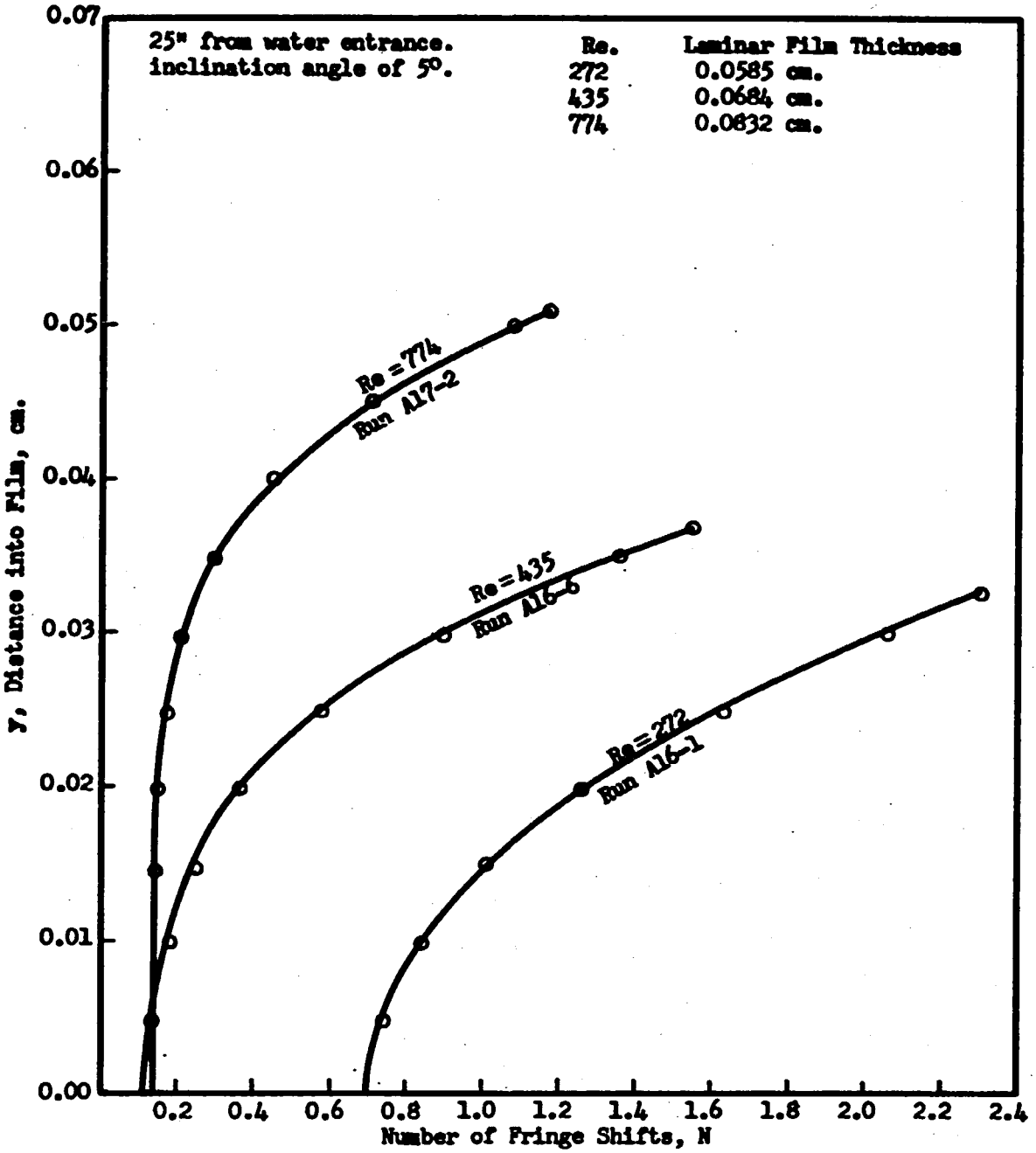

Figure 18. EXPERIMENTAL CONCENTRATION PROFILES.

average value of N was 2.8472 at a temperature of 24°C.

It was found that the fringes were essentially straight at higher flow rates. In order to decide whether the CO_2 penetrated to the bottom as suggested by Jepsen, a series of samples were taken with a small diameter hypodermic needle and syringe. It was found that at 30 inches from the water entrance, the CO_2 concentration at the bottom was 0.0024 to 0.0053 gram/liter at 24°C, for $\beta = 10°$ and a Reynolds number of 1917. This corresponded to a fringe shift of 0.0048 to 0.0107.

From these results and the general behavior of the penetration as a function of flow rate and angle, it was decided that when the bottom part of the fringe was straight, the fringe was considered to not be shifted significantly at the bottom. At low flow rates, a fringe would not have a straight section at the bottom, and it was necessary to correct the location of the fringe using the titration value as indicated by Jepsen. At 5°, for Reynolds numbers of 774, 1144, 1544, and 1917, the bottom of the fringe was straight, at Reynolds numbers of 435 and 272 the fringe was bent at bottom. When β was 15°, for Reynolds numbers of 435 and 774 the fringe was bent at the bottom; at Reynolds numbers of 1544 and 1917 the bottom portion was straight, and it was difficult to tell whether it was bent or not at a Reynolds number of 1144. It may be worth noting that the concentration profiles shown in figure 18 are completely different in shape and magnitude from those suggested by laminar flow combined

with molecular diffusion. For the experimental conditions of figure 18, the molecular diffusion profiles calculated from any of the theories, for example from equation 17.5-15 of Bird (5), show carbon dioxide penetrating only 40% into the film at a Reynolds number of 272 (film thickness of 0.0585 cm.) and much less at the higher Reynolds numbers.

The velocity profile was not measured during this research work. However the literature seems to establish that it should be parabolic at a Reynolds number of 4 when waves were present (see Wilkes (43)). The shapes of a parabolic velocity profile and a logarithmic velocity profile were compared and the results presented in Appendix F. The range of dimensionless film thickness, η (see equation 45), in this experiment was about 20 to 30, and the shape of these profiles was very similar in this range. The major contrastive feature was that the parabolic velocity profile had a small surface layer with nearly constant velocity, which satisfied the condition that the shear must be zero at surface. The equation for the velocity profile used in this thesis was therefore (see page 39 of reference 5):

$$V_x = 3V_o \left(\frac{y}{h_o} - \frac{y^2}{2h_o^2} \right) \qquad (53)$$

And whenever V_o was not equal to $\frac{g \sin \beta \, h_o^2}{3\nu}$ as most authors use for the laminar falling liquid film, the experimental value of V_o was used, that is:

$$V_o = Q/h_o \qquad (54)$$

where Q was the average volumetric flow rate measured by the rotameter. Therefore, the velocity profile used in this thesis should not be too far from the true velocity profile.

In order to calculate the total diffusivity, $(D + \epsilon)$, a mass balance was made on the solute in the falling water film at various locations in the film:

$$(x_2 - x_1)(D + \epsilon) \left.\frac{dC}{dy}\right|_{\frac{x_1+x_2}{2}} = \int_0^y V_x C \, dy \Big|_{x_2} - \int_0^y V_x C \, dy \Big|_{x_1} \qquad (55)$$

Solving for $(D + \epsilon)$, the above equation became

$$(D + \epsilon) = \frac{\int_0^y V_x C \, dy \Big|_{x_2} - \int_0^y V_x C \, dy \Big|_{x_1}}{\Delta x \left.\frac{dC}{dy}\right|_{\frac{x_1+x_2}{2}}} \qquad (56)$$

Since the number of fringe shifts, N, is directly proportional to concentration, the calculations in equation 56 can be done in terms of N as well as concentration. The two terms of the numerator were obtained by graphical integration of the product of the velocity calculated for laminar flow ($V_s/V_o = 1.5$) and concentration profile obtained from the interferometer photographs at two different positions down the cell. The values of $\frac{dC}{dy}$ were found by a numerical procedure. A small interval ΔC was chosen and Δy was obtained from the plot of C vs y. Then a plot of $\Delta C/\Delta y$ vs y was made. For the smooth curve, if the Δy and ΔC were small enough, the difference between dC/dy and $\Delta C/\Delta y$ would be negligible. Using Mickley's (27a) suggestion (Chapter 1 of reference 27a)

the error was not more than 3%. The greatest difficulty with this calculation was that one must use photographs showing the same film thickness (for the same Reynolds number) at various cell positions. Because of the fluctuating nature of the phenomena, sometimes the camera captured the profile under a crest, and at others a trough or some place between. High speed motion pictures taken during this study showed that even at low angles of inclination and low flow rates, the shape of the fringe was not quite the same underneath a trough as under crest. Therefore, one could not compress or expand the fringes very far in order to obtain comparable profiles at different cell positions to obtain a certain film thickness (see page 108 of reference 17). In addition, if a fringe profile was expanded or compressed, the average velocity of the falling liquid film had to be changed according to the film thickness and this could introduce a serious change in the value of $(D + \epsilon)$. The values of $(D + \epsilon)$ calculated from the interferometric patterns are plotted as functions of film thickness in figures 19a,b,c,d and e and 20a,b,c, and d.

These show that total diffusivity increases for positions toward the center of the film. At 15° and the highest Reynolds number, 1917, a maximum is observed. The total diffusivity is a strong function of angle. At a Reynolds number of 435 the total diffusivity is 5 times the molecular diffusivity with a marked decreasing trend toward the wall. The molecular diffusivity for this system is

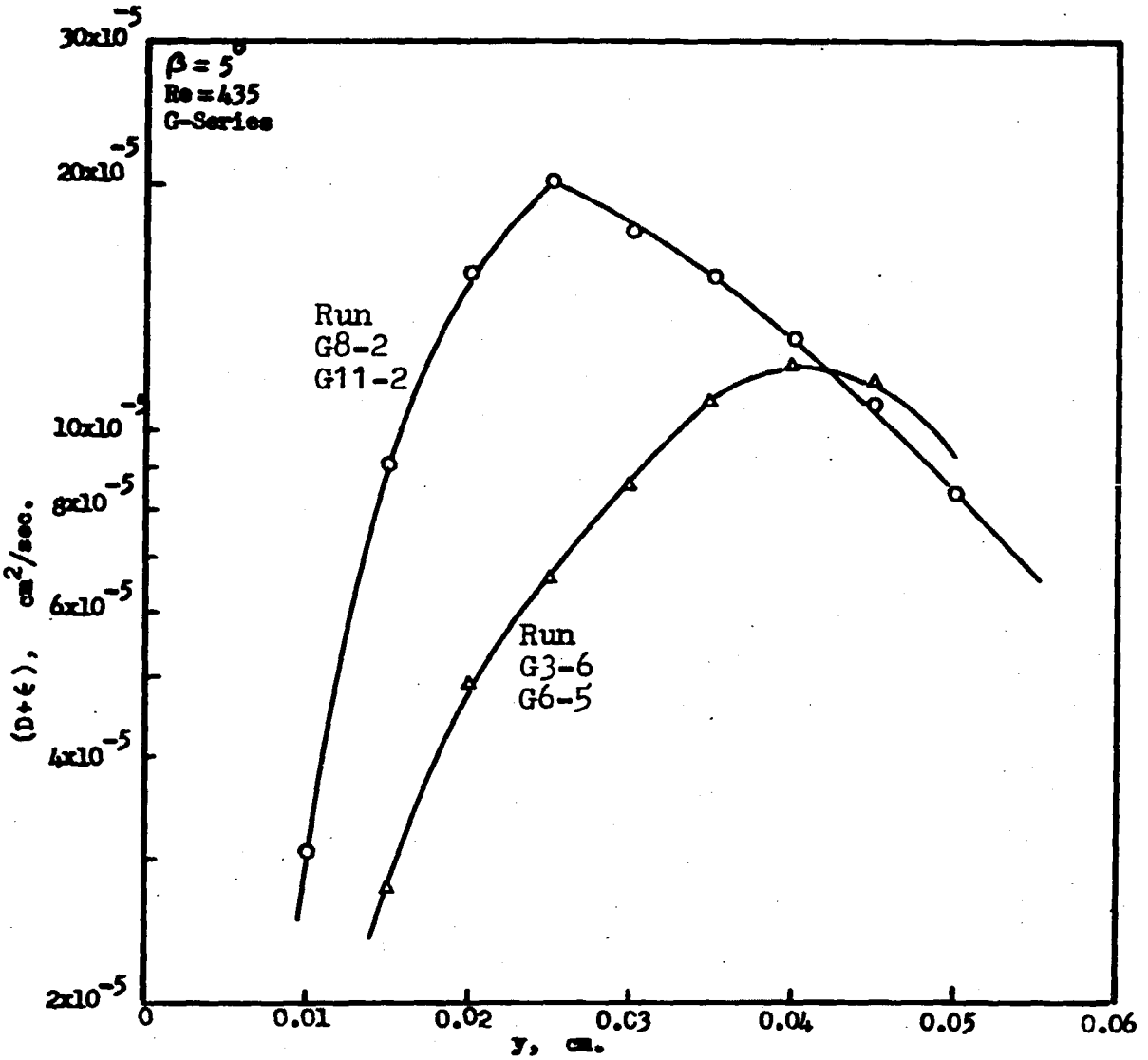

Figure 19A. TOTAL DIFFUSIVITIES, $\beta = 5^{\circ}$.

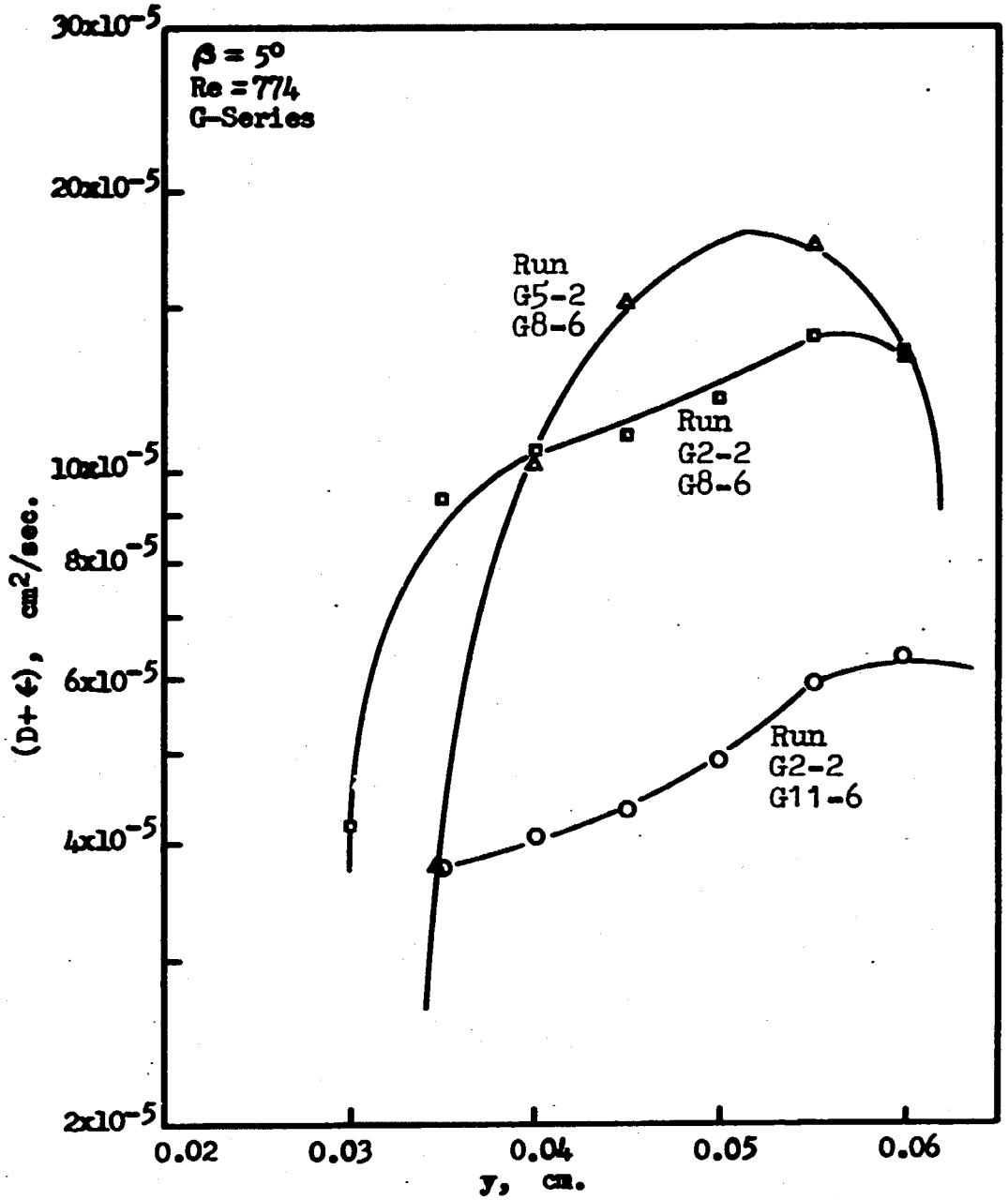

Figure 19B. TOTAL DIFFUSIVITIES, $\beta = 5^{\circ}$.

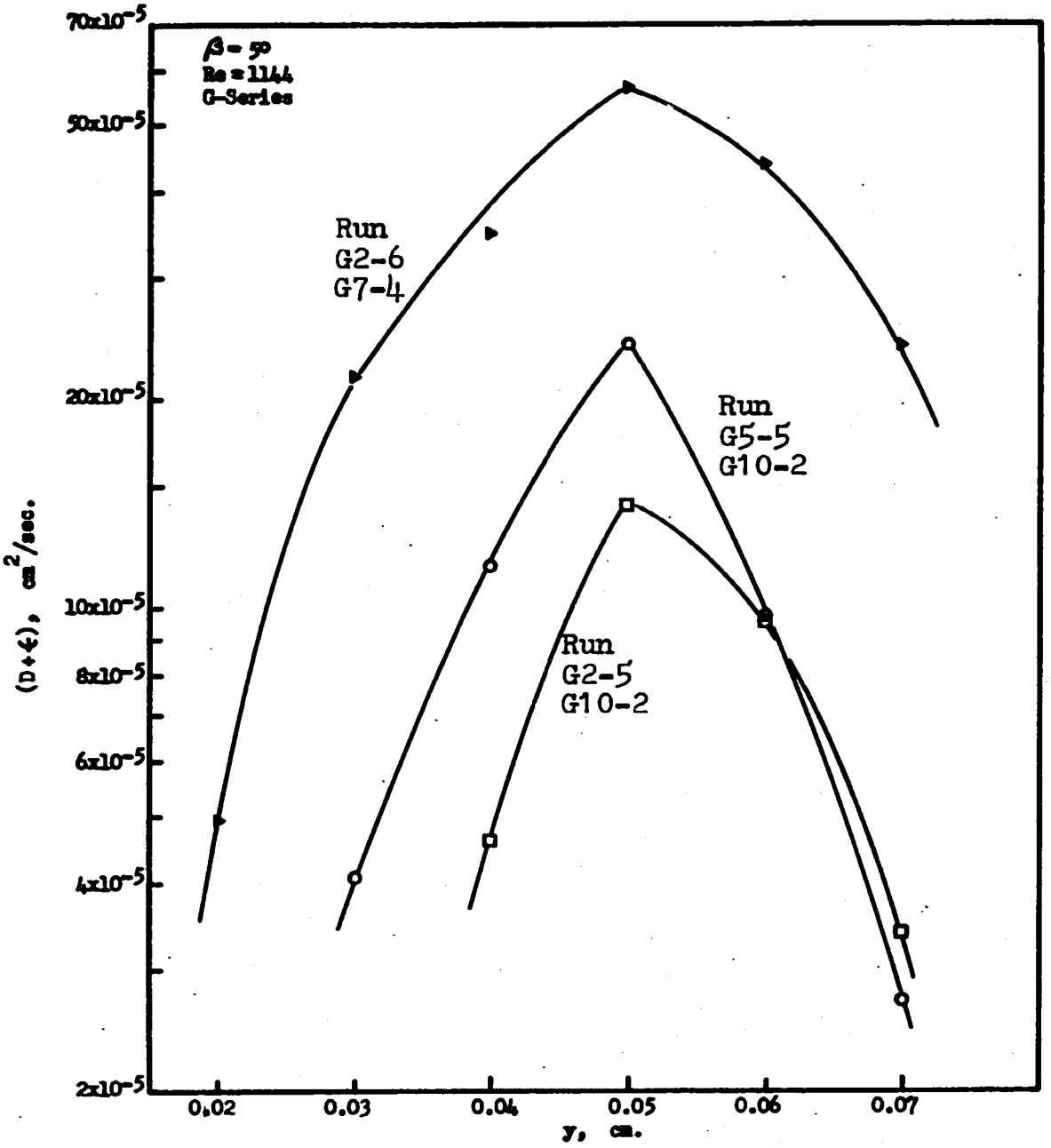

Figure 19C. TOTAL DIFFUSIVITIES, $\beta = 5°$.

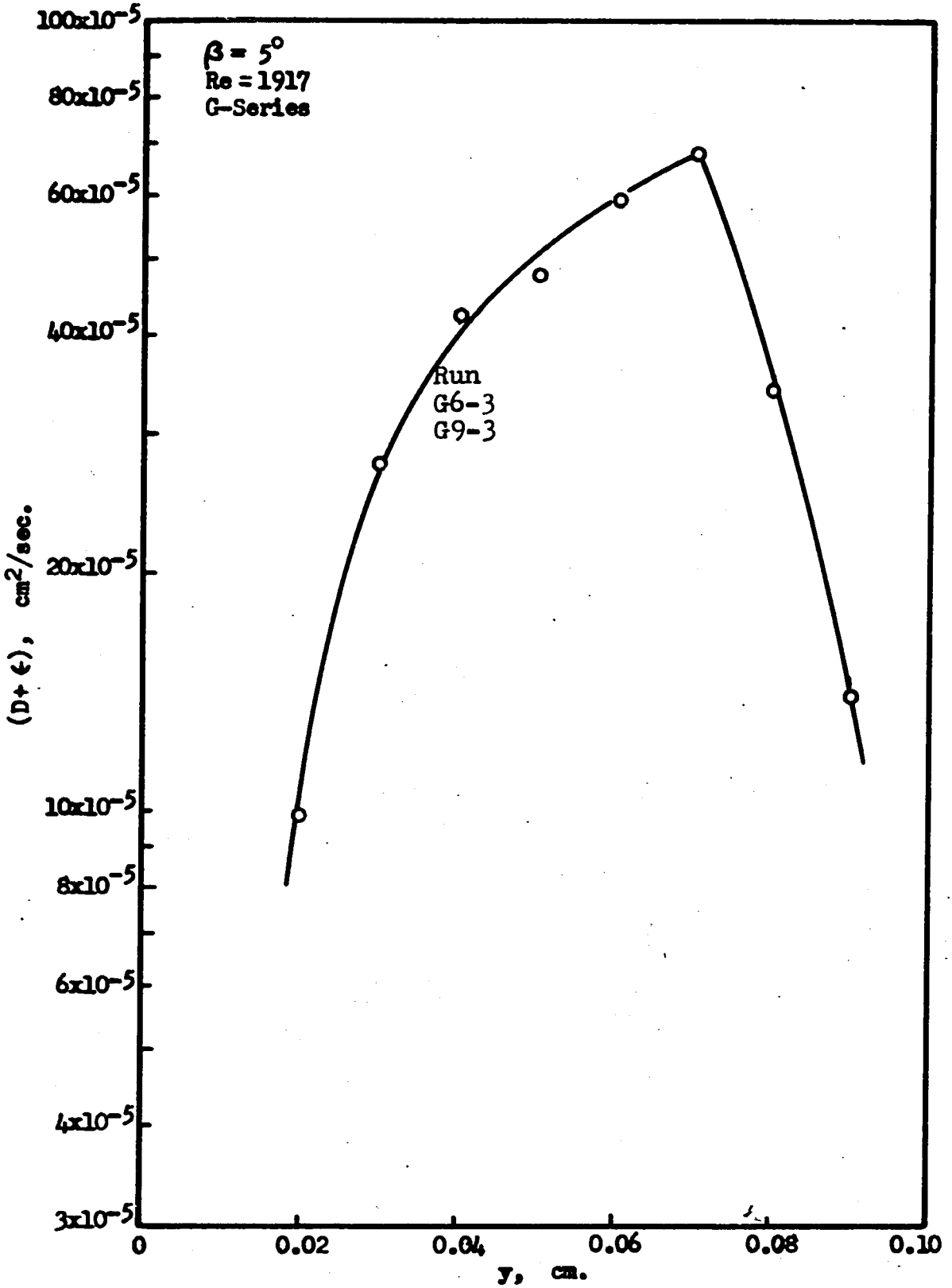

Figure 19D. TOTAL DIFFUSIVITIES, $\beta = 5^{\circ}$.

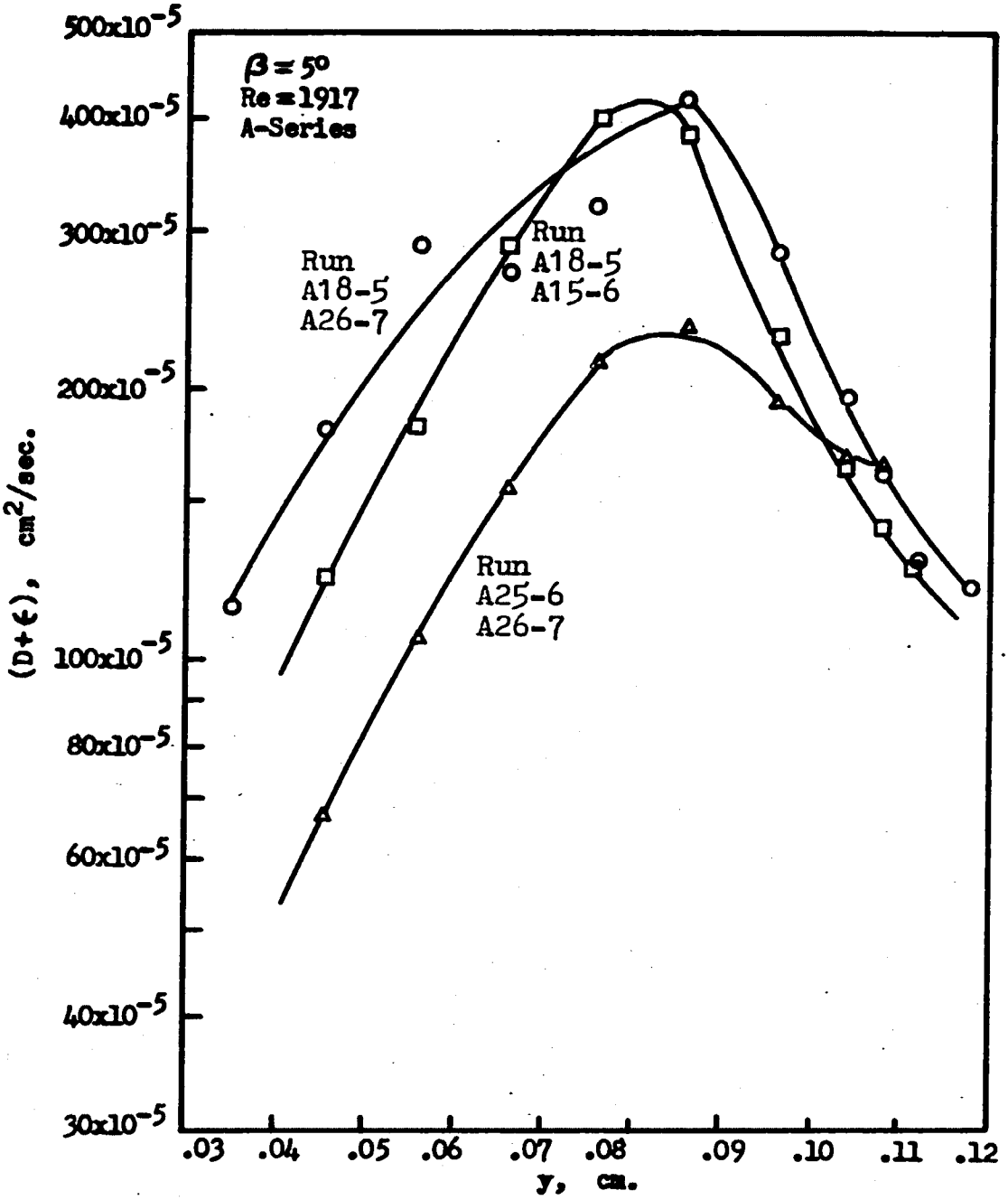

Figure 19E. TOTAL DIFFUSIVITIES, $\beta = 5°$.

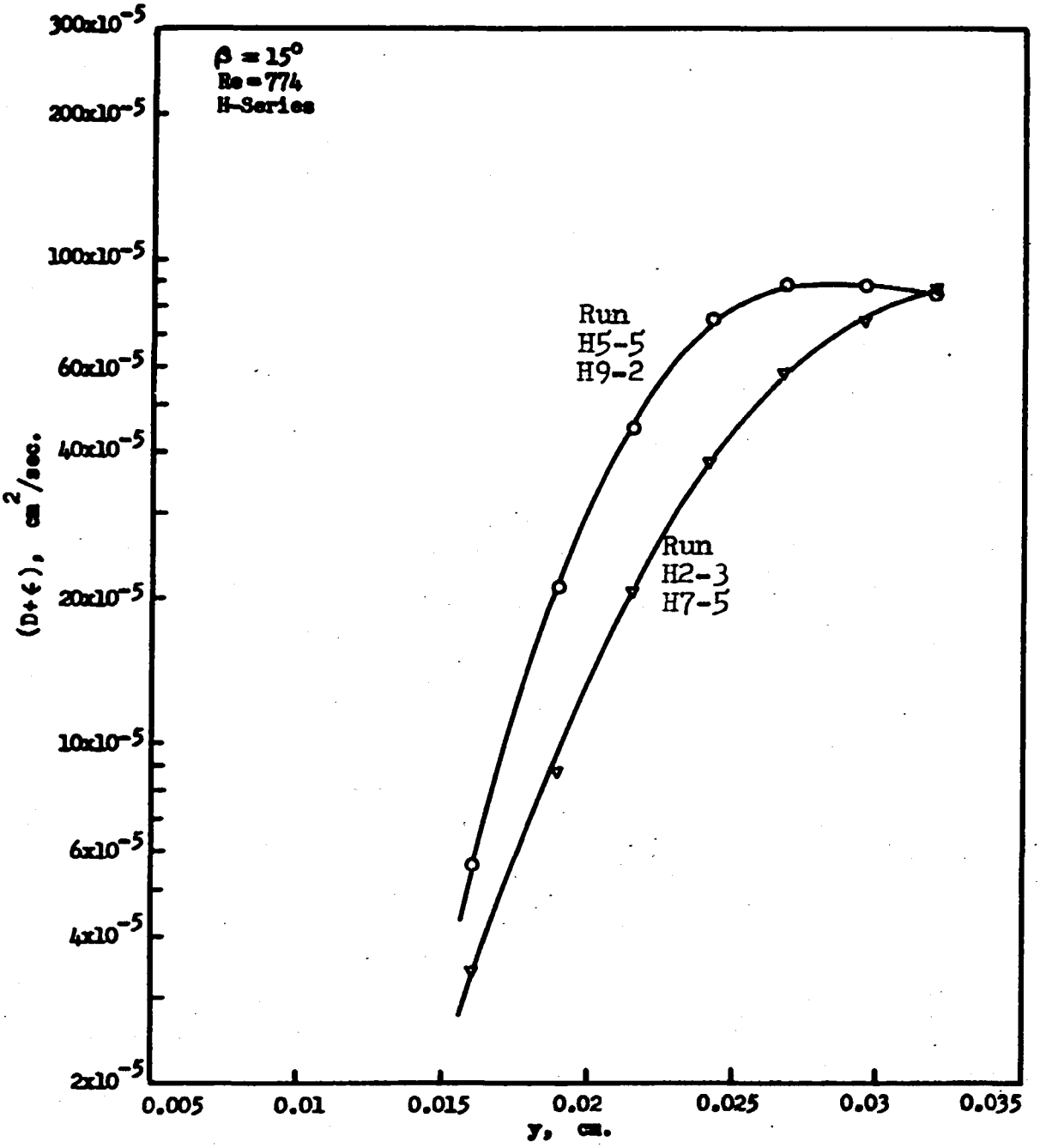

Figure 20A. TOTAL DIFFUSIVITIES, $\beta = 15°$.

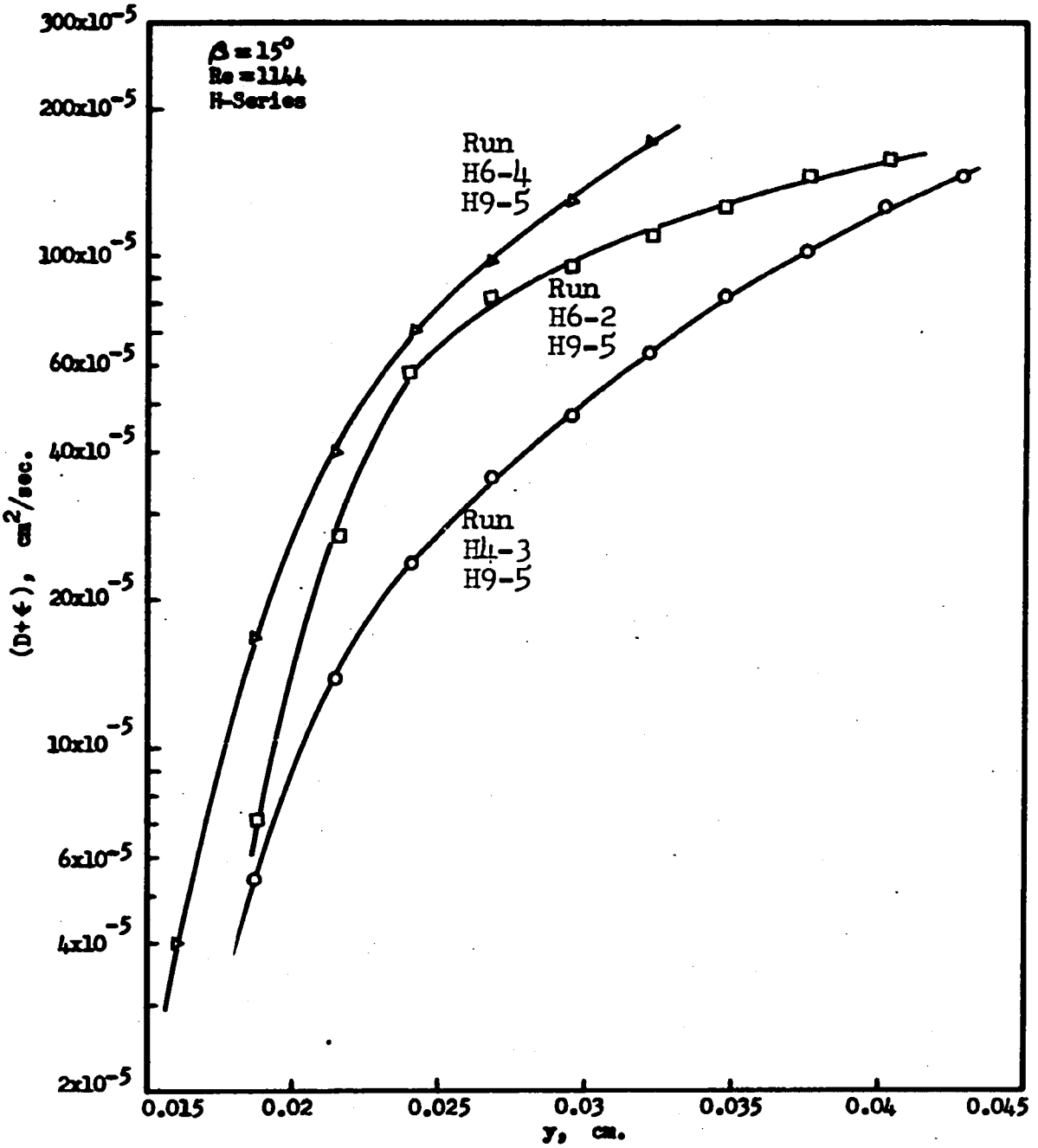

Figure 20B. TOTAL DIFFUSIVITIES, $\beta = 15°$.

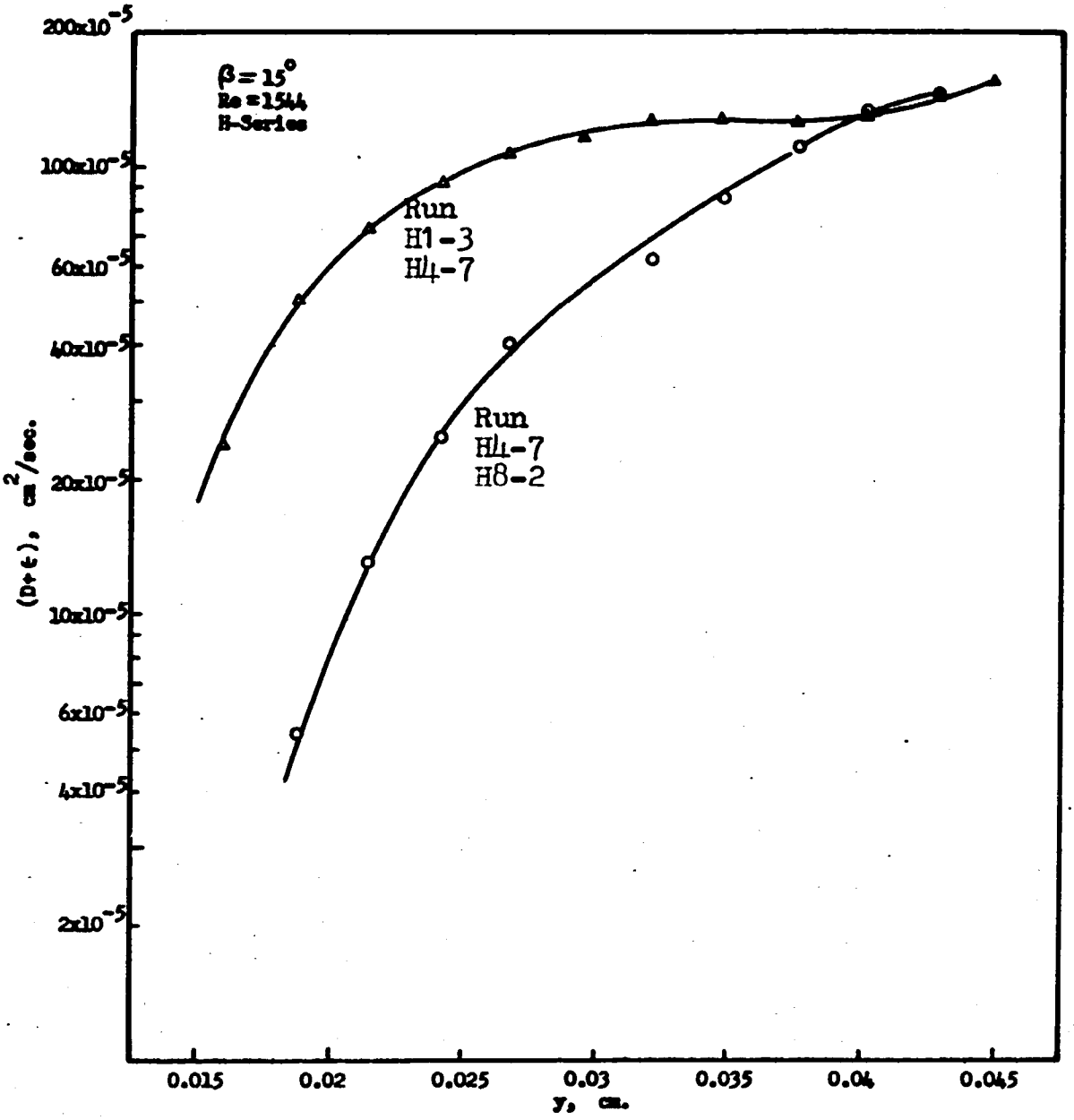

Figure 20C. TOTAL DIFFUSIVITIES, $\beta = 15^{\circ}$.

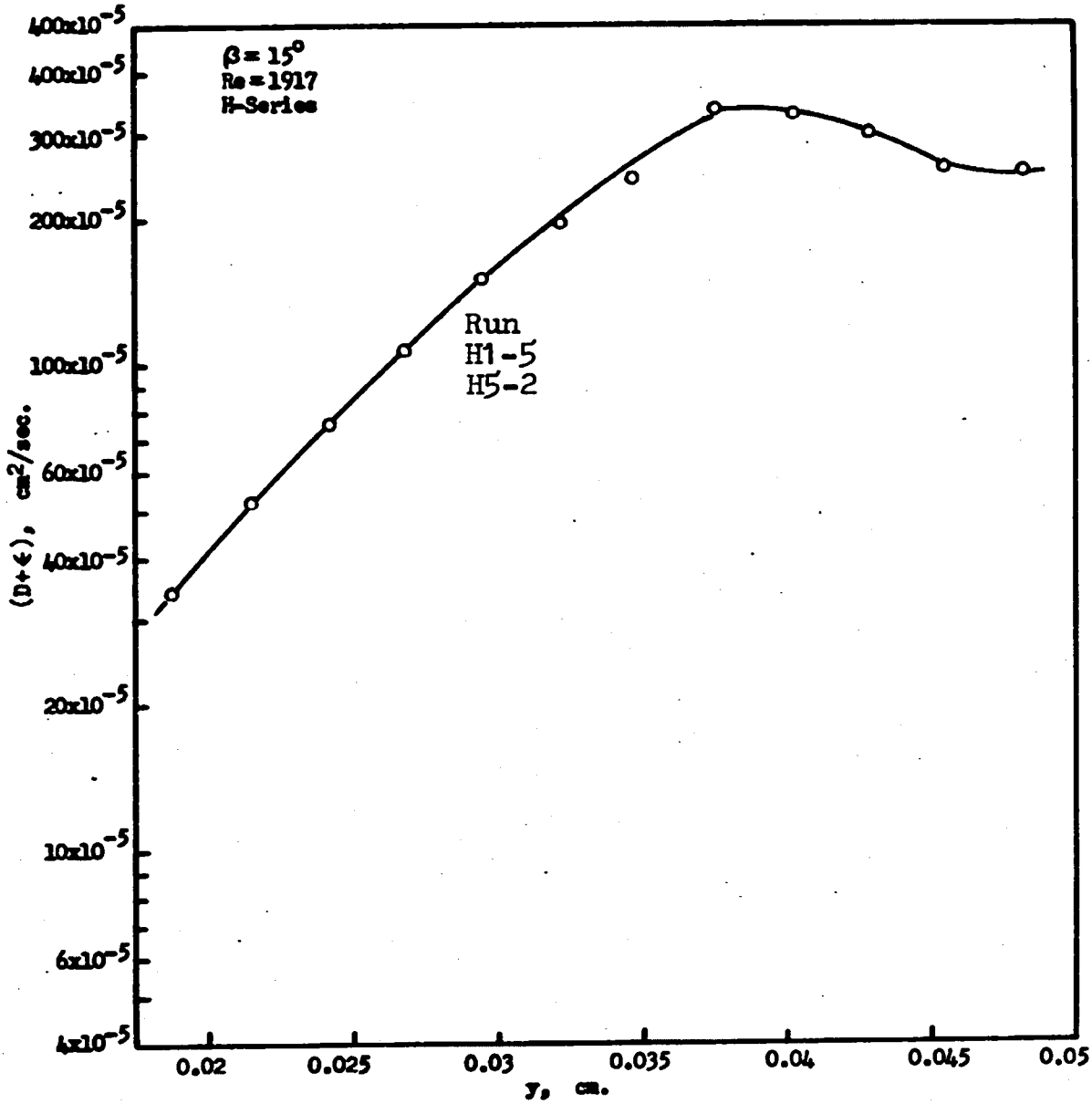

Figure 20D. TOTAL DIFFUSIVITIES, $\beta=15^{\circ}$.

1.9×10^{-5} cm^2/sec for comparison. These results at 15° differ from Jepsen because he showed definite decreasing trends at both the wall and the surface. This could conceivably be the result of his calculation procedure combined with a large amount of data whose average permits better definition towards the surface than was possible in this study. The slight difference in temperature between this study (24°C) and that of Jepsen (22°C) is of no consequence. The diffusivities obtained in this thesis basically agree with Jepsen's results. Both indicated that the diffusivity was a function of Reynolds number and angle of inclination. Jepsen's numerical results of the diffusivity at an inclination angle of 10° are between the numerical values of the diffusivity of this thesis ($\beta = 5°$ and 15°). In this thesis, the diffusivity shows a maximum even at a Reynolds number as low as 435 at $\beta = 5°$.

The results show no change in behavior for a Reynolds number of 1000. This result is consistent with the wave property behavior, in that the laminar turbulent transition Portalski observed in the film thickness at 90° was not observed at these lower angles. The increased mass transfer, and its associated empirical total diffusivity seems to be related strictly to the waves. Although the decrease of total diffusivity toward the surface is less well defined, such a trend toward the molecular diffusivity must be present. The overall mass transfer rates are much too small to permit so large a diffusivity to exist at the surface.

Therefore, the results show a pronounced increase in diffusion rate within the central region of the film at angles from 5° to 15° for Reynolds numbers as low as 435 to as high as 2000 with no indication of a transition in flow mechanism.

Effective diffusion coefficients so much larger than the molecular diffusivity indicate some type of mixing action within the film. Velocity measurements usually supply the basis for describing such an increased action in terms of a non-laminar velocity profile. In all cases, the change from a purely laminar profile need be only very slight in order to indicate an eddy momentum transfer action which can influence mass transfer. The transitions observed at 90° would permit the suggestion of a "universal" velocity profile to describe the transport within the film. Some workers have already applied this to measurements of film thickness.

The shear stress, τ, in the fluid is a linear function of the distance from the bottom of the cell, and

$$\frac{\tau}{\tau_o} = \frac{h_o - y}{h_o} = 1 - \frac{y}{h_o} \tag{58}$$

where τ_o is the shear stress when y equal to zero or the shear stress at the bottom of the cell and h is the film thickness of the water film. Then if

$$\frac{\tau g_c}{\rho} = (\nu + \varepsilon) \frac{dV_x}{dy} \tag{59}$$

it follows that: $$(\nu + \varepsilon) = \frac{\tau_o \left(1 - \frac{y}{h_o} \right) g_c}{\rho \frac{dV_x}{dy}} \tag{60}$$

where ν is the kinematic viscosity. In this context, ϵ is a number which describes any deviation from a purely laminar velocity profile by being not identically zero. As usual, ϵ must become zero at a wall, and anywhere the velocity derivative becomes zero. For any assumed profile, calculations using equation 60 will determine the value and behavior of ϵ. The quantity, ϵ, applies strictly to momentum transfer, but one usually assumes that the eddy diffusivities for momentum and mass transfer are equal.

The usual dimensional arguments suggest:

$$\epsilon = k^2 y^2 \frac{dV_x}{dy} \tag{61}$$

is successful for pipe flow. If von Karman's universal velocity distribution were used for the falling water film (refer to Appendix F), then

$$\frac{dV_x}{dy} = \frac{dU^+}{dy^+} \frac{U^*}{\nu} = \frac{5.0}{y^+} \frac{U^*}{\nu} ; \qquad 5 < y^+ < 30 \tag{62}$$

substituting equation 62 into equation 60 gives

$$(\nu + \epsilon) = \frac{\left(1 - \frac{y}{h_o}\right)\nu}{\frac{5.0}{y^+}} = \frac{\left(\frac{y}{h_o} - \frac{y^2}{h_o^2}\right)\sqrt{h_o^3 \, g \sin \beta}}{5.0} \tag{63}$$

The numerical values of ϵ from equation 63 were calculated using the kinematic viscosity of water at 24°C, and plotted in figure 21. The film thickness, h_o, required to use equation 63 was assumed to be the laminar film thickness. From laminar theory, the film thickness of the falling liquid

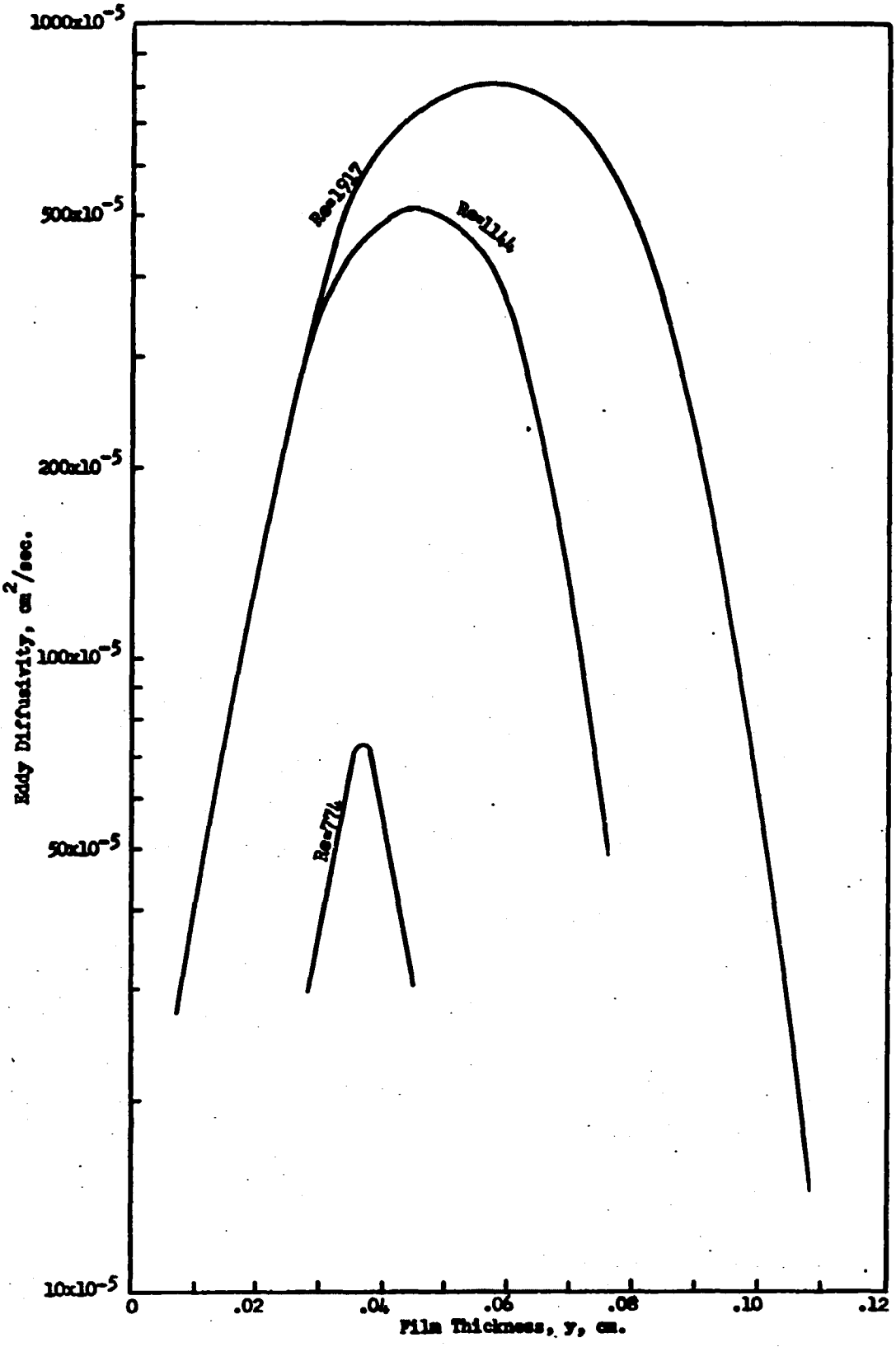

Figure 21. EDDY DIFFUSIVITIES CALCULATED FROM EQUATION 63, $\beta = 5^{\circ}$.

film is:

$$h_o^3 = \frac{3\nu Q}{g \sin \beta}$$

or
$$\sqrt{h_o^3 g \sin \beta} = \sqrt{3\nu Q} \qquad (64)$$

From the wave theory the film thickness is:

$$h_o^3 = \frac{3\nu Q}{g \sin \beta} \phi$$

or
$$\sqrt{h_o^3 g \sin \beta} = \sqrt{3\nu Q \phi} \qquad (65)$$

From equations 63, 64, and 65 the following conclusions are obtained:

1. The maximum total diffusivity should be located ~~at~~ the center of the water film.
2. At the same inclination angle, for the high Reynolds number, ~~and~~ the film thickness becomes larger. According to equations 63 and 64 the total diffusivity will increase when the Reynolds number increases.
3. At the same Reynolds number, when the inclination angle increases, according to equations 63 and 65, the total diffusivity will increase according to $\sqrt{\phi}$.

On the other hand, since

$$g_c \tau_o = \rho g \sin \beta \, h_o \qquad (66)$$

substitution into equations 58 and 59 yields:

$$h_o \, g \sin \beta \left(1 - \frac{y}{h_o} \right) = \left(\nu + k^2 y^2 \frac{dV_x}{dy} \right) \frac{dV_x}{dy} \qquad (67)$$

a non-linear differential equation. The first approximation

to the solution, probably adequate for this case is obtained in the following discussion. Assuming the velocity profile is parabolic, that is

$$V_x = \frac{g \sin \beta}{\nu} \left(h_o y - \frac{y^2}{2} \right) \tag{68}$$

and

$$\frac{dV_x}{dy} = \frac{g \sin \beta}{\nu} (h_o - y) \tag{69}$$

from equations 61 and 69 the total diffusivity will be

$$\epsilon = k^2 y^2 \frac{dV_x}{dy} = k^2 \frac{g \sin \beta}{\nu} (h_o y^2 - y^2)$$

$$= k^2 \frac{g}{\nu} h_o^3 \sin \beta \left(\frac{y^2}{h_o^2} - \frac{y^3}{h_o^3} \right) \tag{70}$$

where k is an universal constant. In order to find the maximum eddy diffusivity, equation 70 is differentiated with respect to y:

$$\frac{d\epsilon}{dy} = \frac{k^2 g \sin \beta}{\nu} (2h_o - 3y)y \tag{71}$$

When $y = 0$ $\quad \frac{d\epsilon}{dy} = 0$ and ϵ is a minimum.

$y = \frac{2}{3} h_o$ $\quad \frac{d\epsilon}{dy} = 0$ and ϵ is a maximum.

This suggests that the maximum eddy diffusivity is located at 2/3 of the total film thickness. The parabolic but non-laminar profile might be assumed from Jackson (16), so that the velocity would have the same form but use $V_s/V_o = 2.0$ instead of 1.5. The constant, k, could be calculated to

agree with the concentration profiles. Finally, one could utilize the profile suggested by Runstadler and obtain similar results.

It appears that a variety of ideas will give the observed behavior and no conclusions can be drawn about any of them. The use of "universal" profiles seems especially inappropriate since not even the normal hydrodynamic transition is observed. The modified laminar profile is purely conjectural, although it may be worth noting that the eddy function need not be strictly associated with turbulence. One concludes that the observed rise in diffusivity is consistent with moderate changes in the velocity profile whatever their cause, and that the most essential knowledge required for further studies is the velocity profile.

Levich (24) has proposed that a quiet film at the surface controls the diffusion process, even in turbulence. These results certainly support this idea, although clear definition of concentration profiles at the surface with pronounced waves was not possible. No suggestion has been made as to how the thickness of this film would be related to the film mechanics, nor how it would be modified as one proceeds from small Reynolds numbers to turbulent films.

Average Concentration of CO_2

The average concentrations of carbon dioxide in the falling water film at various cell locations were calculated from the titration data in the usual way. Sample calculations

are shown in Appendix D. The results are plotted in figures 22, 23, and 24.

The total amount of CO_2 transferred from gas phase into the liquid phase per unit time increased as the liquid flow rate and angle increased. The values of average CO_2 concentration for the laminar flow (without ripples) were calculated from Pigford and Johnstone's equation and shown in figure 22-24. The values were calculated using the experimental results for the film thickness because the comparison of mass transfer at equal Reynolds numbers is meaningful only if the films have the same velocity profile. If the Johnstone-Pigford equation were used without this correction, calculated exit concentrations would be in some cases larger than the experimental values. The measurements of Vyazovov as reported by Sherwood and Pigford (reference 35 page 267) are an example. Jepsen (17) assumed the initial concentration to be equal to the average concentration at some position in the cell and compared the resulting increase according to the Johnstone-Pigford theory with his experimental results. His method slightly underestimates the amount of mixing action. The comparison shows that the slope of the experimental values was greater than the slope of the calculated values at an angle of 25°, and was only slightly larger at an angle of 15° and about the same at 5°. The vertical difference between the experimental and theoretical values on the figure represents the effect of waves, bulk mixing and the increase in interfacial area. This difference was larger at higher

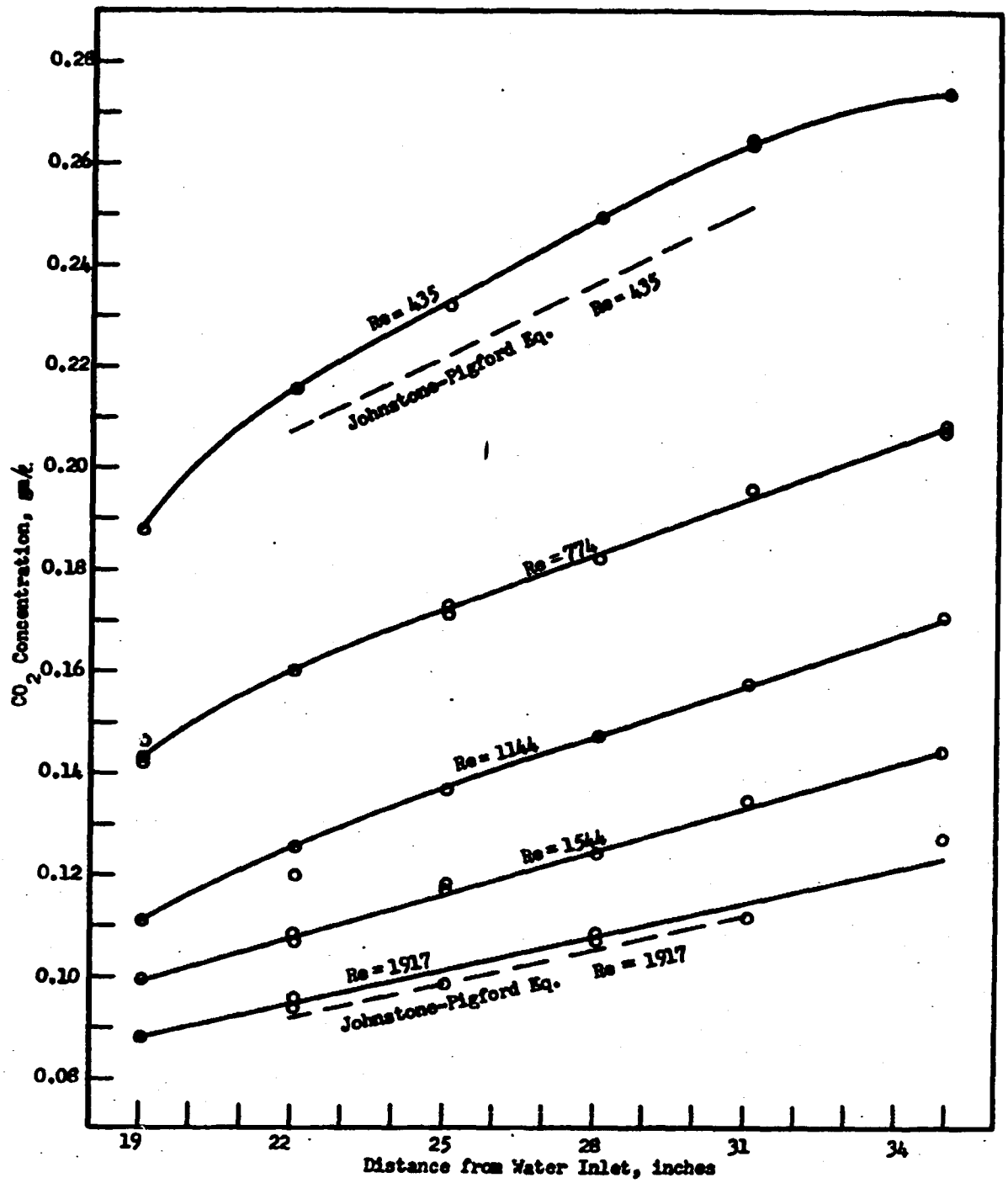

Figure 22. AVERAGE CO_2 CONCENTRATION. $\beta = 5^{\circ}$.

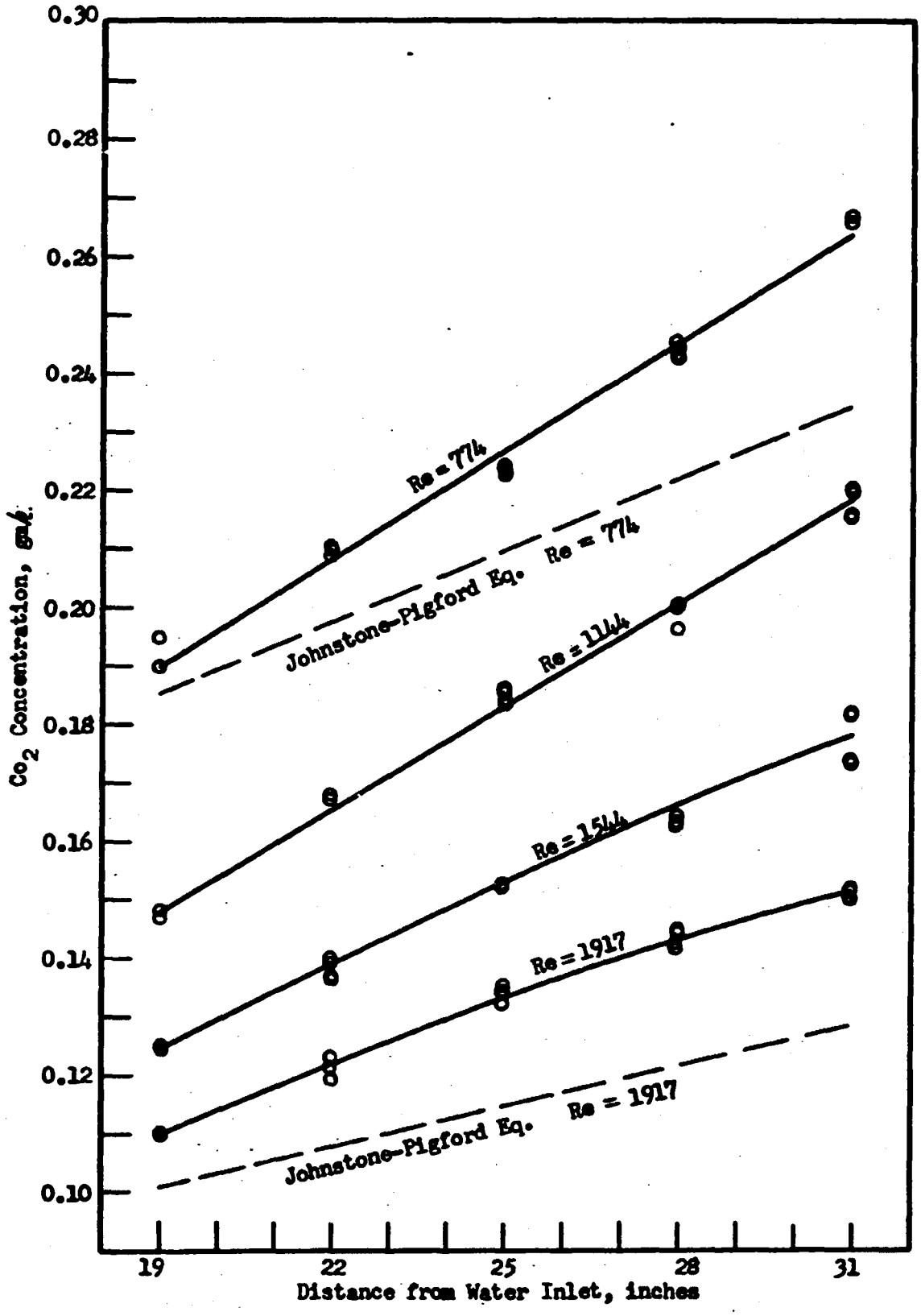

Figure 23. AVERAGE CO_2 CONCENTRATION. $\beta = 15^{\circ}$.

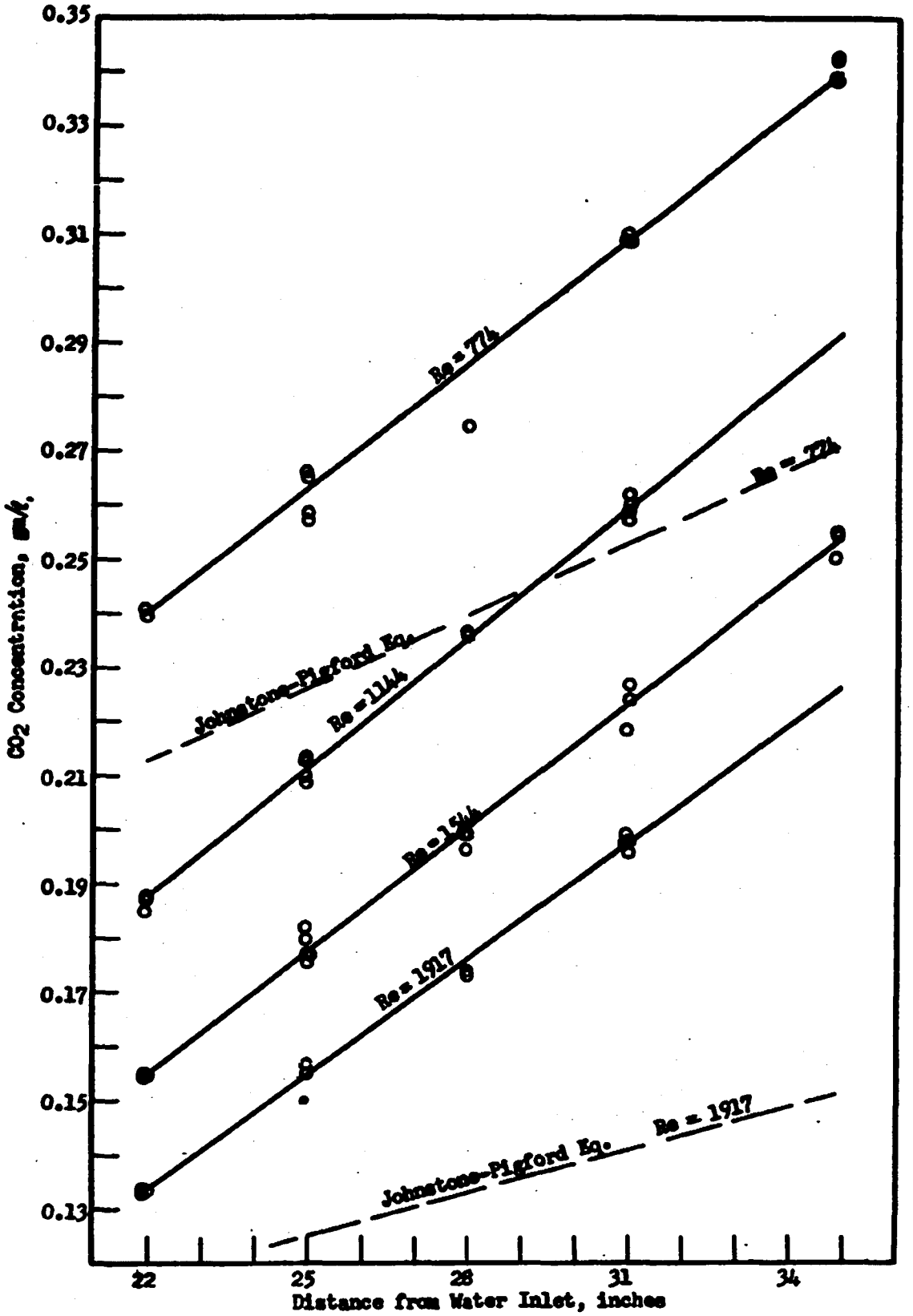

Figure 24. AVERAGE CO_2 CONCENTRATION. $\beta = 25°$.

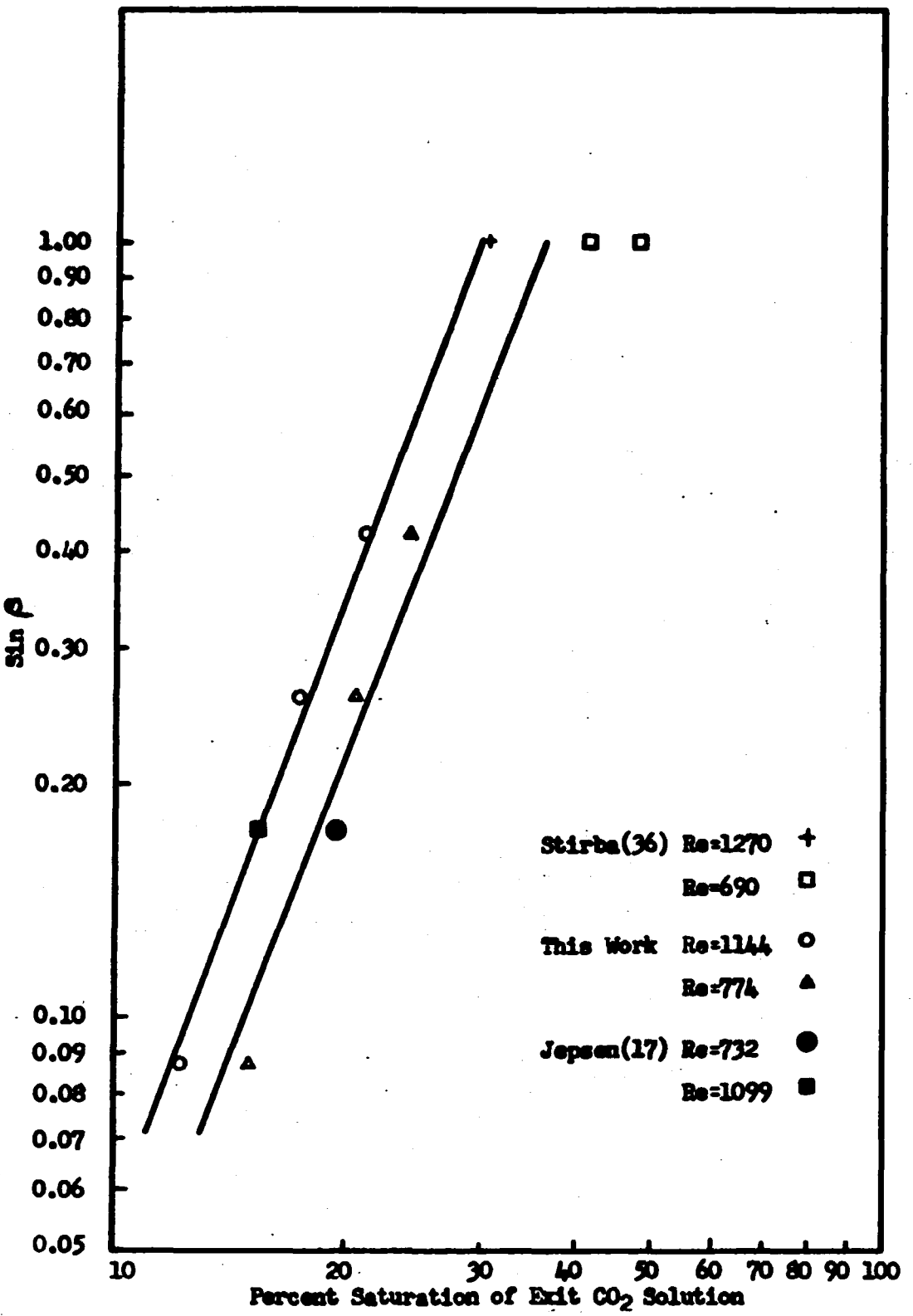

Figure 25. A COMPARISON OF AVERAGE EXIT CO_2 CONCENTRATION, FOR A 36 INCH CONTACTING ZONE.

inclination angle than at lower inclination angle. Thus, the effects of the wave and bulk mixing appear more clearly at higher inclination angle than at lower inclination angles. Furthermore, the eddy diffusivity must be a function of inclination angle and Reynolds number.

One of the purposes of this work was to establish a connection between the data obtained at angles below 25° and experimental results on vertical films. The total mass transfer measurements are essentially consistent with results obtained by others at 90°. According to laminar film diffusion theory a logarithmic plot of average exit concentration as the abscissa at constant Reynolds number should be a straight line as a function of the sine of the angle with a slope of 6 ~~(Ibid)~~.(reference 35 page 267).

Stirba (36) used a 36 inches long, 0.852 in I.D. tube to measure the exit concentration of pure CO_2 and water system at 31.2° to 31.5°C. His results were:

Re	% Saturation of Exit Liquid
380	56.8
690	41.5
690	48.1
1270	30.6

His results are compared with the results of this work in figure 25. The line is straight, with a slope of about 3; no correction for difference in Reynolds number was applied. This does not lead to any proper extrapolation of other results to vertical inclination. The average concentration seems consistent, but the other behavior, such as the

transition, film thickness variation, wave frequency and amplitude are not. The trends cannot be extrapolated to vertical inclinations with any degree of certainty.

The most significant results of the concentration measurements are that the magnitude of the total diffusivity and location of its maximum were functions of the angle of inclination and Reynolds number. Theoretical discussion showed that both laminar wave and turbulent interaction could explain such results.

If the large diffusivities obtained in the central region existed at the surface, this would imply far greater total mass transfer than was observed. Therefore, one concludes that a relatively quiet film at the surface must control the diffusion into the film.

CHAPTER VII

CONCLUSIONS

Mean film thickness and wave phase velocity, frequency and amplitude, for waves appearing on laminar falling films were found to be dependent on both angle of inclination and Reynolds number. Mean film thickness varied from 0% to 50% higher than theoretical prediction at Reynolds numbers greater than 1000 and the phase velocity was also slightly larger (10% at $\beta = 5°$). Experimental frequencies and amplitudes were lower than theoretical.

The experimental values of surface area increase due to the waves were slightly higher than theoretical values but generally not sufficient to account for the increase in mass transfer.

A maximum total diffusivity varying from 10 to 200 times the molecular diffusivity exists within the films. This diffusivity and its position changes with angle and Reynolds number. This behavior could be explained by either a modified laminar or turbulent velocity profile.

CHAPTER VIII

FUTURE RESEARCH

In order to obtain more accurate diffusivity data from the concentration profile and to make the theoretical analysis conclusive, it will be necessary to measure the velocity profile in the water film. Because the carbon dioxide diffusion process seems to be controlled at the surface of the water film, it becomes essential to know the true velocity profile near the interfacial surface. These measurements should establish whether the dynamic mechanisms were turbulent or modified laminar.

Film thickness and frequency at higher Reynolds number will be necessary to establish the nature of the transition Reynolds number. The wave velocities could be obtained by using two capacitometers, high speed moving pictures would establish the increase in interfacial surface area and provide a check on the increase measured by the capacitometer.

Measurements at low angles and velocities would establish more clearly how the interface behaves as the waves begin to appear, and whether the Johnson-Pigford equation is a proper basis for deciding whether the waves enhance the mass transfer.

BIBLIOGRAPHY

1. Benjamin, T. Brooke, "Wave Formation in Laminar Flow Down an Inclined Plane", J. Fluid Mechanics 2, 554, (1957).

2. Benjamin, T. Brooke, "The Development of Three Dimensional Disturbance in an Unstable Film of Liquid Down an Inclined Plane", J. Fluid Mechanics 10, 401, (1961).

3. Binnie, A. M., "Experiments on the Onset of Wave Formation on a Film of Water Flowing Down a Vertical Plate", J. Fluid Mechanics 2, 551, (1957).

4. Binnie, A. M., "Instability in a Slightly Inclined Water Channel", J. Fluid Mechanics 5, 561, (1959).

5. Bird, R. B., W. E. Stewart and E. N. Lightfoot, Transport Phenomena. New York: John Wiley and Sons, Inc., 1960.

6. Danckwerts, P. V., "Significance of Liquid Film Coefficients in Gas Absorption", Ind. & Eng. Chem. 43, 1460, (1951).

7. Davidson, J. F. and E. J. Cullen, "The Determination of Diffusion Coefficients for Sparingly Soluble Gases in Liquids", Trans. Instn. Chem. Engrs. 35, 51, (1957).

8. Dukler, A. E. and O. P. Bergelin, "Characteristics of Flow in Falling Liquid Films", Chem. Eng. Progress 48, 557, (1952).

9. Dukler, A. E., "Dynamics of Vertical Falling Film Systems", Chem. Eng. Progress 55, 62 (1959).

10. Emmert, R. E. and R. L. Pigford, "A Study of Gas Absorption in Falling Liquid Films", Chem. Eng. Progress 50, 87, (1954).

11. Friedman, S. J. and C. O. Miller, "Liquid Film in the Viscous Flow Region", Ind. & Eng. Chem. 33, 885, (1941).

12. Grimley, S. S., "Liquid Flow Conditions in Packed Towers", Trans. Instn. Chem. Engrs. 23, 228, (1945).

13. Hanratty, T. J. and A. Hershman, "Initiation of Roll Waves", AIChE Journal 7, 488, (1961).

14. Harvey, E. A., "The Absorption of CO_2 by a Quiescent Liquid", Ph.D. Thesis, University of London, 1958.

15. Hodgman, C. D., Handbook of Chemistry and Physics, 40th ed., Cleveland, Ohio: Chemical Rubber Publishing Co., 1958.

16. Jackson, M. L., "Liquid Film in Viscous Flow", AIChE Journal 1, 231, (1955).

17. Jepsen, J. C., "The Effect of Wave Induced Turbulence on the Rate of Absorption of Gases in Falling Liquid Films", Ph.D. Thesis, University of Oklahoma, 1964.

18. Kapitsa, P. L., "Zhurn. Eksper. Teoret. Fiz. 18, 3, (1948).

19. Kapitsa, P. L. and Kapitsa, S. P., Zhurn. Eksper. Teoret. Fiz. 19, 105, (1949).

20. Kapitsa, P. L., Zhurn. Eksper. Teoret. Fiz. 21, 964, (1951).

21. Knudsen, J. G. and D. L. Katz, Fluid Dynamics and Heat Transfer. New York: McGraw-Hill Book Co., Inc., 1958.

22. Konobeev, B. I., Malyusov, V. A. and Zhavoronkov, N. M., Dokl. Akad. Nauk. SSSR 117, 671, (1957).

23. Landau, L. D. and E. M. Lifshitz, Fluid Mechanics. Mass.: Addison-Wesley Pub. Co., 1959.

24. Levich, V. G., Physiochemical Hydrodynamics. Englewood Cliffs, N. J.: Prentice Hall, Inc., 1962.

25. Lin, C. C., The Theory of Hydrodynamics Stability. Cambridge University Press, 1955.

26. Lin, C. S., Ph.D. Thesis, University of Washington, 1952.

27. Lynn, S., "The Acceleration of the Surface of a Falling Film", AIChE Journal 6, 703, (1960).

27a. Mickley, H. S., Sherwood, T. S. and Reed, C. E., Applied Mathematics in Chemical Engineering. 2nd ed. New York: McGraw-Hill Book Co., Inc., 1957.

28. Nijsing, R. A. O. T., Hendriksz, R. H. and H. Kramers, "Absorption of CO_2 in Jets and Falling Film of Electrolyte Solutions, with and without Chemical Reaction", Chem. Eng. Science 10, 88, (1959).

29. Perry, J. H., Chemical Engineering Handbook, 3rd ed. New York: McGraw-Hill Book Co., Inc., 1950.

30. Portalski, S., "Study of Falling Liquid Film Flow", Chem. Eng. Science 18, 787, (1963).

30a. Portalski, S., Ph.D. Thesis, University of London, 1960.

31. Portalski, S., "Eddy Formation in Film Flow Down a Vertical Plate", Ind. & Eng. Chem. Fundamentals 3, 49, (1964).

32. Rossum, J. J. Van, "Experimental Investigation of Horizontal Liquid Film Wave Formation, Atomization, Film Thickness", Chem. Eng. Science, 11, 35, (1959).

33. Scriven, L. E. and R. L. Pigford, "Absorption into an Accelerating Film", AIChE Journal 4, 382, (1958).

34. Scriven, L. E. and R. L. Pigford, "One Phase Equilibrium at the Surface of the Gas-Liquid Interface", AIChE Journal 4, 439, (1958).

35. Sherwood, T. K. and R. L. Pigford, Absorption and Extraction. New York: McGraw-Hill Book Co., Inc., 1952.

35a. Sorum, C. H., Introduction to Semimicro Qualitative Analysis. Englewood Cliffs, N. J.: Prentice-Hall, Inc., 1960.

36. Stirba, C. and Hurt, D. M., "Turbulence in Falling Liquid Films", AIChE Journal 1, 178, (1955).

37. Struble, R. A., Nonlinear Differential Equations. New York: McGraw-Hill Book Co., Inc., 1962.

38. Tailby, S. R. and S. Portalski, "The Hydrodynamics of Liquid Films Falling on a Vertical Surface", Trans. Instn. Chem. Engrs., 38, 324, (1960).

39. Tailby, S. R. and S. Portalski, "The Optimum Concentration of Surface Active Agent for the Suppression of Ripples", Trans. Instn. Chem. Engrs., 39, 328, (1961).

40. Tailby, S. R. and S. Portalski, "Wave Inception on a Liquid Film Flowing Down a Hydrodynamically Smooth Plate", Chem. Eng. Science 17, 283, (1962).

41. Thomas, W. J. and S. Portalski, "Countercurrent Flow in Wall Columns", Ind. & Eng. Chem. 50, 1081, (1958).

42. Treadwell, F. P. and Hall, W. T., Analytical Chemical. New York: John Wiley and Sons, Inc., 1942.

43. Whitaker, S., "Effect of Surface Active Agents on the Stability of Falling Liquid Films", Ind. & Eng. Chem. Fundamentals 3, 132, (1964).

43a. Wilkes, J. O. and Nedderman, R. M., "The Measurement of Velocities in Thin Films of Liquid", Chem. Eng. Science 17, 177 (1962).

44. Yih, C. S., "Stability of Liquid Flow Down an Inclined Plane", Phys. Fluids 6, 321, (1963).

45. Zhivaikin, L. Y., "Liquid Film Thickness in Film-Type Unites", International Chemical Eng. 2, 37, (1962).

NOMENCLATURE

A,B	constant
C	concentration of CO_2, gram/liter
C_s	saturated concentration of CO_2, gram/liter
c	wave velocity, cm./sec.
D	diffusion coefficient, $cm.^2/sec.$
g	acceleration of gravity, $cm./sec.^2$
g_c	conversion to force units, $g.-cm./g._{force}-sec.^2$
G	function defined by equation 35-a
H	function defined by equation 35-b
h_o	mean film thickness in wavy flow, cm.
h	varying film thickness, cm.
j	function defined by equation 23
K	function defined by equation 22
k	constant used in equation 61
M	magnification ratio $M_1 = 98.384$ $M_2 = 37.258$
N	number of fringe shifts
N_s	number of fringe shifts that correspond to water saturated with CO_2
Q	volumetric flow rate, $cm.^3/cm.-sec.$
R	function defined by equation 32
Re	Reynolds number, $= 4\Gamma/\mu$

S interfacial area, $cm.^2$

ΔS %area increase caused by waves, ~~$cm.^2$~~

t time, sec.

U^+ dimensionless velocity, $= V_x/U^*$

U^* friction velocity, $= \sqrt{\frac{\tau_w g}{\rho}}$

V_o mean stream velocity at film thickness h_o from equation 17, cm./sec. $V_o = Q/h_o$

$\bar{V}$ mean stream velocity, cm./sec., defined by equation 1

V_x instantaneous velocity in the x direction, cm./sec.

V_y instantaneous velocity in the y direction, cm./sec.

x Cartesian coordinate, distance from leading edge of the flat bottom plate, cm.

X fringe spacing

y Cartesian coordinate; distance measured normal to the bottom plate, cm.

Y_{MF} average crest height, cm.

Y_{MT} average trough height, cm.

Y_T minimum trough height, cm.

α amplitude of wave motion

β angles of inclination of the cell

Γ mass flow rate, gr./cm.-sec.

ϵ eddy diffusivity, $cm.^2/sec.$

η value of y^+ at the interface

λ wave length, cm.

μ viscosity, gr./cm.-sec.

ν kinematic viscosity, $= \mu/\rho$, $cm.^2/sec.$

ρ density, $gr./cm.^3$

σ surface tension, dyne/cm.

τ shear stress, dyne/cm.^{2}

τ_o wall shear stress, dyne/cm.^{2}

ξ function defined by equation 27

φ function defined by equation 9

ω wave frequency, sec.$^{-1}$

δ Levich diffusion film thickness, cm.

APPENDIX A

EXPERIMENTAL VALUE OF WAVE PROPERTIES

angle of inclination = 5°
water temperature = 24°C
ρ = 0.9973 gr./cm.^{3}
μ = 0.9142 cp.

Q cm.^{3}/cm.-sec.	0.9977	1.775	2.622	3.538	4.393
Re	435	774	1144	1544	1917
h_o, inch	0.0203	0.0286	0.0352	0.0407	0.0448
cm.	0.0516	0.0726	0.0894	0.1034	0.1138
V_o, cm./sec.	19.34	24.45	29.33	34.22	38.60
c, cm./sec.	31.95	42.56	52.67	64.68	70.93
c/V_o	1.65	1.74	1.80	1.89	1.84
ω, sec.$^{-1}$	5.32	9.05	13.39	16.98	19.60
$K = \frac{\omega}{c} 2\pi$ rad./cm.	1.04	1.34	1.60	1.65	1.74
Y_{MF}, inch	0.0207	0.0312	0.0377	0.0434	0.0474
cm.	0.0527	0.0793	0.0957	0.1103	0.1204
Y_{MT}, inch	0.0196	0.0267	0.0326	0.0373	0.0419
cm.	0.0498	0.0678	0.0828	0.0947	0.1064
Y_T, inch	0.0137	0.0217	0.0288	0.0339	0.0393
cm.	0.0348	0.0551	0.0732	0.0861	0.0998
α	0.305	0.24	0.182	0.167	0.121

angle of inclination = 15°

Q $cm.^3/cm.-sec.$	0.9977	1.775	2.622	3.538	4.393
Re	435	774	1144	1544	1917
h_o, inch	0.0188	0.0264	0.0301	0.0350	0.0371
cm.	0.04775	0.0671	0.0765	0.0889	0.0942
V_o, cm./sec.	21.89	26.45	34.27	39.80	46.63
c, cm./sec.	49.38	63.20	73.23	80.44	
c/V_o	2.26	2.28	2.11	2.02	
ω, $sec.^{-1}$	6.77	15.73	24.50	31.85	39.70
$K = \frac{\omega}{c} 2\pi$ rad./cm.	0.86	1.56	2.11	2.49	
Y_{MF}, inch	0.0219	0.0299	0.0345	0.0382	0.0402
cm.	0.0556	0.0759	0.0876	0.0970	0.1021
Y_{MT}, inch	0.0173	0.0236	0.0294	0.0332	0.0350
cm.	0.0439	0.0599	0.0747	0.0843	0.0889
Y_T, inch	0.0158	0.0216	0.0270	0.0298	0.0320
cm.	0.0401	0.0549	0.0686	0.0757	0.0813
α	0.16	0.18	0.102	0.148	0.135

angle of inclination = 25°

Q $cm.^3/cm.-sec.$	0.9977	1.775	2.622	3.538	4.393
Re	435	774	1144	1544	1917
h_o, inch	0.0167	0.0223	0.0289	0.0318	0.0337
cm.	0.0424	0.0566	0.0733	0.0808	0.0855
V_o, cm./sec.	23.53	31.36	35.77	43.79	51.38

APPENDIX B

CONCENTRATION PROFILES

Séries A

Inclination angle = 5°

Water temperature = 24°C

Room temperature = 24° ± 2°C

Magnification ratio = 98.384

N_s = 2.8472

C_s = 1.415 gr. CO_2/liter

Run A16-1
Re = 272
Cell position 25

y, cm.	C, gr./l.
0.0051	0.368
0.0102	0.418
0.0152	0.502
0.0203	0.626
0.0254	0.808
0.0305	1.026
0.0330	1.145

Run A16-6
Re = 435
Cell position 25

y, cm.	C, gr./l.
0.0051	0.065
0.0102	0.085
0.0152	0.124
0.0203	0.184
0.0254	0.286
0.0305	0.445
0.0356	0.676
0.0373	0.768

Run A17-2
Re = 774
Cell position 25

y, cm.	C, gr./l.
0.0051	0.070
	0.070
0.0051	0.072
0.0203	0.085
0.0254	0.103
0.0305	0.147
0.0356	0.226
0.0407	0.354
0.0457	0.536
0.0508	0.584
0.0518	

Run A17-6
Re = 1144
Cell position 25

y, cm.	C, gr./l.
0.0051	0.268
0.0356	0.268
0.0407	0.277
0.0457	0.299
0.0508	0.340
0.0559	0.408
0.0610	0.506
0.0646	0.599

Run A18-3
Re = 1544
Cell position 25

y, cm.	C, gr./l.
0.0051	0.122
0.0508	0.122
0.0559	0.128
0.0610	0.154
0.0661	0.219
0.0711	0.336
0.0749	0.460

Run A18-5
Re = 1917
Cell position 25

y, cm.	C, gr./l.
0.0051	0.052
0.0559	0.052
0.0610	0.057
0.0661	0.090
0.0771	0.172
0.0754	0.281

Run A20-3
Re = 272
Cell position 28

y, cm.	C, gr./l.
0.0051	0.350
0.0102	0.403
0.0152	0.495
0.0203	0.638
0.0254	0.872
0.0272	0.915

Run A20-6
Re = 435
Cell position 28

y, cm.	C, gr./l.
0.0051	0.251
0.0102	0.271
0.0152	0.311
0.0203	0.378
0.0254	0.480
0.0305	0.628
0.0356	0.845
0.0396	1.069

Run A21-2
Re. = 774
Cell position 28

y, cm.	C, gr./l.
0.0051	0.224
0.0152	0.224
0.0203	0.226
0.0254	0.234
0.0305	0.241
0.0356	0.271
0.0407	0.338
0.0457	0.450
0.0508	0.611
0.0540	0.764

Run A21-5
Re. = 1144
Cell position 28

y, cm.	C, gr./l.
0.0051	0.442
0.0305	0.442
0.0356	0.442
0.0407	0.460
0.0457	0.485
0.0508	0.524
0.0559	0.581
0.0610	0.715
0.0647	0.917

Run A22-1
Re. = 1544
Cell position 28

y, cm.	C, gr./l.
0.0051	0.027
0.0508	0.027
0.0559	0.030
0.0610	0.035
0.0661	0.077
0.0711	0.191
0.0762	0.370
0.0770	0.393

Run A26-6
Re. = 1917
Cell position 28

y, cm.	C, gr./l.
0.0051	0.077
0.0508	0.077
0.0559	0.087
0.0610	0.100
0.0661	0.124
0.0711	0.161
0.0748	0.189

Run A26-7
Re. = 1917
Cell position 28

y, cm.	C, gr./l.
0.0051	0.050
0.0457	0.050
0.0508	0.057
0.0559	0.066
0.0610	0.077
0.0661	0.093
0.0711	0.112
0.0762	0.139
0.0813	0.180
0.0864	0.236
0.0901	0.292

Run A23-5
Re. = 435
Cell position 30

y, cm.	C, gr./l.
0.0051	0.221
0.0102	0.250
0.0152	0.293
0.0203	0.365
0.0254	0.475
0.0305	0.625
0.0356	0.795
0.0407	0.980
0.0448	1.139

Run A23-6
Re. = 435
Cell position 30

y, cm.	C, gr./l.
0.0051	0.264
0.0102	0.286
0.0152	0.316
0.0203	0.400
0.0254	0.502
0.0305	0.634
0.0356	0.793
0.0407	0.979
0.0457	1.185
0.0480	1.334

Run A24-1
Re. = 774
Cell position 30

y, cm.	C, gr./l.
0.0051	0.201
0.0152	0.201
0.0203	0.209
0.0254	0.221
0.0305	0.251
0.0356	0.297
0.0407	0.363
0.0457	0.452
0.0508	0.562
0.0545	0.656

Run A24-2
Re. = 774
Cell position 30

y, cm.	C, gr./l.
0.0051	0.181
0.0203	0.181
0.0254	0.186
0.0305	0.200
0.0356	0.234
0.0407	0.281
0.0457	0.368
0.0508	0.517
0.0559	0.708
0.0610	0.972
0.0616	1.004

Run A24-5
Re. = 1144
Cell position 30

y, cm.	C, gr./l.
0.0051	0.492
0.0305	0.492
0.0356	0.500
0.0407	0.514
0.0457	0.537
0.0508	0.572
0.0559	0.624
0.0610	0.713
0.0661	0.833
0.0711	0.973
0.0728	1.021

Run A27-2
Re. = 1544
Cell position 30

y, cm.	C, gr./l.
0.0051	0.181
0.0457	0.181
0.0508	0.186
0.0559	0.191
0.0610	0.199
0.0661	0.211
0.0711	0.243
0.0762	0.303
0.0813	0.413
0.0864	0.577
0.0915	0.840
0.0929	0.917

Run A25-6
Re. = 1917
Cell position 30

y, cm.	C, gr./l.
0.0051	0.174
0.0356	0.174
0.0407	0.181
0.0457	0.191
0.0508	0.201
0.0559	0.211
0.0610	0.236
0.0661	0.261
0.0711	0.291
0.0762	0.349
0.0813	0.452
0.0864	0.579
0.0894	0.654

Series G

Inclination angle = 5°

Water temperature = 24°C.

Room temperature = 24°C. ±2°C.

Magnification ratio = 37.258

N_s = 2.8472

C_s = 1.415 gr. CO_2/l.

Run G11-2
Re. = 435
Cell position 19

y, cm.	C, gr./l.
0.0107	0.00
0.0215	0.058
0.0322	0.184
0.0429	0.571
0.0533	1.208

Run G11-6
Re. = 774
Cell position 19

y, cm.	C, gr./l.
0.0107	0.420
0.0215	0.420
0.0322	0.430
0.0429	0.443
0.0537	0.549
0.0644	1.054
0.0611	1.072

Run G11-7
Re. = 774
Cell position 19

y, cm.	C, gr./l.
0.0107	0.408
0.0215	0.408
0.0322	0.413
0.0429	0.430
0.0537	0.516
0.0644	0.862
0.0668	0.997

Run G10-2
Re. = 1144
Cell position 19

y, cm.	C, gr./l.
0.0107	0.418
0.0429	0.418
0.0537	0.425
0.0644	0.488
0.0698	0.651
0.0751	0.880
0.0759	0.917

Run G10-5
Re. = 1544
Cell position 19

y, cm.	C, gr./l.
0.0107	0.022
0.0322	0.022
0.0429	0.030
0.0537	0.043
0.0644	0.060
0.0751	0.099
0.0852	0.170

Run G10-7
Re. = 1544
Cell position 19

y, cm.	C, gr./l.
0.0107	0.039
0.0322	0.039
0.0429	0.044
0.0537	0.055
0.0644	0.082
0.0751	0.138
0.0830	0.214

Run G9-2
Re. = 1917
Cell position 19

y, cm.	C, gr./l.
0.0107	0.460
0.0537	0.460
0.0644	0.462
0.0751	0.467
0.0859	0.500
0.0966	0.644
0.1065	1.061

Run G9-3
Re. = 1917
Cell position 19

y, cm.	C, gr./l.
0.0107	0.477
0.0537	0.477
0.0644	0.486
0.0751	0.503
0.0859	0.591
0.0967	1.019

Run G8-2
Re. = 435
Cell position 22

y, cm.	C, gr./l.
0.0107	0.400
0.0215	0.455
0.0322	0.591
0.0429	0.932
0.0523	1.428

Run G8-4
Re. = 435
Cell position 22

y, cm.	C, gr./l.
0.0107	0.370
0.0215	0.418
0.0322	0.532
0.0429	0.872
0.0515	1.387

Run G8-6
Re. = 774
Cell position 22

y, cm.	C, gr./l.
0.0107	0.071
0.0322	0.071
0.0429	0.077
0.0537	0.144
0.0590	0.296
0.0644	0.494
0.0662	0.561

Run G8-7
Re. = 774
Cell position 22

y, cm.	C, gr./l.
0.0107	0.062
0.0322	0.062
0.0429	0.072
0.0537	0.135
0.0590	0.244
0.0644	0.425
0.0673	0.549

Run G7-4
Re. = 1144
Cell position 22

y, cm.	C, gr./l.
0.0107	0.450
0.0429	0.450
0.0537	0.452
0.0644	0.469
0.0751	0.631
0.0860	0.999

Run G7-5
Re. = 1544
Cell position 22

y, cm.	C, gr./l.
0.0107	0.117
0.0537	0.117
0.0644	0.127
0.0751	0.164
0.0859	0.343
0.0894	0.465

Run G7-6
Re. = 1544
Cell position 22

y, cm.	C, gr./l.
0.0107	0.124
0.0537	0.124
0.0644	0.132
0.0751	0.176
0.0859	0.410
0.0908	0.607

Run G6-3
Re. = 1917
Cell position 22

y, cm.	C, gr./l.
0.0107	0.052
0.0537	0.052
0.0644	0.065
0.0751	0.084
0.0859	0.164
0.0913	0.350
0.0966	0.629
0.0996	0.847

Run G6-4
Re. = 1917
Cell position 22

y, cm.	C, gr./l.
0.0107	0.032
0.0537	0.032
0.0644	0.049
0.0751	0.077
0.0859	0.129
0.0966	0.321
0.1061	0.761

Run G6-5
Re. = 435
Cell position 25

y, cm.	C, gr./l.
0.0107	0.286
0.0215	0.326
0.0322	0.475
0.0376	0.609
0.0429	0.817
0.0483	1.109
0.0537	1.486

Run G6-7
Re. = 435
Cell position 25

y, cm.	C, gr./l.
0.0107	0.360
0.0215	0.401
0.0322	0.568
0.0376	0.716
0.0429	0.875
0.0483	1.248
0.0537	1.615

Run G5-2
Re. = 774
Cell position 25

y, cm.	C, gr./l.
0.0107	0.077
0.0322	0.077
0.0429	0.098
0.0537	0.207
0.0590	0.375
0.0644	0.604
0.0648	0.625

Run G5-3
Re. = 774
Cell position 25

y, cm.	C, gr./l.
0.0107	0.077
0.0322	0.077
0.0429	0.087
0.0537	0.181
0.0590	0.336
0.0644	0.545
0.0679	0.711

Run G5-5
Re. = 1144
Cell position 25

y, cm.	C, gr./l.
0.0107	0.027
0.0322	0.027
0.0429	0.039
0.0537	0.051
0.0644	0.108
0.0747	0.358

Run G5-6
Re. = 1144
Cell position 25

y, cm.	C, gr./l.
0.0107	0.049
0.0322	0.049
0.0429	0.059
0.0537	0.074
0.0644	0.191
0.0671	0.251

Run G4-4
Re. = 1544
Cell position 25

y, cm.	C, gr./l.
0.0107	0.196
0.0537	0.196
0.0644	0.214
0.0751	0.371
0.0758	0.390

Run G4-5
Re. = 1917
Cell position 25

y, cm.	C, gr./l.
0.0107	0.084
0.0537	0.084
0.0644	0.089
0.0751	0.103
0.0859	0.151
0.0966	0.430
0.0997	0.533

Run G2-2
Re. = 774
Cell position 28

y, cm.	C, gr./l.
0.0107	0.055
0.0215	0.055
0.0322	0.072
0.0429	0.110
0.0537	0.306
0.0644	0.852
0.0667	1.046

Run G2-4
Re. = 774
Cell position 28

y, cm.	C, gr./l.
0.0107	0.074
0.0215	0.074
0.0322	0.087
0.0429	0.147
0.0537	0.321
0.0644	0.698
0.0711	1.240

Run G2-5
Re. = 1144
Cell position 28

y, cm.	C, gr./l.
0.0107	0.754
0.0215	0.754
0.0322	0.760
0.0429	0.773
0.0537	0.798
0.0644	0.870
0.0751	1.163
0.0812	1.432

Run G2-6
Re. = 1144
Cell position 28

y, cm.	C, gr./l.
0.0107	0.724
0.0215	0.724
0.0322	0.732
0.0429	0.743
0.0537	0.768
0.0644	0.836
0.0751	1.079
0.0822	1.452

Run G1-2
Re. = 1544
Cell position 28

y, cm.	C, gr./l.
0.0107	0.414
0.0537	0.414
0.0644	0.414
0.0751	0.432
0.0859	0.465
0.0966	0.588
0.1050	0.912

Run G1-4
Re. = 1544
Cell position 28

y, cm.	C, gr./l.
0.0107	0.508
0.0429	0.408
0.0537	0.408
0.0644	0.414
0.0751	0.435
0.0859	0.455
0.0966	0.549
0.1010	0.621

Run G1-5
Re. = 1917
Cell position 28

y, cm.	C, gr./l.
0.0107	0.094
0.0644	0.094
0.0751	0.103
0.0859	0.109
0.0966	0.133
0.1074	0.226
0.1171	0.492

Series H

Inclination angle = 15°

Water temperature = 24°C.

Room temperature = 24°C ±2°C.

Magnification ratio = 37.258

N_s = 2.8472

C_s = 1.415 gr. CO_2/l.

Run H2-2
Re. = 774
Cell position 19

y, cm.	C, gr./l.
0.0161	0.464
0.0215	0.482
0.0268	0.774
0.0322	0.619
0.0331	0.614

Run H2-3
Re. = 774
Cell position 19

y, cm.	C, gr./l.
0.0161	0.503
0.0215	0.513
0.0268	0.551
0.0322	0.645
0.0376	0.831
0.0407	0.954

Run H2-5
Re. = 1144
Cell position 19

y, cm.	C, gr./l.
0.0107	0.197
0.0161	0.297
0.0215	0.313
0.0268	0.330
0.0304	0.369

Run H2-7
Re. = 1144
Cell position 19

y, cm.	C, gr./l.
0.0107	0.263
0.0161	0.263
0.0188	0.264
0.0215	0.291
0.0242	0.335
0.0274	0.393

Run H1-3
Re. = 1544
Cell position 19

y, cm.	C, gr./l.
0.0107	0.260
0.0161	0.260
0.0215	0.262
0.0268	0.273
0.0322	0.292
0.0376	0.321
0.0445	0.362

Run H1-4
Re. = 1544
Cell position 19

y, cm.	C, gr./l.
0.0107	0.285
0.0161	0.285
0.0215	0.290
0.0268	0.308
0.0331	0.369

Run H1-5
Re. = 1917
Cell position 19

y, cm.	C, gr./l.
0.0107	0.051
0.0161	
0.0215	0.051
0.0268	0.058
0.0322	0.064
0.0376	0.072
0.0429	0.085
0.0504	0.125

Run H5-5
Re. = 774
Cell position 2

y, cm.	C, gr./l.
0.0107	0.469
0.0161	0.469
0.0215	0.472
0.0268	0.496
0.0322	0.606
0.0363	0.665

Run H5-7
Re. = 774
Cell position 22

y, cm.	C, gr./l.
0.0107	0.457
0.0161	0.457
0.0215	0.458
0.0268	0.482
0.0328	0.580

Run H4-3
Re. = 1144
Cell position 22

y, cm.	C, gr./l.
0.0107	0.190
0.0161	0.190
0.0215	0.206
0.0268	0.231
0.0322	0.248
0.0376	0.267
0.0429	0.387
0.0467	0.537

Run H4-4
Re. = 1144
Cell position 22

y, cm.	C, gr./l.
0.0161	0.224
0.0215	0.243
0.0268	0.269
0.0322	0.322
0.0354	0.400

Run H4-6
Re. = 1544
Cell position 22

y, cm.	C, gr./l.
0.0107	0.123
0.0161	0.123
0.0215	0.125
0.0268	0.130
0.0322	0.138
0.0376	0.148
0.0429	0.169
0.0483	0.208
0.0537	0.281
0.0586	0.388

Run H3-3
Re. = 1917
Cell position 22

y, cm.	C, gr./l.
0.0161	0.454
0.0215	0.464
0.0268	0.483
0.0322	0.509
0.0376	0.553
0.0429	0.627
0.0442	0.653

Run H7-5
Re. = 774
Cell position 25

y, cm.	C, gr./l.
0.0107	0.163
0.0161	0.278
0.0188	0.355
0.0215	0.440
0.0245	0.544

Run H7-7
Re. = 774
Cell position 25

y, cm.	C, gr./l.
0.0107	0.150
0.0161	0.255
0.0188	0.321
0.0215	0.393
0.0242	0.467

Run H6-2
Re. = 1144
Cell position 25

y, cm.	C, gr./l.
0.0107	0.323
0.0161	0.337
0.0188	0.354
0.0215	0.385
0.0242	0.431
0.0282	0.533

Run H6-4
Re. = 1144
Cell position 25

y, cm.	C, gr./l.
0.0107	0.308
0.0161	0.325
0.0215	0.355
0.0268	0.409
0.0322	0.509
0.0376	0.584
0.0398	0.747

Run H6-7
Re. = 1544
Cell position 25

y, cm.	C, gr./l.
0.0107	0.132
0.0161	0.147
0.0215	0.172
0.0268	0.191
0.0322	0.216
0.0376	0.242
0.0429	0.276
0.0483	0.326
0.0537	0.448
0.0581	0.641

Run H5-2
Re. = 1917
Cell position 25

y, cm.	C, gr./l.
0.0107	0.316
0.0161	
0.0215	0.316
0.0268	0.321
0.0322	0.331
0.0376	0.343
0.0429	0.372
0.0483	0.460
0.0535	0.559

Run H9-2
Re. = 774
Cell position 28

y, cm.	C, gr./l.
0.0107	0.474
0.0161	0.501
0.0215	0.538
0.0242	0.558
0.0268	0.579
0.0301	0.604

Run H9-5
Re. = 1144
Cell position 28

y, cm.	C, gr./l.
0.0107	0.011
0.0161	0.027
0.0215	0.069
0.0268	0.114
0.0322	0.219
0.0340	0.480

Run H8-2
Re. = 1544
Cell position 28

y, cm.	C, gr./l.
0.0107	0.485
0.0161	0.494
0.0215	0.511
0.0268	0.534
0.0322	0.565
0.0379	0.611

Run H8-7
Re. = 1917
Cell position 28

y, cm.	C, gr./l.
0.0107	0.055
0.0161	0.055
0.0215	0.058
0.0268	0.062
0.0322	0.071
0.0376	0.083
0.0429	0.102
0.0483	0.127
0.0537	0.153
0.0590	0.191
0.0625	0.219

APPENDIX C

TOTAL DIFFUSIVITIES

Re. = 435
Run A16-6 & A20-6
Cell position 25 & 28

y cm	$(D + \epsilon) \times 10^5$ cm.^{2}/sec.
0.0051	
0.0152	
0.0254	2.57
0.0356	5.04
0.0433	7.95
0.0489	7.62
0.0503	7.32
0.0517	7.11

Re. = 435
Run A16-6 & A23-5
Cell position 25 & 30

y cm	$(D + \epsilon) \times 10^5$ cm.^{2}/sec.
0.0051	
0.0152	
0.0254	7.04
0.0356	12.90
0.0443	19.13
0.0489	21.18
0.0503	21.67
0.0517	22.31

Re. = 435
Run A20-6 & A23-5
Cell position 28 & 30

y cm.	$(D + \epsilon) \times 10^5$ cm.^{2}/sec.
0.0051	
0.0152	
0.0254	10.74
0.0356	17.4
0.0443	26.1
0.0489	28.3
0.0503	28.2
0.0517	28.1

Re. = 774
Run A17-2 & A21-2
Cell position 25 & 30

y cm.	$(D + \epsilon) \times 10^5$ cm.^{2}/sec.
0.0051	95.7
0.0152	137
0.0254	204
0.0356	111
0.0457	42.4
0.0553	22.4
0.0629	15.2
0.0691	10.8
0.0757	8.39

Re. = 774
Run A17-2 & A24-1
Cell position 25 & 30

y cm.	$(D + \epsilon) \times 10^5$ cm.^{2}/sec.
0.0051	
0.0152	
0.0254	10.67
0.0356	8.13
0.0457	9.73
0.0553	11.80
0.0629	12.54
0.0691	11.20
0.0757	

Re. = 1144
Run A17-6 & A21-5
Cell position 25 & 28

y cm.	$(D + \epsilon) \times 10^5$ cm.^{2}/sec.
0.0051	
0.0152	
0.0254	
0.0356	82.38
0.0457	170.8
0.0559	228.9
0.0661	181.8
0.0762	124.4
0.0821	92.84
0.0846	81.93
0.0884	65.20
0.0931	

Re. = 1144
Run A17-6 & A24-5
Cell position 25 & 30

y cm.	$(D + \epsilon) \times 10^5$ cm.^{2}/sec.
0.0254	
0.0356	
0.0457	21.14
0.0559	23.99
0.0661	25.46
0.0762	26.74
0.0821	30.21
0.0846	32.73
0.0884	37.07
0.0931	42.85

Re. = 1544
Run A21-5 & A24-5
Cell position 28 & 39

y cm.	$(D + \epsilon) \times 10^5$ cm.^{2}/sec.
0.0254	94.15
0.0356	113.8
0.0457	134.4
0.0559	167.9
0.0661	221.1
0.0762	210.1
0.0864	159.5
0.0931	120.5
0.0972	108.2
0.1021	103.5
0.1075	

Re. = 1544
Run A18-3 & A22-1
Cell position 25 & 28

y cm.	$(D + \varepsilon) \times 10^5$ cm.^{2}/sec.
0.0152	155.7
0.0254	191.4
0.0356	235.1
0.0457	291.3
0.0559	331.1
0.0661	367.5
0.0762	307.5
0.0864	127.1
0.0931	108.0
0.0972	87.1
0.1021	78.4
0.1075	78.8

Re. = 1917
Run A18-5 & A26-7
Cell position 25 & 28

y cm.	$(D + \varepsilon) \times 10^5$ cm.^{2}/sec.
0.0254	
0.0356	113.9
0.0457	182.3
0.0559	291.6
0.0661	273.9
0.0762	326.3
0.0864	425.6
0.0966	284.6
0.1042	196.4
0.1086	160.5
0.1123	128.8
0.1181	121.8

Re. = 1917
Run A18-5 & A25-6
Cell position 25 & 30

y cm.	$(D + \varepsilon) \times 10^5$ cm.^{2}/sec.
0.0254	
0.0356	
0.0457	123.0
0.0559	183.4
0.0661	291.1
0.0762	401.1
0.0864	383.1
0.0966	229.7
0.1042	163.6
0.1086	141.4
0.1123	127.9
0.1181	131.1

Re. = 1917
Run A25-6 & A26-7
Cell position 28 & 30

y cm.	$(D + \varepsilon) \times 10^5$ cm.^{2}/sec.
0.0254	
0.0356	
0.0457	66.6
0.0559	105.0
0.0661	155.8
0.0762	215.2
0.0864	231.9
0.0966	193.2
0.1042	166.1
0.1086	164.0
0.1123	172.5
0.1181	

Re. = 435
Run G11-2 & G8-2
Cell position 19 & 22

y cm.	$(D + \epsilon) \times 10^5$ cm.^{2}/sec.
0.01	3.05
0.015	9.09
0.02	15.5
0.025	20.2
0.03	17.4
0.035	15.4
0.04	12.9
0.045	10.7
0.05	8.4

Re. = 435
Run G6-5 & G3-6
Cell position 25 & 28

y cm.	$(D + \epsilon) \times 10^5$ cm.^{2}/sec.
0.01	
0.015	2.73
0.02	4.86
0.025	6.55
0.03	8.63
0.035	10.78
0.04	11.93
0.045	11.51
0.05	

Re. = 774
Run G11-6 & G2-2
Cell position 19 & 28

y cm.	$(D + \epsilon) \times 10^5$ cm.^{2}/sec.
0.02	
0.025	
0.03	2.05
0.035	3.78
0.04	4.04
0.045	4.36
0.05	4.91
0.055	5.94
0.06	6.36
0.065	

Re. = 774
Run G8-6 & G5-2
Cell position 22 & 25

y cm.	$(D + \epsilon) \times 10^5$ cm.^{2}/sec.
0.02	
0.025	
0.03	
0.035	3.73
0.04	10.25
0.045	15.18
0.05	13.77
0.055	17.54
0.06	13.45
0.065	

Re. = 774
Run G8-6 & G2-2
Cell position 22 & 28

y cm.	$(D + \varepsilon) \times 10^5$ cm.^{2}/sec.
0.02	
0.025	1.1
0.030	4.26
0.035	9.38
0.04	10.60
0.045	10.94
0.05	11.80
0.055	13.81
0.06	17.60
0.065	

Re. = 1144
Run G10-2 & G5-5
Cell position 19 & 25

y cm.	$(D + \varepsilon) \times 10^5$ cm.^{2}/sec.
0.02	
0.03	4.05
0.04	12.57
0.05	22.0
0.06	9.72
0.07	2.71
0.08	

Re. = 1144
Run G10-2 & G2-5
Cell position 19 & 28

y cm.	$(D + \varepsilon) \times 10^5$ cm.^{2}/sec.
0.02	
0.03	
0.04	4.58
0.05	14.04
0.06	9.65
0.07	3.40
0.08	

Re. = 1144
Run G7-4 & G2-6
Cell position 22 & 28

y cm.	$(D + \varepsilon) \times 10^5$ cm.^{2}/sec.
0.02	4.97
0.03	20.8
0.04	35.0
0.05	57.1
0.06	44.3
0.07	24.1
0.08	

Re. = 1544
Run G10-5 & G7-5
Cell position 19 & 22

y cm.	$(D + \epsilon) \times 10^5$ cm.^{2}/sec.
0.0067	
0.0201	35.2
0.0336	82.56
0.0470	144.2
0.0604	159.5
0.0738	115.9
0.0872	41.9
0.0943	36.6
0.0970	40.7
0.1020	51.5
0.1075	

Re. = 1917
Run G9-3 & G6-3
Cell position 19 & 22

y cm.	$(D + \epsilon) \times 10^5$ cm.^{2}/sec.
0.02	9.86
0.03	27.6
0.04	42.6
0.05	47.6
0.06	59.5
0.07	67.9
0.08	34.2
0.09	14.1
0.10	

Re. = 774
Run H5-5 & H9-2
Cell position 22 & 28

y cm.	$(D + \epsilon) \times 10^5$ cm.^{2}/sec.
0.0134	
0.0161	5.65
0.0188	20.96
0.0215	44.90
0.0242	75.62
0.0268	88.39
0.0295	87.92
0.0322	86.50
0.0348	
0.0376	

Re. = 774
Run H2-3 & H7-5
Cell position 19 & 25

y cm.	$(D + \epsilon) \times 10^5$ cm.^{2}/sec.
0.0134	
0.0161	3.36
0.0188	8.73
0.0215	20.57
0.0242	38.29
0.0268	58.14
0.0295	74.97
0.0322	89.67
0.0348	

Re. = 1144
Run H4-3 & H9-5
Cell position 22 & 28

y cm.	$(D + \epsilon) \times 10^5$ cm.^{2}/sec.
0.0134	
0.0161	
0.0188	5.42
0.0215	13.78
0.0242	23.89
0.0268	35.15
0.0295	47.36
0.0322	63.34
0.0348	82.72
0.0376	103.5
0.0403	126.2
0.0429	146.5

Re. = 1144
Run H4-3 & H6-2
Cell position 22 & 25

y cm.	$(D + \epsilon) \times 10^5$ cm.^{2}/sec.
0.0134	
0.0161	2.4
0.0188	7.9
0.0215	12.7
0.0242	17.3
0.0268	18.06
0.0295	17.3
0.0322	19.64
0.0348	31.29
0.0376	56.02
0.0403	90.92
0.0429	

Re. = 1144
Run H6-2 & H9-5
Cell position 25 & 28

y cm.	$(D + \varepsilon) \times 10^5$ cm.^{2}/sec.
0.0134	
0.0161	
0.0188	7.17
0.0215	27.08
0.0242	58.42
0.0268	82.02
0.0295	96.24
0.0322	112.5
0.0348	127.6
0.0376	146.2
0.0403	156.9
0.0429	

Re. = 1144
Run H6-4 & H9-5
Cell position 25 & 28

y cm.	$(D + \varepsilon) \times 10^5$ cm.^{2}/sec.
0.0134	
0.0161	4.04
0.0188	16.9
0.0215	40.65
0.0242	70.42
0.0268	99.26
0.0295	131.03
0.0322	170.16
0.0348	
0.0376	

Re. = 1544
Run H4-7 & H8-2
Cell position 22 & 28

y cm.	$(D + \varepsilon) \times 10^5$ cm.^{2}/sec.
0.0134	
0.0161	
0.0188	5.04
0.0215	13.07
0.0242	24.67
0.0268	40.33
0.0295	37.25
0.0322	60.98
0.0348	85.55
0.0376	110.89
0.0403	132.82
0.0429	145.58

Re. = 1544
Run H1-3 & H4-7
Cell position 19 & 22

y cm.	$(D + \varepsilon) \times 10^5$ cm.^{2}/sec.
0.0134	
0.0161	24.76
0.0188	50.61
0.0215	73.05
0.0242	91.83
0.0268	105.88
0.0295	115.90
0.0322	126.39
0.0348	127.25
0.0375	127.05
0.0403	131.41
0.0429	141.80
0.0456	155.0

Re. = 1544
Run H4-6 & H6-7
Cell position 22 & 25

y cm.	$(D + \epsilon) \times 10^5$ cm.^{2}/sec.
0.0134	
0.0161	
0.0188	11.44
0.0215	46.32
0.0242	108.72
0.0268	198.53
0.0295	312.0

Re. = 1917
Run H1-5 & H5-2
Cell position 19 & 25

y cm.	$(D + \epsilon) \times 10^5$ cm.^{2}/sec.
0.0188	34.03
0.0215	52.47
0.0242	75.63
0.0268	107.77
0.0295	149.84
0.0322	195.69
0.0348	240.12
0.0376	334.37
0.0403	327.6
0.0429	301.1
0.0456	251.47
0.0483	253.83
0.0510	294.95

APPENDIX D

TITRATION PROCEDURE

The error of the titration could be found by the following analysis: (42)(35a)

$$Ba^{++} + CO_2^{--} \rightleftharpoons BaCO_3 \quad (72)$$

$$OH^- + H^+ \rightleftharpoons H_2O \quad (73)$$

$$BaCO_3 + H_2O \rightleftharpoons Ba^{++} + HCO_3^- + OH^- \quad (74)$$

At 20°C., the solubility product of equation 72 is

$$K_s = [Ba^{++}][CO_3^{--}] = 1.6 \times 10^{-9} \quad (75)$$

and the ionization constant of the carbonic acid is

$$K_2 = \frac{[H^+][CO_3^{--}]}{[HCO_3^-]} = 4.8 \times 10^{-11} \quad (76)$$

and

$$K_w = [H^+][OH^-] = 1 \times 10^{-14} \quad (77)$$

From equations 75, 76 and 77, give

$$[Ba^{++}][HCO_3^-][OH^-] = \frac{K_s K_w}{K_2} = 3.33 \times 10^{-13} \quad (78)$$

The pH range of Phenolphthalein is 8.3 to 10. It means that the color of the solution will change from red to colorless while the concentration of hydrogen ion is decreased from $[H^+] = 10^{-8.3}$ to $[H^+] = 10^{-10}$ or the hydroxide ion is increased from $[OH^-] = 10^{-5.7}$ to $[OH^-] = 10^{-4}$. Substituting the $[OH^-]$ ion concentration into equation 78 gives $[Ba^{++}][HCO_3^-] = 3.33 \times 10^{-7}$ (red) to 3.33×10^{-9} (colorless). Therefore a little excess of $BaCl_2$ solution being added to the sample will decrease the error to negligible.

APPENDIX E

FILM THICKNESS OF ACCELERATING FALLING FILM

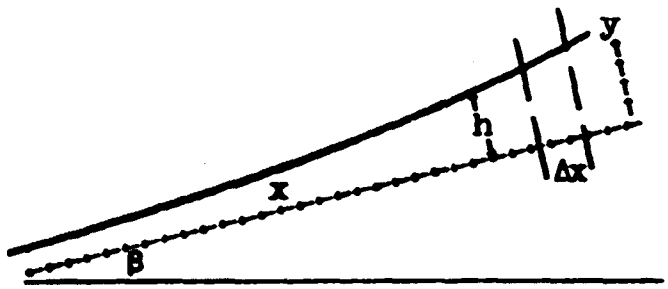

Let h = instantaneous height of the water film near the water entrance

h_o = average film thickness

Assuming near the water entrance, the velocity profile in the water film is parabolic

$$V_x = 3\bar{V}\left(\frac{y}{h} - \frac{y^2}{2h^2}\right)$$

$$= \frac{3Q}{h^3}\left(hy - \frac{y^2}{2}\right) \qquad (79)$$

Momentum balance over Δx gives

$$\frac{\partial}{\partial x}\int_o^h \rho V_x^2\, dy = \rho h g \sin\beta - \mu\left(\frac{\partial V_x}{\partial y}\right)_{y=0} - h\frac{\partial P}{\partial x} \qquad (80)$$

From equation 79 gives

$$\left(\frac{\partial V_x}{\partial y}\right)_{y=0} = \frac{3Q}{h^2} \qquad (81)$$

and

$$\frac{\partial}{\partial x}\int_o^h \rho V_x^2\, dy = -\frac{6}{5}\frac{Q^2\rho}{h^2}\frac{\partial h}{\partial x} \qquad (82)$$

From equation 4 gives

$$\frac{\partial P}{\partial x} = \rho g \cos \beta \frac{\partial h}{\partial x} - \sigma \frac{\partial^3 h}{\partial x^3} \qquad (83)$$

Substituting equations 81, 82, 83 in equation 80 gives

$$\sigma h h''' + \left(\frac{6}{5} \frac{Q^2 \rho}{h_o^3} - h\rho g \cos \beta \right) h' + \rho g h \sin \beta - \mu \frac{3Q}{h^2} = 0 \qquad (84)$$

Multiply equation 84 by h^2/h_o^3

$$\sigma \frac{h^3}{h_o^3} h''' + \left(\frac{6Q^2\rho}{5h_o^3} - \frac{h^3}{h_o^3} \rho g \cos \beta \right) h' + \rho g \sin \beta \frac{h^3}{h_o^3} - \mu \frac{2Q}{h_o^3} = 0 \qquad (85)$$

From equation 28 gives

$$Q = \frac{g \sin \beta}{3\nu} h_o^3$$

and let $$H = \frac{h}{h_o} \; ; \quad X = \frac{x}{h_o}$$

Equation 85 becomes

$$\frac{\sigma}{\rho g \sin \beta \, h_o^2} H^3 H''' + \left(\frac{2Q}{5\nu} - \cot \beta \, H^3 \right) H' + H^3 - 1 = 0 \qquad (86)$$

If $$h/h_o = H = 1 + \theta$$

where θ is a small value, and $Re = 4Q\rho/\mu$. Equation 86 becomes

$$\frac{\sigma}{\rho g \sin \beta \, h_o^2} \theta''' + \left(\frac{Re}{10} - \cot \beta \right) \theta' + 3\theta = 0 \qquad (87)$$

If both Reynolds number and inclination angle are small, then

$$\left(\frac{Re}{10} - \cot \beta \right) \to 0$$

equation 87 becomes

$$\frac{\sigma}{\rho g \sin \beta \, h_o^2} \theta''' + 3\theta = 0 \qquad (88)$$

In this thesis, the longest region for the acceleration of the water film at the entrance was at $\beta = 5^\circ$ and $Re = 435$. Substituting these values into equation 87 gives

$$3170\theta''' + 32.2\theta' + 3\theta = 0 \qquad (89)$$

Assuming $3170\theta'''$ is negligible, then equation 89 becomes

$$10.7\theta' + \theta = 0 \qquad (90)$$

Boundary conditions are: when $X = 0$ $\quad \theta = \theta_o$

$$X = \infty \quad \theta = 0$$

The solution of equation 90 is

$$\theta = \theta_o e^{-X/10.7} \qquad (91)$$

The values of θ/θ_o vs X are listed in the following table.

X	0	10	10.7	20	50	100
θ/θ_o	1	0.393	0.368	0.154	0.009	0.00009

From the above table, it is easy to find out that at $\beta = 5^\circ$, $Re = 435$, gives

$$X = x/h_o = 100$$

$$\theta/\theta_o = 0.00009$$

or, $$x = 100\ h_o = 100 \cdot 0.0516 = 5.16 \text{ cm.}$$

$$h/h_o = 1 + \theta = 1 + 0.00009\ \theta_o$$

This shows that at 5.16 cm. away from the water entrance, the value of h/h_o is near to one.

APPENDIX F

COMPARISON OF THE VELOCITY PROFILE

For laminar flow

$$V_x = 3V_o \left(\frac{y}{h_o} - \frac{y^2}{2h_o^2} \right) = \frac{g \sin \beta}{\nu} \left(h_o y - \frac{y^2}{2} \right) \qquad (92)$$

Let

$$U^+ = V_x / U^* \qquad (38)$$

$$y^+ = yU^*/\nu \qquad (39)$$

where $$U^* = \sqrt{\frac{\tau_w g}{\rho}} = \sqrt{\frac{h_o \rho \sin \beta \, g}{\rho}} = \sqrt{h_o g \sin \beta} \qquad (93)$$

Substituting equations 92, 39, 93 in equation 38

$$U^+ = \frac{g \sin \beta}{\nu U^*} \left(h_o y^+ \frac{\nu}{U^*} - y^{+2} \frac{\nu^2}{U^{*2} g} \right) = y^+ - \frac{\nu}{2\sqrt{h_o^3 \, g \sin \beta}} y^{+2}$$

$$= y^+ - \frac{1}{2\eta} y^{+2} \qquad (94)$$

For turbulent flow

$$U^+ = y^+ \qquad y^+ < 5 \qquad (40)$$

$$U^+ = -30.5 + 5.0 \ln y^+ \qquad 5 < y^+ < 30 \qquad (41)$$

$$U^+ = 5.5 + 2.5 \ln y^+ \qquad 30 < y^+ < \eta \qquad (42)$$

Equations 94, 40, 41, and 42 are plotted in Figure 26.

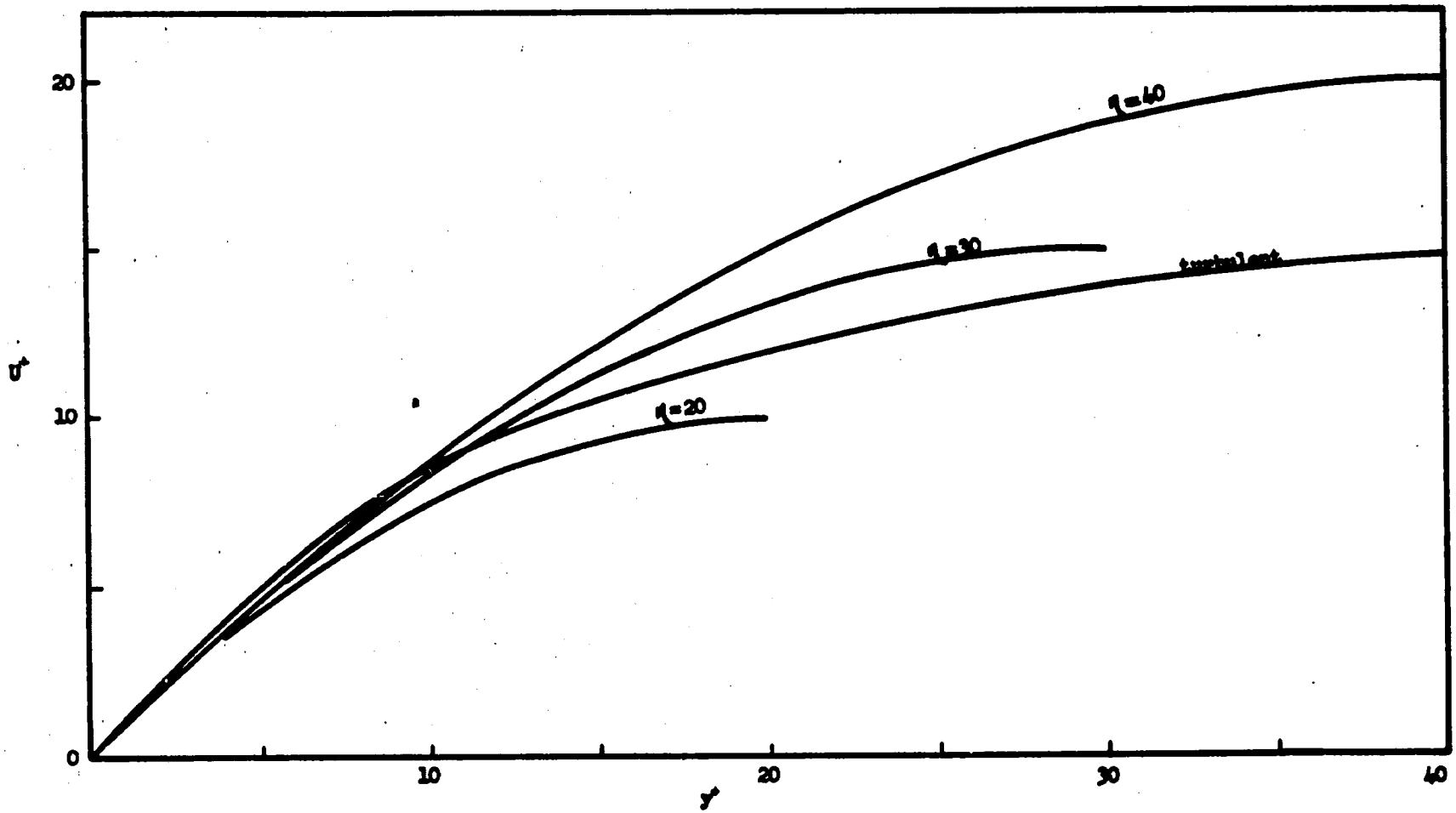

Figure 26. VELOCITY PROFILES.

APPENDIX G

COMPARISON OF DIFFERENT THEORETICAL FILM THICKNESSES OF FALLING WATER FILMS

Temperature = 24°C.
ρ = 0.9973 gr./cm.^{3}
μ = 0.9142 cp.
Film thickness in inches

$\beta = 5°$

Re	435	744	1144	1544	1917
Laminar	0.0269	0.0328	0.0371	0.0408	0.0439
Dukler	0.0259	0.0324	0.0381	0.0434	0.0483
Portalski	0.0251	0.0326	0.0391	0.0453	0.0504
Equation 28	0.0235	0.0287	0.0325	0.0357	0.0384

$\beta = 15°$

Laminar	0.0187	0.0228	0.0258	0.0285	0.0306
Dukler	0.0180	0.0226	0.0265	0.0302	0.0336
Portalski	0.0174	0.0228	0.0272	0.0313	0.0351
Equation 28	0.0164	0.0200	0.0226	0.0249	0.0268

$\beta = 25°$

Laminar	0.0159	0.0194	0.0219	0.0242	0.0260
Dukler	0.0151	0.0191	0.0225	0.0256	0.0286
Portalski	0.0148	0.0193	0.0231	0.0267	0.0298
Equation 28	0.0139	0.0170	0.0192	0.0212	0.0228

APPENDIX H

DERIVATION OF EQUATION 37 AND THE VALUES OF INCREASE IN INTERFACIAL AREA

I. Proof of $dy/dx < 1$:

From equations 9 and 24 gives

$$y = h_o(1 + \varphi)$$

$$= h_o\left(1 + \alpha \sin Kx + \frac{\alpha^2 j}{12 K^2} \cos 2Kx\right) \qquad (9)$$

$$y' = h_o\left(\alpha K \cos Kx - \frac{\alpha^2 j}{6K} \sin 2Kx\right) \qquad (95)$$

Since $j/K^2 = 3$ equation 95 becomes

$$y' = h_o \alpha K \cos Kx \,(1 - \alpha \sin Kx) \qquad (96)$$

Let $\alpha = 0.5$ and $c/V_o = 2.0$ gives

$$K^2 = \frac{V_o^2 \,(c/V_o - 1)(c/V_o - 0.9) - h_o g \cos \beta}{\sigma h_o/\rho}$$

$$= 1.1 \, V_o^2/\sigma h_o \qquad (97)$$

From equations 17 and 28 gives

$$V_o^2 = \frac{h_o Q g \sin \beta}{3\nu\rho} \qquad (98)$$

Substituting equation 98 into equation 97 gives

$$K^2 = 0.4 \, \frac{Qg \sin \beta}{\nu\sigma} \qquad (99)$$

The maximum Q used in this thesis is 4.4. Substituting equation 99 into equation 96 gives

$$y' = h_o \cdot 0.5 \sqrt{0.4 \, \frac{4.4 \cdot 980 \sin \beta}{0.00941 \cdot 72.13}} \cos Kx \,(1 - \alpha \sin Kx)$$

$$= 25.6 \, h_o \sqrt{\sin \beta} \cos Kx \,(1 - \alpha \sin Kx) \qquad (100)$$

In order to find the maximum value of y', let

$$F = \cos x \,(1 - 0.5 \sin x)$$

$$F' = -\sin x \,(1 - 0.5 \sin x) - \cos x \,(0.5 \cos x) = \sin^2 x - \sin x - 0.5$$

when $F' = 0$ gives $\sin x = 1.36$ or -0.4

when $\sin x = -0.4$ gives $\cos x = 0.9$ and $F = 1.08$. Substituting the above values into equation 100 gives

$$y' = 27.8\, h_o \sqrt{\sin \beta}$$

That is, as long as $h_o \sqrt{\sin \beta} < 0.036$ then $y' < 1$

II. Derivation of equation 37

From equation 36 gives

$$\Delta S = \frac{1}{\lambda}\int_o^\lambda \frac{1}{2} y'^2 dx - \frac{1}{\lambda}\int_o^\lambda \frac{1}{8} y'^4 dx + \frac{1}{\lambda}\int_o^\lambda \frac{1}{16} y'^6 dx \qquad (36)$$

where $$y' = G \cos Kx - H \sin 2Kx \qquad (34)$$

$$y'^2 = G^2 \cos^2 Kx - 2GH \cos Kx \sin 2Kx + H^2 \sin^2 2Kx$$

Therefore the first term of equation 36 becomes

$$\frac{1}{\lambda}\int_o^\lambda \frac{1}{2} y'^2 dx = \frac{1}{2\lambda}\left[\frac{G^2}{K}\int_o^\lambda \cos^2 Kx\, dKx \right.$$

$$\left. - \frac{4GH}{K}\int_o^\lambda (1 - \sin^2 Kx)\sin Kx\, dx + \frac{H^2}{2K}\int_o^\lambda \sin^2 2Kx\, d2Kx \right.$$

$$= \frac{1}{2\lambda}\left[\frac{G^2}{K}\frac{1}{2}K\lambda + \frac{H^2}{2K}\frac{1}{2}2K\lambda \right] = \frac{1}{4}(G^2 + H^2)$$

$$y'^4 = G^4 \cos^4 Kx - 4G^3 \cos^3 Kx\, H \sin 2Kx + 6G^2 \cos^2 Kx\, H^2 \sin^2 2Kx$$
$$- 4G \cos Kx\, H^3 \sin^3 2Kx + H^4 \sin^4 2Kx$$

The second term of equation 36 becomes

$$\frac{1}{\lambda}\int_0^{\lambda}\frac{1}{8}y'^4dx = \frac{1}{8\lambda}\left[\frac{G^4}{K}\int_0^{\lambda}\cos^4 Kx\,dKx - \frac{8G^3H}{K}\int_0^{\lambda}\cos^4 Kx\sin Kx\,dKx \;\to 0\right.$$

$$+\frac{6G^2H^2}{K}\int_0^{\lambda}4(\cos^4 Kx - \cos^6 Kx)dKx$$

$$-\frac{32GH^3}{K}\int_0^{\lambda}\cos^4 Kx\sin^3 Kx\,dKx \;\to 0$$

$$\left.+\frac{H^4}{2K}\int_0^{\lambda}\sin^4 2Kx\,d2Kx\right] = \frac{3}{64}(G^2+H^2)^2 + \frac{3}{32}G^2H^2$$

$$y'^6 - G^6\cos^6 Kx - 6G^5\cos Kx\,H\sin 2Kx + 15\,G^4\cos^4 Kx\,H^2$$
$$\cdot\sin^2 2Kx - 20\,G^3\cos^3 Kx\,H^3\sin^3 2Kx + 15\,G^2\cos^2 Kx\,H^4$$
$$\cdot\sin^4 2Kx - 6G\cos Kx\,H^5\sin^5 2Kx + H^6\sin^6 2Kx$$

The third term of equation 36 becomes

$$\frac{1}{\lambda}\int_0^{\lambda}\frac{1}{16}y'^6dx = \frac{1}{16K\lambda}\left[\frac{5}{16}G^6 + \frac{15\times4}{16}G^4H^2 + \frac{15\times3}{16}G^2H^4 + \frac{5}{16}H^6\right]$$

$$= \frac{5}{256}(G^2+H^2)^3 + \frac{45}{256}G^4H^2 + \frac{30}{256}G^2H^4$$

After substituting all these values into equation 36 gives

$$\Delta S = \frac{1}{4}(G^2+H^2) - \frac{3}{64}(G^2+H^2)^2 + \frac{5}{256}(G^2+H^2)^3$$
$$-\frac{3}{64}G^2H^2\left(1 - \frac{15}{4}G^2 - \frac{10}{4}H^2\right)$$

Both G and H are small values and less than 1. Therefore

$$\Delta S = \frac{1}{4}(G^2+H^2) - \frac{3}{64}(G^2+H^2)^2 + \frac{5}{256}(G^2+H^2)^3 - \ldots \quad (37)$$

III. Surface area increase, %

Re	435	774	1144	1544	1917
$\beta = 5°$	0.7	2.31	4.57	7.79	10.8
$\beta = 15°$	1.54	3.47	6.31	9.09	12.1
$\beta = 90°$	4.69		12.27		20.03

Portalski

Re	442	530	619	1060	1414	1766
$\beta = 90°$	5.1	6.9	8.7	21.7	36.2	52.2

IV. Calculation of the experimental value of ΔS:

Let
$$y = \alpha \sin Kx \tag{101}$$
$$y' = \alpha K \cos Kx \tag{102}$$

Then the length of the arc from $x = 0$ to $x = \lambda$ is given by

$$L = \int_0^{\lambda} \sqrt{1 + \alpha^2 K^2 \cos^2 Kx}\, dx$$

$$= \frac{\sqrt{1 + \alpha^2 K^2}}{K} \int_0^{\lambda} \sqrt{1 - \frac{\alpha^2 K^2}{1 + \alpha^2 K^2} \sin^2 Kx}\, dKx \tag{103}$$

where K is the wave number, α is the amplitude and λ is the wave length. Let

$$Kx = \theta$$

$$\frac{\alpha^2 K^2}{1 + \alpha^2 K^2} = a^2$$

$$\frac{\sqrt{1 + a^2K^2}}{K} = b$$

equation 103 becomes

$$L = b \int_0^{K\lambda} \sqrt{1 - a^2 \sin^2\theta}\, d\theta \qquad (104)$$

Equation 104 is elliptic integrals of the second kind. The values of L are listed on pages 234-237 of reference 15. One wave trace at inclination angle of 5° with a Reynolds number of 774 was measured by fitting 24 inches of thread on to the wave curve, and the length of the base line is 20.25". The chart speed is 10''/sec., the wave velocity is 16.75"/sec. The wave number is 1.336, the theoretical amplitude is 0.6, and one inch of the visicorder reading corresponds to 0.016" air gap. The correct factor for the thread fitting method is found by the following procedures.

From equation 101

$$y = 0.6 \sin 1.336x \qquad (105)$$

After correct by velocity difference and visicorder reading difference, gives

$$y = 0.6 \cdot 0.016 \sin 1.336 \frac{x}{1.675} \qquad (106)$$

By means of equation 104 the arc length of equation 105 is

$$L = 1.8 \text{ (for x from 0 to } \pi/2)$$

The arc length of equation 106 is

$$L = 1.57 \text{ (for x from 0 to } \pi/2)$$

Correct factor = 1.8/1.57 = 1.145

Real curve length = 24"/1.145 = 20.95 inch

$$\Delta S = \frac{20.95 - 20.25}{20.25} \times 100\% = 3.46\%$$

APPENDIX I

DERIVATION OF EQUATIONS 31 AND 33

From equation 24 gives

$$\varphi = \alpha \sin Kx + \frac{\alpha^2 j}{12 K^2} \cos 2Kx$$

$$= \alpha \sin Kx + \alpha^2 R \cos 2Kx \qquad (24\text{-a})$$

where $R = \frac{1}{12} \frac{j}{K^2}$ and $K\lambda = 2\pi$

$$\frac{1}{\lambda} \int_0^\lambda \varphi \, dx = 0$$

$$\frac{1}{\lambda} \int_0^\lambda \varphi^2 dx = \frac{\alpha^2}{2} + \frac{\alpha^4}{2} R^2$$

$$\frac{1}{\lambda} \int_0^\lambda \varphi^3 dx = -\frac{3}{4} \alpha^4 R$$

$$\frac{1}{\lambda} \int_0^\lambda \varphi^4 dx = \frac{3}{8} \alpha^4 + \frac{3}{2} \alpha^6 R^2 + \frac{3}{8} \alpha^8 R^4$$

$$\frac{1}{\lambda} \int_0^\lambda \varphi^5 dx = -\frac{5}{4} \alpha^6 R - \frac{15}{8} \alpha^8 R^3$$

$$\frac{1}{\lambda} \int_0^\lambda \varphi^6 dx = \frac{5}{16} \alpha^6 R + \frac{105}{32} \alpha^8 R^2 + \frac{45}{16} \alpha^{10} R^4 + \frac{5}{16} \alpha^{12} R^6$$

$$\frac{1}{\lambda} \int_0^\lambda \varphi^7 dx = \frac{105}{64} \alpha^8 R - \frac{105}{16} \alpha^{10} R^3 - \frac{105}{32} \alpha^{12} R^5$$

$$\frac{1}{\lambda}\int_0^{\lambda} \varphi^8 dx = \frac{35}{128}\alpha^8 + \frac{35 \times 13}{80}\alpha^{10}R^2 + \frac{35 \times 11}{32}\alpha^{12}R^4$$

$$\frac{1}{\lambda}\int_0^{\lambda} \varphi^9 dx = -\frac{63}{32}\alpha^{19}R - \frac{21 \times 23}{32}\alpha^{12}R^3$$

$$\frac{1}{\lambda}\int_0^{\lambda} \varphi^{10} dx = \frac{63}{64 \times 4}\alpha^{10} + \frac{45 \times 49}{64 \times 4}\alpha^{12}R^2$$

$$\frac{1}{\lambda}\int_0^{\lambda} \varphi^{11} dx = -\frac{63 \times 55}{16 \times 12 \times 8}\alpha^{12}R$$

$$\frac{1}{\lambda}\int_0^{\lambda} \varphi^{12} dx = \frac{21 \times 11}{64 \times 16}\alpha^{12}$$

Both R and α are less than 1 and all the terms containing α^{14}, α^{16}, etc. are negligible. Substituting the above values in equation 30 give

$$\begin{aligned}
\Phi = {} & 1 + 3\alpha^2 + (3R^2 + 7.5R + 5.625)\alpha^4 + (22.5R^2 + 26.25R + 8.75)\alpha^6 \\
& + (5.625R^4 + 39.375R^3 + 91.875R^2 + 59.06R + 12.30)\alpha^8 \\
& + (78.75R^4 + 236.25R^3 + 255.94R^2 + 108.28R + 16.242)\alpha^{10} \\
& + (8.75R^6 + 118.15R^5 + 54.14R^4 + 830.15R^3 + 568.5R^2 \\
& \quad + 351.9R + 20.528)\alpha^{12} \\
& - c/V_o[3\alpha^2 + (3R^2 + 9R + 7.5)\alpha^4 \\
& \qquad + (30R^2 + 37.5R + 13.125)\alpha^6 \\
& \qquad + (7.5R^4 - 56.25R^3 + 275.6R^2 + 91.875R + 19.688)\alpha^8
\end{aligned}$$

$$+ (118.12R^4 + 367.5R^3 + 346.5R^2 + 177.19R + 27.07)\alpha^{10}$$
$$+ (13.125R^6 + 183.75R^5 + 866.25R^4 + 1358.4R^3$$
$$+ 947.46R^2 + 297.77R + 351.9)\alpha^{12}]$$
$$+ c^2/V_o^2[0.5\alpha^2 + (0.5R^2 + 2.25R + 2.25)\alpha^4$$
$$+ (9R^2 + 12.5R + 4.688)\alpha^6$$
$$+ (2.25R^4 + 18.75R^3 + 98.437R^2 + 34.45R + 7.686)\alpha^8$$
$$+ (42.188R^4 + 137.8R^3 + 159.2R^2 + 70.88R + 11.07)\alpha^{10}$$
$$+ (4.688R^6 + 68.91R^5 + 336.87R^4 + 543.37R^3 + 387.6R^2$$
$$+ 124.07R + 14.89)\alpha^{12}] \qquad (31)$$

Differentiating equation 31 with respect to α^2 gives

$$\frac{d\phi}{d(\alpha^2)} = 3 + (6R^2 + 15R + 11.25)\alpha^2$$
$$+ (67.5R^2 + 78.75R + 26.25)\alpha^4$$
$$+ (22.5R^4 + 157.5R^3 + 367.5R^2 + 236.3R + 49.22)\alpha^6$$
$$+ (393.8R^4 + 1181R^3 + 1280R^2 + 541.4R + 31.21)\alpha^8$$
$$+ (52.5R^6 + 708.8R^5 + 3248R^4 + 4981R^3 + 3411R^2$$
$$+ 2111R + 123.2)\alpha^{10}$$
$$- c/V_o[3 + (6R^2 + 18R + 15)\alpha^2$$
$$+ (90R^2 + 112.5R + 39.38)\alpha^4$$
$$+ (30R^4 + 225R^3 + 1103R^2 + 367.5R + 78.75)\alpha^6$$
$$+ (551.2R^4 + 1837.5R^3 + 2047.5R^2 + 885.9R$$
$$+ 135.4)\alpha^8$$
$$+ (78.75R^6 + 1103R^5 + 5198R^4 + 8151R^3 + 5685R^2$$
$$+ 1787R + 211.1)\alpha^{10}]$$
$$+ c^2/V_o^2[0.5 + (R^2 + 4.5R + 4.5)\alpha^2$$
$$+ (27R^2 + 37.5R + 14.06)\alpha^4$$

$$+ (9R^4 + 75R^3 + 393.8R^2 + 137.8R + 30.63)\alpha^6$$
$$+ (210.9R^4 + 689.1R^3 + 159.25R^2 + 354.37R + 55.37)\alpha^8$$
$$+ (28.13R^6 + 413.4R^5 + 2021R^4 + 3260R^3 + 2326R^2 + 744.4R + 89.33)\alpha^{10}] \quad (33)$$

APPENDIX J

SAMPLE CALCULATION

I. Average fringe shift from interferometric data:

$$\bar{N} = \frac{a \sum_{o}^{Y_{MT}} V_x \, \Delta y_i \, N_i + w \sum_{o}^{Y_{MF}} b_i V_x \, \Delta y_i \, N_i}{\sum_{o}^{Y_{MT}} V_x \, \Delta y_i + w \sum_{Y_{MT}}^{Y_{MF}} b_i \, V_x \, \Delta y_i}$$

where $V_x = 3V_o \left(\frac{y}{h_o} - \frac{y^2}{2h_o^2} \right)$ cm./sec.

ΔS = frequency, sec.$^{-1}$

b_T = time width for travelling one wave space, sec.

$a = 1 - wb_T$

Example: Run A17-2
Magnification ratio $M_1 = 98.384$
$w = 9.05$ sec.$^{-1}$
Re. = 774
$M_1 Y_{MF} = 7.804$ cm.
$M_1 Y_{MT} = 5.874$ cm.

M_1Y internal		V_x	$V_x \Delta y_i$	b_i	$b_i V_x \Delta y_i$
0	to 1.0	4.92	4.92		
1.0	2.0	13.92	13.92		
2.0	3.0	21.30	21.30		
3.0	4.0	27.12	27.12		
4.0	5.0	31.66	31.66		
5.0	5.874	34.60	34.60		
5.874	6.5	36.06		0.099	2.243
6.5	7.1	35.59		0.075	1.658
7.1	7.804	36.62		0.0428	1.108

The value of b_i was calculated from the following equation

$$b_i = (\pi - 2x_i)\frac{b_T}{\pi} \qquad (107)$$

After several trials, the value of b_T was 0.1105. The value of x_i was found from x_i = arc sin y_i, where

$$y_i = \frac{\frac{5.874 + 6.5}{2} - 5.874}{7.804 - 5.874} = \frac{0.313}{1.93} = 0.162$$

where $x_i = 0.162$

From equation 107 $b_i = 0.099$

In the same way

$$y_i = \frac{6.8 - 5.874}{1.93} = 0.48 \; ; \; x_i = 0.5 \; ; \; b_i = 0.075$$

$$y_i = \frac{7.452 - 5.874}{1.93} = 0.818 \; ; \; x_i = 0.96 \; ; \; b_i = 0.0428$$

$$\sum_{o}^{Y_{MT}} V_x \, \Delta y_i + w \sum_{Y_{MT}}^{Y_{MF}} V_x \, \Delta y_i \, b_i = 129.16 + 45.33 = 174.49$$

$M_1Q = 174.63$ Check!

Calculation Sheet

β = 5°

Date _____

Position = 25

Mag. ratio = 98.384

Flow rate = 12

$a = 1 - b_T w$ = 0

Plate No. = A17-2

w = 9.05

M_1y internal		$V_x\Delta y_i$	N_i	$V_x\Delta y_i N_i$	$V_x\Delta y_i b_i$	N_i	$V_x\Delta y_i N_i b_i$
0	to 1.0	9.92				0.145	0.0788
1.0	2.0	13.92				0.145	0.2230
2.0	3.0	21.30				0.145	0.3413
3.0	4.0	27.12				0.160	0.4795
4.0	5.0	31.66				0.20	0.6997
5.0	5.874	30.24				0.295	0.9858
5.874	6.5				2.243	0.475	1.0654
6.5	7.1				1.658	0.690	1.1440
7.1	7.804				1.108	0.980	1.0858
					Total		6.1024

$a\Sigma V_x\Delta y_i N_i$ = 0

$w\Sigma V_x\Delta y_i N b_i$ = 55.227 } total = 55.227

Q = 174.63

$\bar{N}$ = 0.3163 $\bar{N}/N_s$ = 0.1111

$\bar{C}$ = 0.1725 $\bar{C}/C_s$ = 0.1217

$\bar{N}/N_s - \bar{C}/C_s$ = -0.01083

II. The calculation of dN/dy:

Example: Run A17-2

N	ΔN	M_1y	$\Delta(M_1y)$	$\Delta N/\Delta(M_1y)$
0.145		0.5		
	0		0.5	0
0.145		1.0		
	0		0.5	0
0.145		1.5		
	0.005		0.5	0.01
0.150		2.0		
	0.02		0.5	0.04
0.170		2.5		
	0.035		0.5	0.07
0.205		3.0		
	0.085		0.5	0.17
0.290		3.5		
	0.155		0.5	0.31
0.455		4.0		
	0.255		0.5	0.51
0.710		4.5		
	0.370		0.5	0.74
1.080		5.0		

III. The calculation of eddy diffusivity:

From equation

$$(D + \epsilon) = \frac{\int_0^y V_x C \, dy\big|_{x_2} - \int_0^y V_x C \, dy\big|_{x_1}}{\Delta x \left.\frac{dC}{dy}\right|_{\frac{x_2+x_1}{2}}} = \frac{\int_0^y V_x \Delta C \, dy}{\Delta x \left.\frac{dC}{dy}\right|_{\frac{x_1+x_2}{2}}}$$

Since $$C = N(C_s/N_s)$$

Therefore $$(D + \epsilon) = \frac{\int_0^y V_x \, \Delta N \, dy}{\Delta x \left.\frac{dN}{dy}\right|_{\frac{x_1+x_2}{2}}}$$

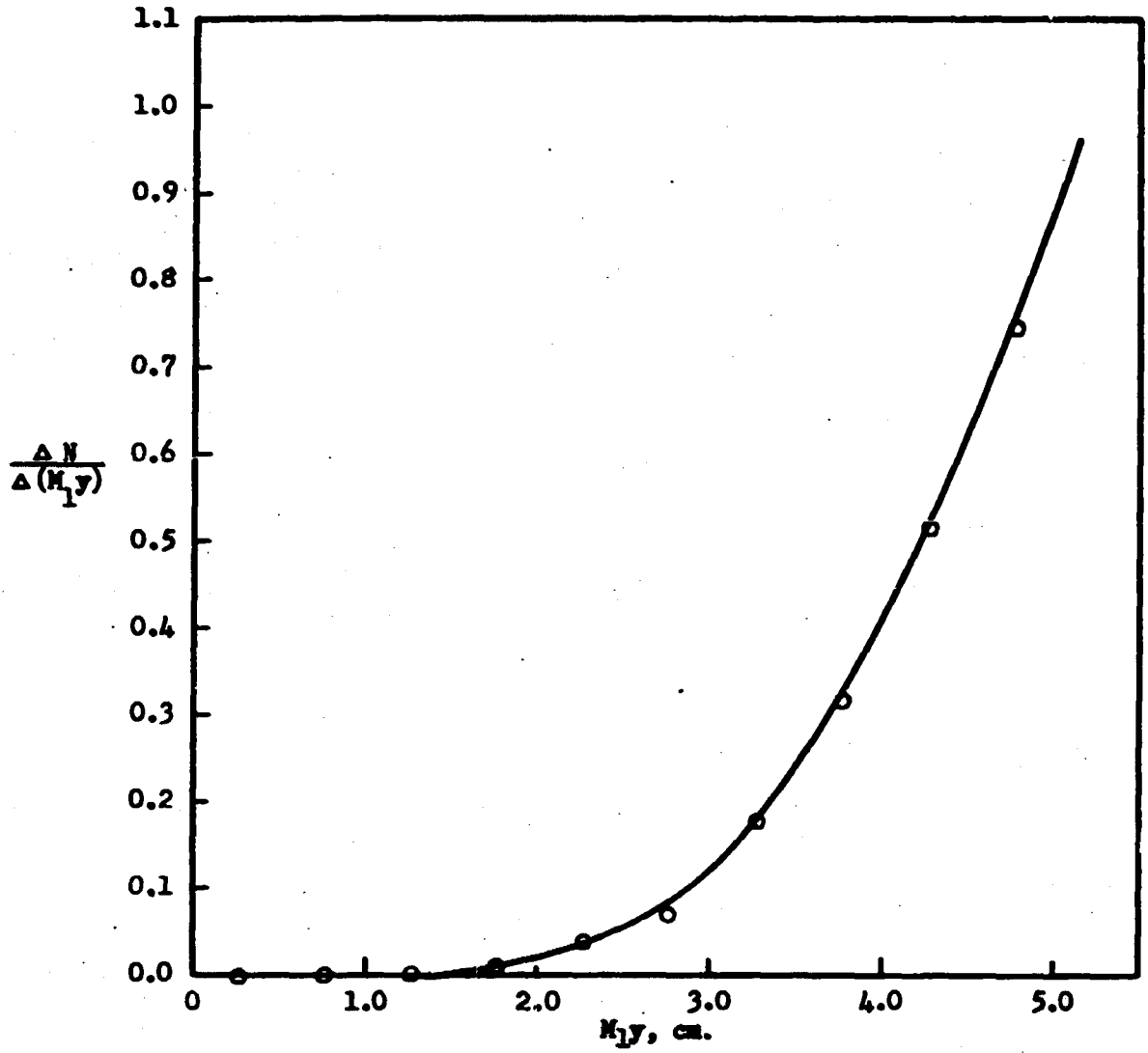

Figure 27. SLOPE OF CONCENTRATION PROFILE.

Calculation Sheet

$\beta = 5^\circ$

Re. = 1144

Magnification ratio = 98.384

Plate No. A17-6 and A21-5

Position 25 and 28

y cm.	V_x cm./sec.	ΔN	$V_x \Delta N$	$\int_0^h V_x \Delta N dy$	$\frac{dN}{dy}_{av.}$	$(D + \epsilon) \times 10^5$ cm.^{2}/sec.
0.0051	4.84	0			0.0108	
0.0152	13.85	0			0.0118	
0.0754	21.5	0.0401	0.8621	0.0011	0.0142	
0.0356	27.92	0.0700	1.954	0.0155	0.0169	82.38
0.0457	33.53	0.100	3.353	0.0423	0.0223	170.8
0.0559	37.9	0.128	4.85	0.0841	0.0331	228.9
0.0661	41.1	0.147	6.042	0.1396	0.0692	181.8
0.0762	42.65	0.135	5.758	0.1992	0.144	124.4
0.0821	43.7	0.135	5.900	0.2333	0.226	92.8
0.0846	43.8	0.130	5.694	0.2481	0.273	81.9
0.0884	43.98	0.165	7.257	0.2727	0.377	65.2
0.0931	44.0	0.240	10.56	0.3146		

$$(D + \epsilon) = 9.0135 \times 10^{-4} \frac{\int_0^y V_x \, \Delta N \, dy}{\frac{dN}{dy}_{av.}}$$

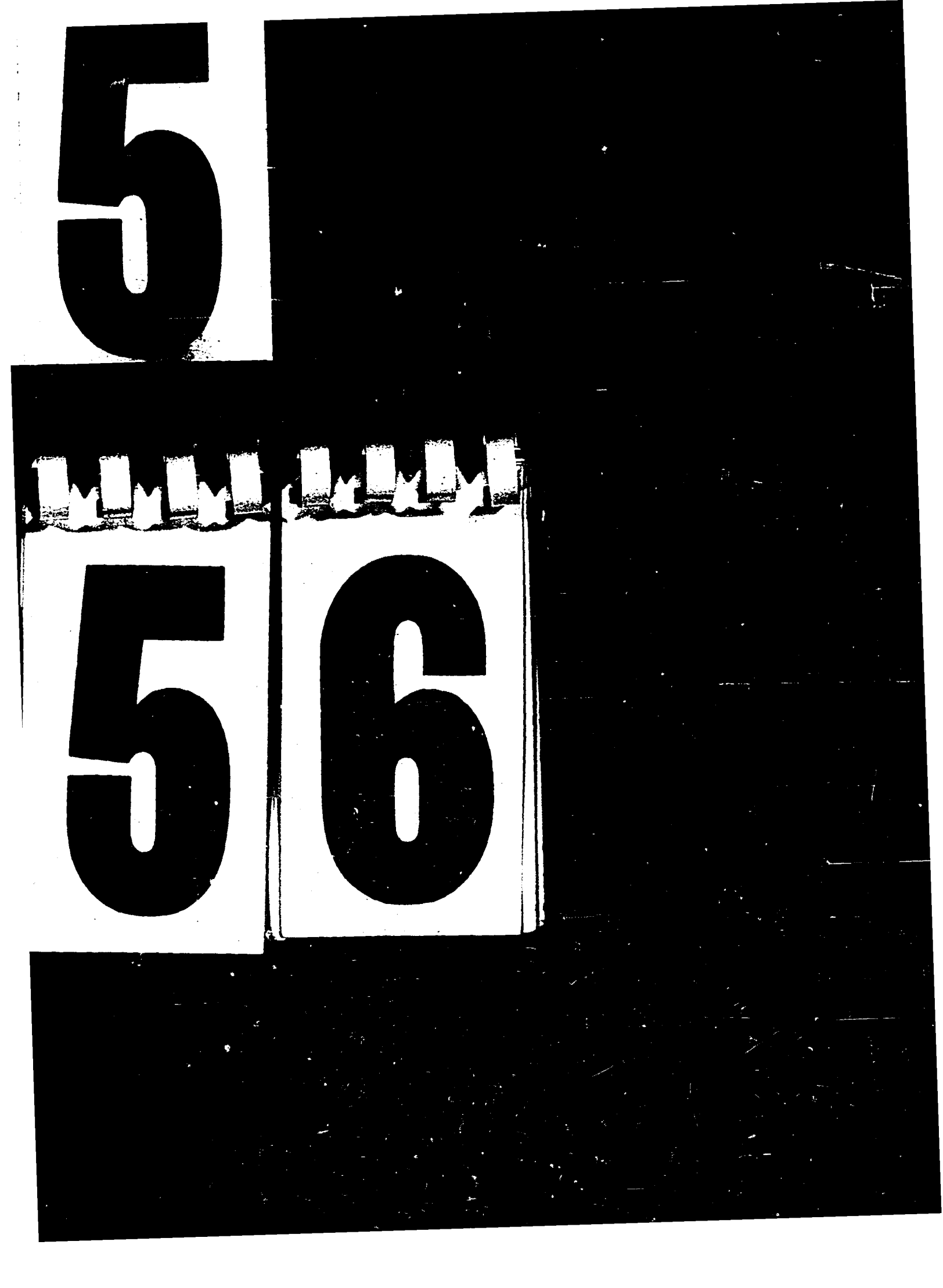
5
56